SANDIA REPORT
SAND2020-10950
Printed September 2020

Sandia National Laboratories

Sandia's Research in Support of COVID-19 Pandemic Response: Materials Science

Grant A. Rossman, Isaac C. Avina, Bradley A. Steinfeldt, Jeffrey Koplow, Kent Smith, Natalia Jouravel, George M. Buffleben, Anupama Sinha, Oscar Negrete, Todd Barnett, Richard Karnesky, Michael A. Melia, Jason M. Taylor, Neil Robert Sorensen, Mark Tucker, Brad H. Jones, George D. Bachand, Brooke N. Harmon, Philip R. Miller, James B. Ricken, Maxwell Stefan, Patrick D. Burton, Matt Tezak, Cody Corbin, Bryce Ricken, Lauren Atencio, Jesse Cahill, Andres Sanchez, Anne Grillet, Sara Dickens, Martin Nemer, Michael A. Melia, Jason M. Taylor, Mark Tucker, Wahid Hermina, and Edward I Cole Jr.

Prepared by
Sandia National Laboratories
Albuquerque, New Mexico
87185 and Livermore,
California 94550

Issued by Sandia National Laboratories, operated for the United States Department of Energy by National Technology & Engineering Solutions of Sandia, LLC.

Available to DOE and DOE contractors from
U.S. Department of Energy
Office of Scientific and Technical Information
P.O. Box 62
Oak Ridge, TN 37831

Telephone: (865) 576-8401
Facsimile: (865) 576-5728
E-Mail: reports@osti.gov
Online ordering: http://www.osti.gov/scitech

Available to the public from
U.S. Department of Commerce
National Technical Information Service
5301 Shawnee Rd
Alexandria, VA 22312

Telephone: (800) 553-6847
Facsimile: (703) 605-6900
E-Mail: orders@ntis.gov
Online order: https://classic.ntis.gov/help/order-methods/

ABSTRACT

Sandia Materials Science Investment Area contributed to the SARS-CoV-2 virus and COVID-19 disease which represent the most significant pandemic threat in over 100 years. We completed a series of 7, short duration projects to provide innovative materials science research and development in analytical techniques to aid the neutralization of COVID-19 on multiple surfaces, approaches to rapidly decontaminate personal protective equipment, and pareto assessment of construction materials for manufacturing personal protective equipment. The developed capabilities and processes through this research can help US medical personnel, government installations and assets, first responders, state and local governments, and multiple federal agencies address the COVID-19 Pandemic.

ACKNOWLEDGEMENTS

The authors gratefully acknowledge the support of Gil Herrera, Ben Cook, Greg Frye-Mason, Donna Chavez, Donna Mullaney, Leigh Cunningham, Ladonna Martin, and Hannah Stangebye. Supported by the Laboratory Directed Research and Development program at Sandia National Laboratories, a multimission laboratory managed and operated by National Technology and Engineering Solutions of Sandia LLC, a wholly owned subsidiary of Honeywell International Inc. for the U.S. Department of Energy's National Nuclear Security Administration under contractDE-NA0003525.

CONTENTS

This page left blank

ACRONYMS AND DEFINITIONS

Abbreviation	Definition
MS	Materials Sciences
COVID-19	2019 novel coronavirus disease
CRO	Chief Research Officer
DOE	Department of Energy
PPE	Personal Protective Equipment
LDRD	Laboratory Directed Research and Development
E-PPE	Emulated-PPE (E-PPE)
CDC	Center for Disease Control
NIOSH	National Institute for Occupational Safety and Health
NPPTL	National Personal Protective Technology Laboratory
BAMPs	Boronic acid-modified polymers
GRAS	generally regarded as safe
SDS	Sodium dodecyl sulfate
DF-200	Decontamination Formulation 200
SFO	Sandia Field Office

1. INTRODUCTION

In mid-March of 2020, the Chief Research Officer (CRO) of Sandia National Laboratories issued an internal call for scientific and engineering research proposals to support national, regional, and local responses to the COVID-19 pandemic. Ideas submitted in response to this call were evaluated through Sandia's Laboratory Directed Research and Development (LDRD) program, and those selected for funding were administered through the program's seven research foundations. To ensure timely impact on the public health, economic, and social challenges posed by the pandemic, COVID-19 projects were expected to execute within a two- to four-week time frame after approval from the LDRD office and concurrence from the Sandia Field Office (SFO) of the U.S. Department of Energy (DOE). The call for proposals closed in mid-May.

During the nearly two months that the call was open, a total of 33 projects were selected for funding. This report describes the seven projects funded under the Materials Science (MS) research foundation.

The 7 MS portfolio projects focused research on innovative methods to aid in the neutralization of COVID-19 on multiple surfaces, approaches to rapidly decontaminate personal protective equipment (PPE), and pareto assessment of construction materials for manufacturing PPE.
.
The goals, procedures, challenges, results, and findings of each of the projects executed under the MS umbrella are summarized in the next section. The report concludes with a discussion of the immediate and ongoing impacts of the MS COVID-19 portfolio in addressing aspects of the pandemic.

2. RESEARCH PROJECTS

This section consists of a series of project overviews. The full reports of each project or pointers to standalone SAND reports are included in the Appendix.

2.1. E-PiPEline: Face Shields and Face Coverings Using Commonly Available Materials

The Center for Disease Control has recommended that the public should wear cloth face coverings in public settings. Face coverings and face shields can be made by using Commonly Available Materials (CAMs). As part of the Sandia COVID-19 LDRD effort (funded under the Materials Science Investment Area), the Sandia E-PiPEline task evaluated design options for face coverings and face shields considering their effectiveness, durability, build difficulty, build cost, and comfort. Observations from this investigation are presented to provide guidelines for home construction of face coverings and face shields. This Appendix Report includes a brief roadmap of the analysis methodology, two one-page handouts geared to be distributed to the public at large (one for face coverings and one for face shields), and additional observations regarding potential solutions for face coverings and face shields included to further support the one-page handouts.

2.2. Supercritical Co_2 for PPE

In response to the COVID-19 outbreak earlier this year, Sandia National Labs stood up several short-duration R&D projects to evaluate various technological countermeasures for this crisis. The present work is directed towards multiple reuse of normally disposable N95 masks used in hospital settings to ensure the safety of medical staff. Exhausting the supply of personal protective equipment (PPE) is one of the most likely scenarios for collapse of our nation's health care infrastructure during a wide-spread pandemic.

N95 masks, such as the 3M model 1860 widely used in the healthcare industry were never meant to be reused. Accordingly, such masks were not designed to withstand the harsh conditions of autoclaving and other traditional sterilization protocols. In fact, the internal structure of such N95 masks is quite delicate because of the mechanism used to achieve high-efficiency particle filtration while minimizing restriction of air flow. High particle filtration efficiency is not achieved be using an extremely fine fabric weave, but rather via electrically poled polymeric fibers that capture particulates by electrostatic attraction (i.e., the induced dipole effect). The challenge is to develop sterilization process that does damage the delicate internal structure of the mask or cause other adverse effects such as degradation of the elastomeric band used to achieve a good seal between the mask and face.

We hypothesized that supercritical CO2 processing in conjunction with a suitable biocidal additive will allow for multi-reuse processing of N95 masks using commercially available equipment that has been developed in the U.S. and abroad for the dry-cleaning industry. In the proposed application, a key attribute of a super critical fluid is that it possesses the characteristics of a gas from standpoint of its ability to permeate into microporous materials and completely fill the volume of internal recesses and cavities independent of aspect ratio (i.e. leaving no place for contaminants to hide) while also having the properties of a liquid from the standpoint of its performance as a solvent. Supercritical CO2's properties as a non-polar solvent allow it to serve as a vehicle for delivery of a variety of candidate biocidal additives. The reason that super-critical CO2 is suitable for use on fabrics having a delicate microstructure is that the strong surface tension forces that can alter fabric microstructure during liquid-to-gas drying at the end of a solvent or water-based washing cycle can be circumvented by keeping carbon dioxide above its critical temperature of 31 C, such that the

liquid-to-gas phase change is prevented from occurring. Finally, the ability of super-critical CO2 to also remove soil is highly desirable in PPE reuse applications.

Data obtained in this brief preliminary study strongly suggest, but do not prove, that processing of 3M model 1860 N95 masks in super-critical carbon dioxide will not impair the function of such masks. Fifteen such masks were subjected to ten consecutive 1-hour cycles of super-critical carbon dioxide cleaning at a temperature of 37 C and a pressure of 1200 psig. These masks, along with five control samples from the same manufacturing lot were sent to the CDC NIOSH NPPTL research facility in Pittsburgh, PA for standardized battery of performance tests. Interpretation of the test results was complicated by the fact the masks were mechanically deformed during insertion into our small pressure chamber. This degraded the ability of the masks to seal properly around the face, allowing some particulate material to bypass. But in quantitative terms, 100% of the reductions in masks particle collection efficiency was attributable to such leakage. We strong suspect that repeating the same experiment with a larger size pressure vessel will definitively demonstrate that super-critical carbon dioxide cleaning is benign to 3M model 1860 N95 masks.

2.3. Spray-On Active Layer

The current COVID-19 pandemic has resulted in globally constrained supplies for face masks and personal protective equipment (PPE). Production capacity is limited in many countries and the future course of the pandemic on the global scale will likely escalate for the foreseeable future. Hence, expectations are that mask reuse, extended wear and similar approaches will play a critical role to enhance the availability of personal protective measures. Repetitive thermal sterilization could be an important option and likely easier implemented in some situations, at least on the small scale, than UV illumination or hydrogen peroxide vapor exposure. An overview on thermal aging and ongoing filtration performance of multiple face mask types is summarized. Some masks have adequate material properties to survive extended thermal exposure, while others are more easily affected (fusing of plastic liner or warping). As guidance, we also show that dilute disinfectants solutions maintain their surface presence over extended time at 25 and 37°C. Dilute and gentle spray-on alcohol-based sterilization solutions, perhaps improvised due to lack of local availability and applied to the top surface only, may complement the now ubiquitous custom-made face masks with their often unknown filtration effectiveness for additional anti-viral properties.

2.4. Boronic Acid-Functionalized Polymers

Boronic acid-modified polymers (BAMPs) can interact with glycoproteins and other glycosylated compounds through covalent binding of the boronic acid moieties to saccharide residues. As a first step toward evaluating the utility of BAMPs as SARS-CoV-2 antiviral agents, this COVID-19 rapid response LDRD was intended to examine the effect of BAMPs on SARS-CoV-2 spike glycoprotein and its subsequent binding with ACE2 receptor protein. Multiple different approaches were attempted in order to determine whether BAMPs based on poly(ethylene glycol) and poly(ethylenimine) bind the spike protein, but failed to produce a definitive answer. However, two different enzyme-linked immunosorbent assays clearly showed no discernable effect of boronic acid in inhibiting spike-ACE2 binding.

2.5. Carboxylic Acids as Sanitizers

Non-toxic disinfectants composed of readily available commodity chemicals are needed for immediate response to the current COVID-19 pandemic. While many disinfectant cleaners are usually available, disruption of standard operations can place supply or logistical constraints on

established materials. It is therefore useful to expand the body of knowledge to include or adapt new or atypical decontaminants.

One such area is the active research field for food-grade sanitization. Freshly harvested produce and food processing equipment have several opportunities for cross-contamination to occur during routine operation. A substantial effort to develop cleaning solutions from non-toxic, and specifically food-grade, ingredients has been directed largely at reducing bacterial pathogens. Combinations of levulinic acid, a five-carbon ketocarboxylic acid, and sodium dodecyl sulfate, have been frequently reported. Levulinic acid is a five-carbon ketocarboxylic acid designated as GRAS (generally regarded as safe) for human use, including consumption. Sodium dodecyl sulfate is a surfactant with wide safety acceptance and common use in consumer products. These ingredients are appealing for food use, since any residue left after cleaning (the surface of food, such as cantaloupe stem scars) must be safe for incidental ingestion. Routine use of the chemical should also be minimally hazardous to operators who will be applying it to high use surfaces frequently. Adapting this technology for virucidal use would be beneficial to near-term use in the COVID-19 pandemic, as well as subsequent routine use.

Levulinic acid has been identified as a renewable feedstock but is not presently in commodity production. Other carboxylic acids, such as acetic acid, may be equally usable and food-safe. Since the literature had very few reports of levulinic acid/SDS (sodium dodecyl sulfate) efficacy towards viruses in general, an evaluation of the solution efficacy was needed. The solution was tested as a decontaminant for MS-2, a non-enveloped bacteriophage used as a surrogate for SARS-CoV2. MS-2 is a non-enveloped virus which is more resistant to decontamination efforts than enveloped viruses, such as coronaviruses.

Neutralization of MS-2 by levulinic or acetic acids, buffers, and salts in SDS solution was investigated in this project. Acidic and buffered solutions were highly effective, yielding no countable surviving organisms. Conjugate salts of each acid were less effective, but still slightly better than 1 wt% SDS alone. Solutions containing potassium salts exhibited a further complication due to formation of a precipitate. A functional mechanism (and comparative activity of acetic and levulinic acids) could not be determined due to the identical behavior of each acid. The high efficacy of each acid may suggest that carboxylic acid sanitizers in general have potential use against viruses.

2.6. Self-Cleaning Coatings

A novel derivative of a previously-published polymeric material has been synthesized and developed into an easily-sprayable coating. Surface characterization of coatings confirm correct elemental presence, and viral assays reveal quantitative elimination of MS2 bacteriophage and Phi6 bacteriophage, surrogates used for SARS-CoV-2, in as little as 5 minutes upon contact. Furthermore, an N95 mask was dip-coated in the polymer solution and analyzed through microscopy and filtration efficacy testing. Though coating was successful, electrostatic interactions between mask layers and polymer reduced filtration efficacy significantly. As such, we expect the current results of this work to be applicable on non-respiratory PPE and on solid substrates of commonly-touched surfaces for rapid self-decontamination.

2.7. The Corrosivity of Disinfectants in Contact with a Shipboard Material, HY80 steel

The variety of decontamination formulations used to eliminate the SARS-CoV-2 virus from surfaces ranges in efficacy and materials compatibility, with corrosion of infrastructure material being of major concern. The Sandia developed Decontamination Formulation DF-200 is a hydrogen peroxide based disinfectant showing high efficacy at seven-9's effectiveness, however there is little quantitative work showing its corrosivity when in contact with alloys critical to infrastructure. The aim of this study is to determine the corrosivity of the DF-200 formulation and bleach (sodium hypochlorite), for comparison, when in contact with a shipboard relevant alloy in HY80 steel.

Traditional electrochemical measurements revealed a similar corrosion rate was caused by the sodium hypochlorite and DF-200 solutions at early immersion times. After 24 hours the corrosion rate cause by sodium hypochlorite remained the same while samples fully immersed with DF-200 saw an order of magnitude reduction in corrosion rate, due to the dissipation of the oxidizer, hydrogen peroxide. Atmospheric corrosion exposures were also carried out on HY80 specimens with crevice forming washers attached to them in order to show the impact these disinfectants, and their residue if left behind after cleaning cycles, have on crevice corrosion in a humid environment. In general, the sodium hypochlorite solution caused the most corrosion when residue remained on the surface, consistently causing more crevice sites to show local attack. The DF-200 formulation, when diluted to 10% strength, showed localized corrosion at the crevices and surrounding area to a similar extent to the control samples (with no disinfectant). The residue left behind from the DF-200 formulation exhibited inhibitor behavior for the exposures performed on specimen with NaCl loading, used to better replicate a marine environment.

APPENDIX A. INDIVIDUAL PROJECT REPORTS

A.1. E-PiPEline: Quick to Market Face Coverings and Face Shields Using Commonly Available Materials

Grant A. Rossman, Isaac C. Avina, Bradley A. Steinfeldt

A.1.1. Overview and Approach

A.1.1.1. Overview

The Center for Disease Control has recommended that the public should wear cloth face coverings in public settings. Face coverings and face shields can be made by using Commonly Available Materials (CAMs). As part of the Sandia COVID-19 LDRD effort (funded under the Materials Science Investment Area), the Sandia E-PiPEline task evaluated design options for face coverings and face shields considering their effectiveness, durability, build difficulty, build cost, and comfort. Observations from this investigation are presented here to provide guidelines for home construction of face coverings and face shields. This executive summary includes a brief roadmap of the analysis methodology, two one-page handouts geared to be distributed to the public at large (one for face coverings and one for face shields), and additional observations regarding potential solutions for face coverings and face shields included to further support the one-page handouts.

A.1.2. Methodology

Analysis methodology techniques that are transparent and defensible were used to provide an analytic framework that articulates the design options, enumerates the assumptions, and provides a semi-quantitative assessment of alternatives while providing a clear linkage between analysis steps. The methodology employed followed the following steps:

1. Understand Design Alternatives in the Literature
2. Define the Design Space Identifying Design Characteristics and Options
3. Enumerate Alternative Designs
4. Develop Evaluation Metrics and Scoring Rubrics
5. Score Alternative Designs
6. Analyze Design Space for Trends and Develop Recommendations

A.1.3. Face Covering Design Space

A large design space was examined for the face coverings (over 200,000 design combinations) using a systematic process. This design space using CAMs includes the following design options

Number of Layers: 1, 2, or 3

Mask Material in Each Layer: (1) Tight Non-Woven Hydrophilic Coated Polypropylene Based, (2), Non-Woven Polypropylene Based, (3) Non-Woven Polypropylene/Polyester Blend Based, (4) Lignocellulosic Based; (5) Non-Woven Cohesive Polyester/Elastomer Blend Based; (6) Woven Cotton Based <600 Thread Count Based; or (7) Tight-Woven Cotton Based >600 Thread Count Based

Layer Connection Location: Around Edge, Around Edges and Center, or None

Layer Connection Mechanism: Staple, Glue, Sew, Friction, or None

Strap Attachment Material: Same as Layer 1, Same as Layer 2, Same as Layer 3, Elastic Band, Tourniquet Band, Velcro Straps, Rubber Band, Cohesive Bandage, or Latex Gloves

Strap Attachment Mechanism: Staple, Glue, Sew, Tape, Compression, or Integrated

A.1.4. Face Shield Design Space

The face shield design space (900 design combinations) using a systematic process includes the following CAM design options

Shield Material: Cellulose Acetate, Polypropylene & Vinyl, Polyethylene Terephthalate, Polypropylene, or Polyester

Structure: Foam, Safety Glasses, Velcro Straps, Cardboard, Tongue Depressor, or Rolled Paper

Strap Attachment Material: Rubber Band, Cotton Fabric, Velcro Straps, Cohesive Bandage, Elastic Band, or Latex Gloves

Strap Attachment Mechanism: Staple, Glue, Sew, Tape, or Compression

A.1.5. One-Page Handouts

A.1.5.1. Face Covering Designs Using Commonly Available Materials

See Page 7 for the one-page handout developed describing Observations Regarding Face Covering Designs Using Commonly Available Materials.

A.1.5.2. Face Shield Designs Using Commonly Available Materials

See Page 8 for the one-page handout developed describing Observations Regarding Face Shield Designs Using Commonly Available Materials.

Observations Regarding Face Covering Designs Using Commonly Available Materials

Sandia National Laboratories

The Center for Disease Control has recommended that the public should wear cloth face coverings in public settings[1]. A Sandia COVID-19 LDRD effort, the Sandia E-PiPEline Team, systematically evaluated design options for face coverings constructed from commonly available materials (CAMs). The design options were analyzed with subject matter expert input considering the design's effectiveness (metric fiber density, material construction, and water saturation), reusability (degree of inertness), producibility (ability to obtain materials, build time), cost, and comfort (fit on face, breathability). Observations for the design of face coverings using CAMs are provided here.

DESIGN SPACE

The principle design characteristics and alternatives considered for the construction of a face covering are listed below.

- Number and materials of layers: 1-3 layers; woven cotton materials, paper-based materials, synthetic fabrics
- Connection method and location between layers: sewn, glued, stapled; around edge or center and edges
- Treatments of the top layer: machine wash, bake in oven, iron, machine dry, none
- Attachment methods: integrated designs, compression straps, Velcro straps

The graphic at top illustrates the results of scoring more than 200,000 designs evaluated for face coverings using CAMs. The normalized design scores are shown in blue, with the best options shown in red. The scores are normalized relative to the highest score in the effectiveness and producibility metrics.

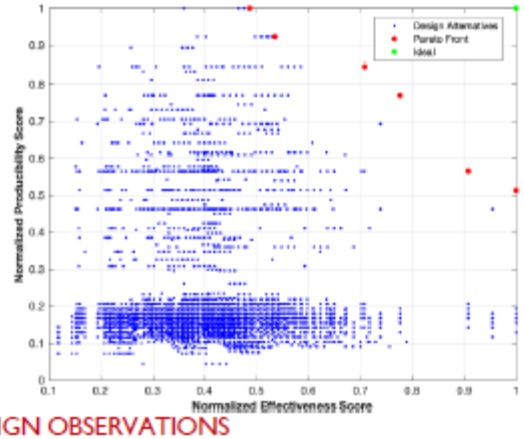

DESIGN OBSERVATIONS

- More layers increase effectiveness
- Full coverage over mouth and nose reduces chances of particles reaching the face
- Mask conformability improves effectiveness

MATERIAL OBSERVATIONS

- Leverage cotton and paper-based materials to capture aerosolized water droplets within the fiber matrix
- The placement of natural-based materials sandwiched between two water repelling synthetic based materials decreases liquid movement towards the face
- Using materials with high fabric density to improve particle filtration while maintaining user breathability
- Prioritize user safety by selecting materials that reduce loose material particle inhalation hazards

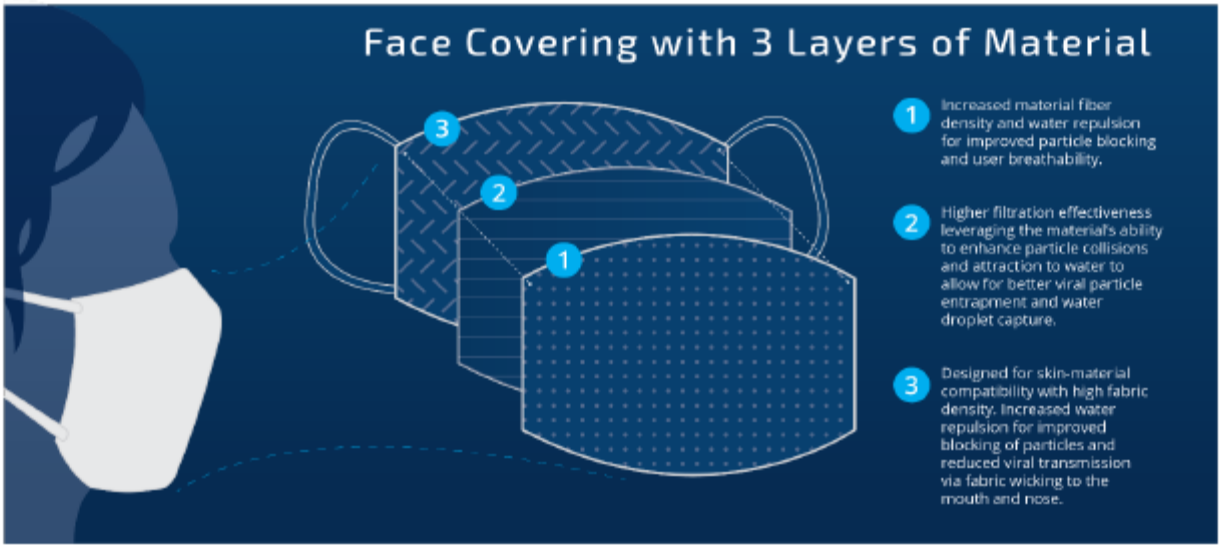

[1] https://www.cdc.gov/coronavirus/2019-ncov/prevent-getting-sick/cloth-face-cover.html

Sandia National Laboratories is a multimission laboratory managed and operated by National Technology & Engineering Solutions of Sandia, LLC, a wholly owned subsidiary of Honeywell International Inc., for the U.S. Department of Energy's National Nuclear Security Administration under contract DE-NA0003525.

Observations Regarding Face Shield Designs Using Commonly Available Materials

Sandia National Laboratories

A Sandia COVID-19 LDRD effort, the Sandia E-PiPEline Team, systematically evaluated design options for face shields constructed from commonly available materials (CAMs). This study is not focused on face shields for medical applications, and as such, has excluded labeling and flammability considerations suggested by the FDA. Design options for face shields were analyzed with subject matter expert input considering the design's **effectiveness** (seal around face), **reusability** (compatibility with solvents, degree of inertness), **producibility** (ability to obtain materials, build time), **cost**, and **comfort** (fit around head, contact surface interface). Observations for the design of face shields using CAMS are provided here.

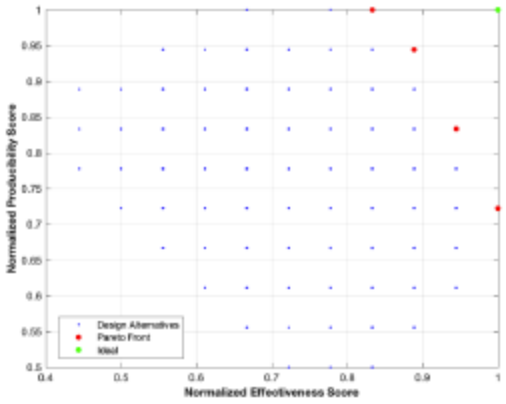

DESIGN SPACE

The principle design variables considered for the construction of a face shield were:

- **Primary shield material**: polyethylene, polypropylene, cellulose acetate
- **Structural material**: foams, safety glasses, cardboard, wood
- **Attachment methods**: sewn, glued, stapled

The graphic at top illustrates the results of scoring more than 900 designs evaluated for face shields using CAMs. The normalized design scores are shown in blue, with the best options shown in red. The scores are normalized relative to the highest score in the **effectiveness** and **producibility** metrics.

DESIGN OBSERVATIONS

- Minimizing the gap between the face shield and the forehead will help reduce the chance of liquid splash to the eyes
- It is important that the face shield extends down below the chin and stretch around the full-face area
- Designs that use compression to attach the face shield to the face were observed to be promising

MATERIAL OBSERVATIONS

- Using foam as the primary frame/face interface material provides splash protection
- For reuse of the face shield, choosing materials that are compatible with common solvents, like polypropylene

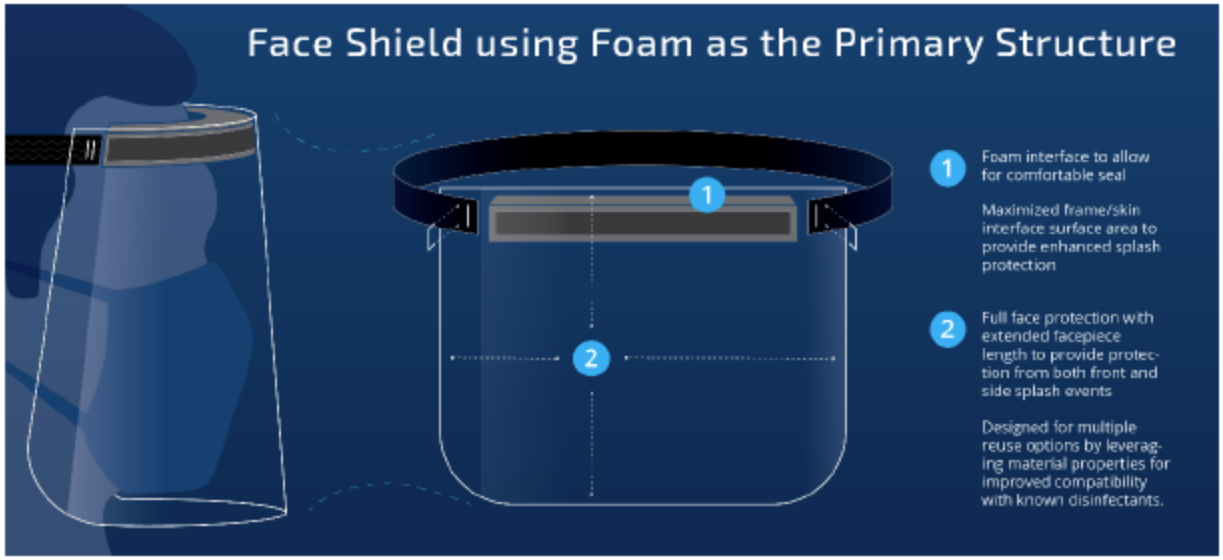

Sandia National Laboratories is a multimission laboratory managed and operated by National Technology & Engineering Solutions of Sandia, LLC, a wholly owned subsidiary of Honeywell International Inc., for the U.S. Department of Energy's National Nuclear Security Administration under contract DE-NA0003525.

A.1.6. Analysis Observations

A.1.6.1. Face Covering Material and Design Observations

Observations

The following observations from the data in the E-PiPEline study were made for the face covering:

- Leverage cotton and paper-based materials to capture aerosolized water droplets within the fiber matrix.
- The placement of natural-based materials sandwiched between two water repelling synthetic based materials decreases liquid movement towards the face
- Using materials with high fabric density to improve particle filtration while maintaining user breathability
- More layers increase effectiveness
- Full coverage over mouth and nose reduces chances of particles reaching the face
- Mask conformability improves filtration effectiveness.

It was observed that the more layers the better. Assuming a three-layer face covering the following observations were made regarding the selection of materials for each layer:

For the *layer furthest from the mouth*, one should increase inertial impaction factor by maximizing fabric fiber density. This will likely increase the probability of blocking aerosolized viral particles. Selecting first layer materials that have a **low water absorption** may also reduce water saturation and increase mask durability and breathability.

The *middle layer* should be designed for material interchangeability. Using **non-woven fabrics with high fiber density** will likely increase filtration effectiveness by providing a tortuous path for particles resulting in increased particle collision and entrapment in the middle layer. Materials with increased water absorbance provide a matrix for aerosolized liquid water capture. Additionally, the middle layer should have design features that allow for material interchange after high particle loading and water saturation which can reduce filtration effectiveness and user breathability.

The *layer closest to the mouth* should be designed for mouth and nose interface compatibility and with **high water repelling properties**. Select materials with a **high fiber density**. Do not select loose materials or weaves to prevent inhalation of material borne particles. By choosing these materials the user can reduce the chance of viral transmission via water wicking to the mouth and nose.

A.1.6.2. Using the Observations for Practical Steps to Materials Selection for Face Coverings

The following are steps to interpret, evaluate, and use the observations provided in the design and creation of a face covering.

1. Understand the material's fiber parameters. Categorize your materials based on whether base fibers are synthetic or natural and if the fibers are small or large in diameter. Synthetic fibers

are usually stronger and more durable for longer use situations as well as usually maintain a low water absorption while small fibers usually indicate a high fiber density.

2. Determine if the material stretches when pulled indicating a knitted or loose weave structure or if conversely the fabric is very stable under tension indicating an increase in fiber density with a non-woven or tight weave structure. Choose materials with a high fiber density that will maintain their shape when put under tension.
3. Determine if the fabric has any coatings, ink, or other surface treatment. A quick way of determining this is simply testing the fabric under water and check if water is repelled or absorbed by the material. Additionally, check if the treatment is applied to one or both sides of the material with the understanding that the water-absorbing material faces should point away from the mouth or nose and placed further away from the mouth. This will minimize water wicking towards the mouth and nose interface of the mask.

A.1.6.3. Material Observations

Table 2-1 provides an assortment of the materials examined in this study for the face coverings, observations regarding these materials, and observations regarding the location in the design of a face covering.

Table 2-1. Practical Description of Materials, Observations, and Locations

Material Types	Examples	Water Saturation Potential	Face Coverings Observations	Highest Scored Face Covering Layer
Cotton with High Fiber Density	Pillowcases, flannel, high tread count clothing	Medium	Easy to wash, absorbent, fairly durable, high fabric density.	Layer closest and furthest from the mouth
Cotton with Medium to Low Fiber Density	Shirts, bandanas, woven gauze, scarfs	Medium	Easy to wash, absorbent, fairly durable, low fabric density	Middle Layer
Polypropylene	Professional/shop towels, Haylard surgical wraps, medical grade fabrics.	Very Low	Low water absorption, high fabric density, very durable	Layer closest and furthest from the mouth
Polyester Blends	Surgical masks, general shop towels, non-woven gauze, sports and performance apparel	Low	Low water absorption, high fabric density, dries quickly, durable	Layer closest and furthest from the mouth
Paper Based	Coffee filters, paper towels, stretcher tissue paper	High	High water absorption, varying degree of fabric	Middle Layer

Material Types	Examples	Water Saturation Potential	Face Coverings Observations	Highest Scored Face Covering Layer
			density	

A.1.6.4. Face Shield Material and Design Observations

The following observations were made from the analysis of the data regarding materials for the face shield.

- The most highly scored options used a foam as the primary frame/face interface material to provide the most effective liquid splash protection
- For reuse of the face shield, choosing materials that are compatible with solvents like polypropylene is crucial.

The following observations were made from the data regarding the design for the face shield.

- Minimizing the gap between the face shield and the forehead will help reduce the chance of liquid splash to the eyes
- It is important that the face shield extends down below the chin and stretch around the full-face area
- Designs that use compression to attach the face shield to the face were observed to be promising

From a design perspective, for the skin to frame interface, it is desired to maximize frame/skin interface surface area to provide enhanced splash protection along with a foam interface for a comfortable seal. For the location of the window, it is desirable for full face protection with extended facepiece length to provide protection from both front and side splash events. Design for multiple reuse options by leveraging material properties for improved compatibility with known disinfects and solvents.

A.2. Supercritical CO2 sterilization of N95 Masks

Jeffrey Koplow, Kent Smith, Natalia Jouravel, George M. Buffleben, Anupama Sinha, Oscar Negrete, Todd Barnett, and Richard Karnesky

A.2.1. Abstract

A preliminary investigation of the use of supercritical carbon dioxide for sterilization of 3M 1860 N95 masks was undertaken to evaluate a potential route to low-cost, scalable, sterilization of N95 masks for multiple reuse in hospital settings. Upon entering the supercritical regime, the normally distinct liquid and gaseous phases of CO_2 merge into a single homogeneous phase that has density, short-range order, and solvation capacity of a liquid, but the volume-filling and permeation properties that of a gas. This enables supercritical CO_2 to function as vehicle for delivery of biocidal agents such peracetic acid into microporous structures. The potentially adverse effect of a liquid-to-gas phase transition on mask filter media is avoided by conducting cleaning operations above 31 C, the critical temperature for carbon dioxide. A sample of fifteen 3M 1860 N95 masks was subjected to ten consecutive cycles of supercritical CO_2 cleaning to determine its effect on mask performance. These 15 masks, along with 5 control samples then underwent a battery of standardized tests at the CDC NIOSH NPPTL research facility in Pittsburgh, PA. The data from these tests strongly suggest (but do not prove) that super-critical carbon dioxide do not damage 3M 1860 N95 masks. Additional tests conducted during this project confirmed the compatibility of supercritical CO_2 with ventilator tubing, which like N95 masks, has been in short supply during portions of the COVID-19 pandemic but cannot be sterilized by conventional means. Finally, a control experiment was also conducted to examine the effect of supercritical CO_2 on a BSL-2 surrogate virus, vesicular stomatitis virus (VSV), Indiana serotype strain. In the absence of biocidal additives, supercritical CO2 exhibited no measurable lethality against VSV. This surrogate virus experiment suggests that a biocidal additive such as peracetic acid will be necessary to achieve required sterilization metrics.

A.2.2. Acknowledgements

The authors of this study would like to acknowledge the assistance provided by Sandia colleagues David Chandler, Paul Schrader, Tim Gilbertson, and David Hopman.

A.2.3. Executive Summary

In response to the COVID-19 outbreak earlier this year, Sandia National Labs stood up several short-duration R&D projects to evaluate various technological countermeasures for this crisis. The present work is directed towards multiple reuse of normally disposable N95 masks used in hospital settings to ensure the safety of medical staff. Exhausting the supply of personal protective equipment (PPE) is one of the most likely scenarios for collapse of our nation's health care infrastructure during a wide-spread pandemic.

N95 masks, such as the 3M model 1860 widely used in the healthcare industry were never meant to be reused. Accordingly, such masks were not designed to withstand the harsh conditions of autoclaving and other traditional sterilization protocols. In fact, the internal structure of such N95 masks is quite delicate because of the mechanism used to achieve high-efficiency particle filtration while minimizing restriction of air flow. High particle filtration efficiency is not achieved be using an extremely fine fabric weave, but rather via electrically poled polymeric fibers that capture particulates by electrostatic attraction (i.e., the induced dipole effect). The challenge is to develop sterilization process that does damage the delicate internal structure of the mask or cause other adverse effects such as degradation of the elastomeric band used to achieve a good seal between the mask and face.

We hypothesized that supercritical CO_2 processing in conjunction with a suitable biocidal additive will allow for multi-reuse processing of N95 masks using commercially available equipment that has been developed in the U.S. and abroad for the dry-cleaning industry. In the proposed application, a key attribute of a super critical fluid is that it possesses the characteristics of a gas from standpoint of its ability to permeate into microporous materials and completely fill the volume of internal recesses and cavities independent of aspect ratio (i.e. leaving no place for contaminants to hide) while also having the properties of a liquid from the standpoint of its performance as a solvent. Supercritical CO_2's properties as a non-polar solvent allow it to serve as a vehicle for delivery of a variety of candidate biocidal additives. The reason that super-critical CO_2 is suitable for use on fabrics having a delicate microstructure is that the strong surface tension forces that can alter fabric microstructure during liquid-to-gas drying at the end of a solvent or water-based washing cycle can be circumvented by keeping carbon dioxide above its critical temperature of 31 C, such that the liquid-to-gas phase change is prevented from occurring. Finally, the ability of super-critical CO_2 to also remove soil is highly desirable in PPE reuse applications.

Data obtained in this brief preliminary study strongly suggest, but do not prove, that processing of 3M model 1860 N95 masks in super-critical carbon dioxide will not impair the function of such masks. Fifteen such masks were subjected to ten consecutive 1-hour cycles of super-critical carbon dioxide cleaning at a temperature of 37 C and a pressure of 1200 psig. These masks, along with five control samples from the same manufacturing lot were sent to the CDC NIOSH NPPTL research facility in Pittsburgh, PA for standardized battery of performance tests. Interpretation of the test results was complicated by the fact the masks were mechanically deformed during insertion into our small pressure chamber. This degraded the ability of the masks to seal properly around the face, allowing some particulate material to bypass. But in quantitative terms, 100% of the reductions in masks particle collection efficiency was attributable to such leakage. We strong suspect that repeating the same experiment with a larger size pressure vessel will definitively demonstrate that super-critical carbon dioxide cleaning is benign to 3M model 1860 N95 masks.

ACRONYMS AND DEFINITIONS

Abbreviation	Definition
SC-CO_2	supercritical carbon dioxide
NIOSH	National Institute of Occupational Safety and Health
CDC	Center for Disease Control (Atlanta, GA)
VSV	vesicular stomatitis virus
PPE	personal protective equipment
PRV	pressure relief valve
COTS	commercial off the shelf

A.2.4. Background and motivation

A.2.4.1. Objective

The objective of this project is to investigate supercritical carbon dioxide sterilization as a non-destructive, high-throughput process for sterilization of N95 masks that can be stood up quickly, widely deployed, uses electricity as the only significant consumable, and that minimizes exposure of personnel to handling of contaminated masks. Multiple reuse of N95 masks has become an important objective for the protection of health care workers fighting the current COVID-19 pandemic, an anticipated 2nd wave of COVID-19 in the fall of 2020, and future communicable-disease public health crises.[1] There are also PPE sterilization applications beyond N95 masks that are driven by the same need to reuse equipment that is normally considered disposable because of current supply chain limitations. Most notably this includes tubing and other components for COVID-19 patient ventilators.

A.2.4.2. Technical background

There are many types of masks on the market with a rating of “N95”, which denotes that such a mask blocks transmission of 95% of particles 0.3 microns or larger in size (95) and that such a mask is not (N) oil resistant. The main challenge in the design and fabrication of any such mask is providing high particle filtration efficiency without an objectionable level of air flow restriction. Such masks must also be very inexpensive to manufacture, because under normal circumstances disposability is a critically important element of the safety provided by such PPE. For example, a physician may change his or her mask before meeting with a new patient as a simple but effective precaution against transmission of disease.

Figure 1: Health care worker wearing personnel protective equipment (PPE) that includes a 3M 1860 N95 mask. These masks are normally considered disposable PPE. Accordingly, such masks were not designed to withstand sterilization processes such as autoclaving.

Applications for N95 masks vary widely as does their design. For example, an N95 mask used on a construction site may feature a one-way valve to reduce flow resistance for worker exhalation because the purpose of such PPE is minimizing inhalation of dust. On the other hand, a mask design that prevents transmission of air-borne contaminants in both directions (inhalation and exhalation) is required in a hospital setting. The present study emphasizes the 3M model 1860 N95 mask because it is the most commonly used mask by health care workers confronting the current COVID-19 crisis. Moreover, other N95 masks that have been employed as alternatives in hospital settings are similar in design.

Such masks are constructed with a multi-layer fiber mesh that is coarse enough to allow adequate air flow, employing electrically poled polymeric filaments to capture particles that would otherwise pass through such a coarse mesh. This electrostatic capture feature is critically important to mask breathability. A frozen-in-place charge separation present in the woven filaments of the inner mask material creates numerous locations among filaments with electric field gradients strong enough to trap particles via the induced dipole effect. Electrical poling of these fibers is carried out by applying a strong electric field during a specific stage of the fiber fabrication process. To avoid destroying the mask, it is vitally important that a candidate sterilization technique not electrically de-pole the fiber material by allowing charge migration, nor leave behind a residue having any significant electrical conductivity.

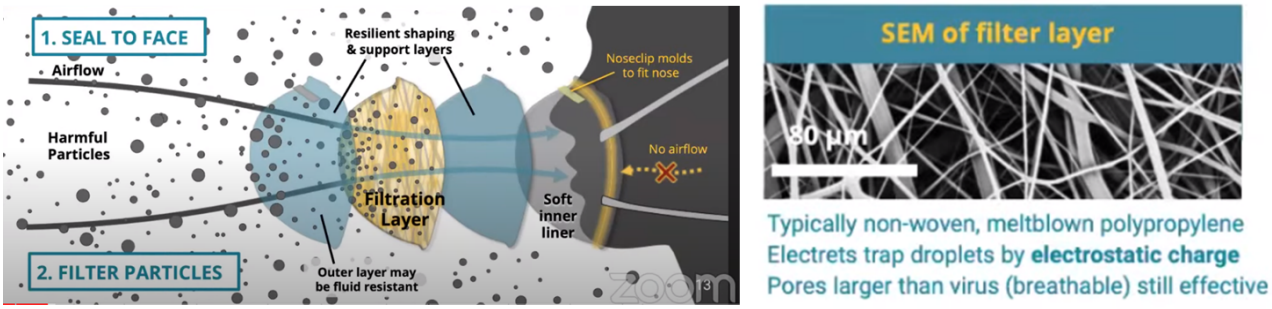

Figure 2: Details of N95 mask design. Any proposed sterilization process must not compromise the integrity/efficacy of the filtration layer, nor compromise mask features that ensure proper fitting of the mask to the face. Source: N95 Decontamination & Reuse Webinar | N95DECON & MGB, https://www.youtube.com/channel/UCG05UXgAI7mtRT_pN9TdSzg

It is important to appreciate that such masks were never intended to be cleaned and reused. They are of delicate construction and can easily be ruined by exposure to traditional sterilization methodologies such as autoclaving or direct application of alcohol. It is also important to remember that mask degradation may comprise (1) a significant reduction in particle filtration efficiency, (2) structural changes that impair proper fitting of the mask when donned, (3) degradation of specific components such as the elastic band used to hold the mask firmly in place, (4) the presence of biocidal agent residue that is toxic or irritating to the respiratory tract, or various combinations thereof.

During the past few months of the COVID-19 crisis, there are three sterilization methodologies that have been pressed into service for reuse of N95 masks on an emergency basis. These include hydrogen peroxide vapor treatment, UVC ultraviolet light treatment, and thermal treatment. A comprehensive review of research conducted on these three methodologies as of May 1, 2020 can be found in the form of a 2-hour video at the Mass General Brigham Center for COVID innovation.[2]

None of these three methodologies provide a fully satisfactory solution for multiple reuse of N95 masks. In the case of thermal methods, researchers have found that the temperature and time duration of heat exposure required to achieve sterilization (defined as a 10^6 reduction in viral load) is in excess of what can be tolerated by the mask. The lesser goal of "decontamination", defined as a 10^3 reduction in viral load appears to be feasible, but this does not meet application requirements.

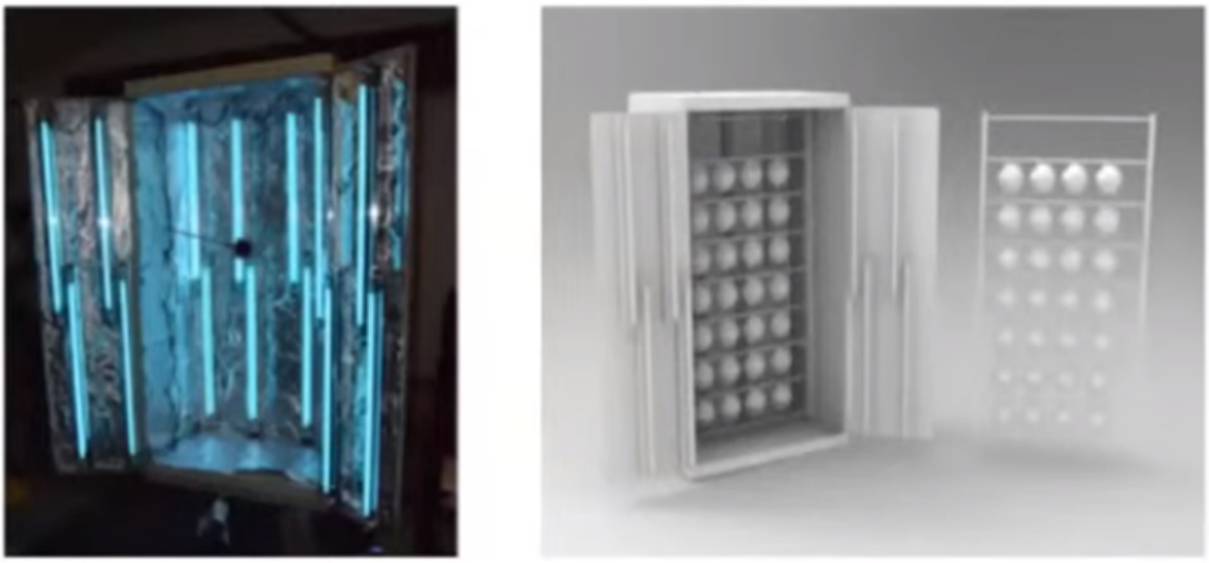

Figure 3: Examples of UVC chambers constructed for N95 mask sterilization.

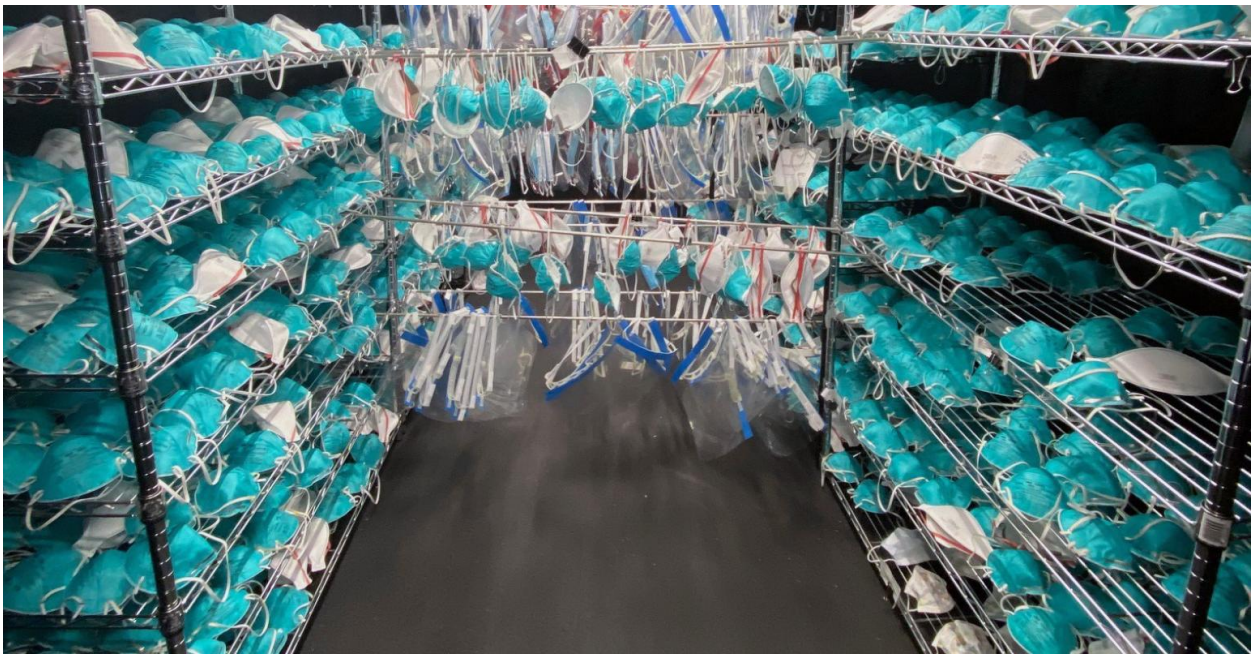

Figure 4: 3M 1860 masks being racked for Batelle's hydrogen peroxide vapor sterilization process.

UVC irradiation at 254 nm by exposure to low-pressure mercury discharge lamps can achieve a 10^6 reduction in viral load, but small numbers of masks must be individually racked to carefully avoid shadowing effects, and a secondary sterilization process must be applied to the elastic band. A further complication is that contaminants deep inside the microporous structure of the

masks are somewhat shielded from UVC light because of absorption and scattering by multiple layers of mask materials. The extent to which this shielding effect reduces the reliability of the UVC method is currently under study.

The hydrogen peroxide vapor (HPV) method provides a 10^6 reduction in viral load but also shares the work-flow impediment that contaminated masks need to be individually racked via manual labor. A lengthy aeration cycle is also required to ensure complete removal of hydrogen peroxide following sterilization because H_2O_2 is very irritating to the respiratory tract. HPV systems are also expensive to build. Batelle was recently awarded a contract to build sixty HPV sterilization modules at a cost of 6.9 million dollars each.[3]

Unlike thermal treatment, in HPV and UVC systems, the precautions required to ensure that all portions of the mask receive adequate biocidal dosage accounts for much of the complexity and tedium of applying these methods. Moreover, personnel tasked with individually racking thousands of contaminated masks by hand each day must exercise extreme caution because of potential COVID-19 transmission. And a major deficiency of all three methods is their inability to remove soil; thermal, UVC, and HPV seek to kill COVID-19 virus in place, but none of these methods clean the mask in a manner that removes foreign material. From the standpoint of aesthetics alone, this discourages the reuse of masks when visible soil is present. But the accumulation of foreign matter such as dried saliva is also a concern from standpoint of reduced air flow, especially in scenarios where individual masks may be reused 10 or more times. Finally, in the case of the UVC and HPV methods, both visible and invisible soil can function as barrier to biocidal infiltration, thereby introducing another unwelcome source of uncertainty.

A.2.5. Proposed Approach

We hypothesize that supercritical CO_2 processing in conjunction with a suitable biocidal additive will allow for multi-reuse processing of N95 masks using commercially available equipment that has been developed in the U.S. and abroad for the dry-cleaning industry. Supercritical carbon dioxide (CO_2) is a unique solvent that is becoming increasingly popular for industrial cleaning and chemical extraction processes. Upon entering the supercritical regime, the normally distinct liquid and gaseous phases of carbon dioxide merge into a single homogeneous phase that has the density, short-range order, and solvation capacity of a liquid, but the volume-filling and permeation properties that of a gas.

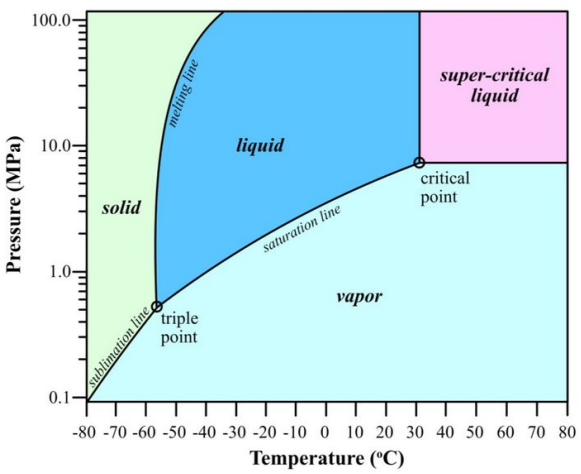

Figure 5: Carbon dioxide phase diagram

Supercritical CO_2 cleaning is becoming increasingly popular in the dry-cleaning industry[4] because it eliminates the need for hazardous solvents such as perchloroethylene, it is suitable for use on even the most delicate fabrics, it can perform the function of a solvent for delivery and removal of chemical additives such as surfactants, and it leaves behind no dampness or chemical residue. It should also be noted that super critical CO_2 processing has long been used for various chemical extraction applications such as decaffeination of coffee beans on an industrial scale. The fact that supercritical CO_2 cleaning equipment is already deployed in the dry-cleaning industry is important to the question of wide-scale, cost-effective, rapid deployment.

Figure 6: COTS SC-CO_2 washing machine

In the proposed application, a key attribute of a super critical fluid is that it possesses the characteristics of a gas from standpoint of its ability to permeate into microporous materials and completely fill the volume of internal recesses and cavities independent of aspect ratio (i.e. leaving no place for contaminants to hide) while also having the properties of a liquid from the standpoint of its performance as a solvent. Supercritical CO_2's properties as a non-polar solvent allow it to serve as a vehicle for delivery of a variety of candidate biocidal additives. The reason that super-critical CO_2 is suitable for use on fabrics having a delicate microstructure is that the strong surface tension forces that can alter fabric microstructure during liquid-to-gas drying at the end of a solvent or water-based washing cycle can be circumvented by keeping carbon dioxide above its critical temperature of 31 C, such that the liquid-to-gas phase change cannot occur. Finally, as alluded to earlier, the ability of super-critical CO_2 to also remove soil is highly desirable in PPE reuse applications.

A.2.6. N95 mask sterilization workflow

We envision a very simple and safe workflow for super-critical CO_2 sterilization of N95 masks. Hospital workers would discard used masks into a container that is lined with a Tyvek bag, perhaps comparable in size to large garbage bag. When the Tyvek bag reaches capacity, it is heat sealed closed, after which its exterior surface is decontaminated (alternatively the Tyvek material could be pretreated with a biocidal agent). A collection of such sealed bags would then be transported to a local CO_2 dry cleaning facility, a CO_2 washing machine installed on site, or a mobile truck-mounted machine. The unopened bags would then be perforated (or perhaps unzipped) to allow rapid ingress/egress of CO_2, processed in super-critical carbon dioxide for tens of minutes, and then resealed for transport or storage. At the end of the cycle, the CO_2 is

pumped back into a storage tank, and converted from supercritical fluid to back to gas as the pressure inside the cleaning vessel ramps down. The resealed sterilized bag and its sterile contents would then be returned to the hospital unopened. If desired, health care workers could write their name on masks when they are newly issued. Alternatively, a passive RFID tag could be applied to each mask to facilitate sorting or barcoded masks could be used.

It will be noted that the proposed sterilization process requires very little labor, avoids exposing personnel to contaminated masks, and preserves masks in an uncontaminated state once sterilized. It is in fact very similar to the workflow used for sterilizing surgical instruments. Used surgical instruments are placed in a heat-sealed Tyvek bag, and then subjected to a penetrating sterilization process such as autoclaving, after which the unopened bags are returned for later use. As with the proposed supercritical CO_2 sterilization scheme, there are no shadowing effects or other uncertainties regarding portions of the mask that may have evaded adequate sterilization. The absence of surface tension in the supercritical state ensures that that even the most remote microporous regions and crevices receive treatment, regardless of the hydrophobicity of hydrophilicity of mask construction materials and any contaminants present. To ensure complete removal of the biocidal agent, if necessary, one or more super-critical CO_2 "rinse cycles" may be employed to ensure its complete removal. And if necessary, activated charcoal may provide a convenient means of any absorbing chemical residue that cannot simply be removed by distillation as CO_2 is converted back to the gas phase.

A.2.7. Sterilization mechanism

We hypothesize that supercritical CO_2 may kill CIVID-19 without the assistance of biocidal additives. One potential lethality mechanism is ultra-dehydration. Water has 0.01 mole fraction of solubility in supercritical carbon dioxide under the temperature and pressure conditions contemplated.[5] Supercritical CO_2 therefore acts as very strong drying agent.[6] Complete removal of water via osmosis through the virus envelope may irreversibly damage proteins and enzymes.

Prior to extraction of water, the high partial pressure of CO_2 present should also acidify water inside the virus envelope to approximately pH = 3.[7] This is analogous to the immediate conversion of deionized water to highly carbonated water upon application of pressurized carbon dioxide. Such a precipitous drop to low pH may also be destructive towards proteins and enzymes.

Finally, unlike proposed sterilization methods based on heat, UV light, or exposure to hydrogen peroxide, the proposed super-critical CO_2 cleaning process has what we refer to as "the elution advantage". That is, virus particles can be destroyed, but they can also be simply washed away.

At the end of the CO_2 washing cycle, supercritical CO_2 containing soil, lint, virus (dead or alive), and other contaminants is re-purified by distillation to CO_2 gas. The small amount of dried

foreign material left behind inside the sump trap of the CO_2 washing machine can then be aggressively sterilized by whatever means is desired (e.g. 200 C heat). The ability of supercritical CO_2 to solvate materials that might otherwise be retained within the mask material is therefore important.

On the other hand, it may be that supercritical CO_2 alone is not capable of killing the COVID-19 virus, or there may be application requirements for the destruction of other less vulnerable pathogens that necessitate the use of biocidal additives. Future work will therefore be required to explore the efficacy of candidate biocidal additives and/or surfactants to ensure adequate sterilization and soil removal, respectively. Biocidal additives currently under consideration include anhydrous materials that can preserve the ultra-dehydration properties of super-critical CO_2, and which we hypothesize will be fully soluble in super-critical CO_2. For example, hydrogen peroxide is known to be highly effective against COVID-19 and a wide variety of other

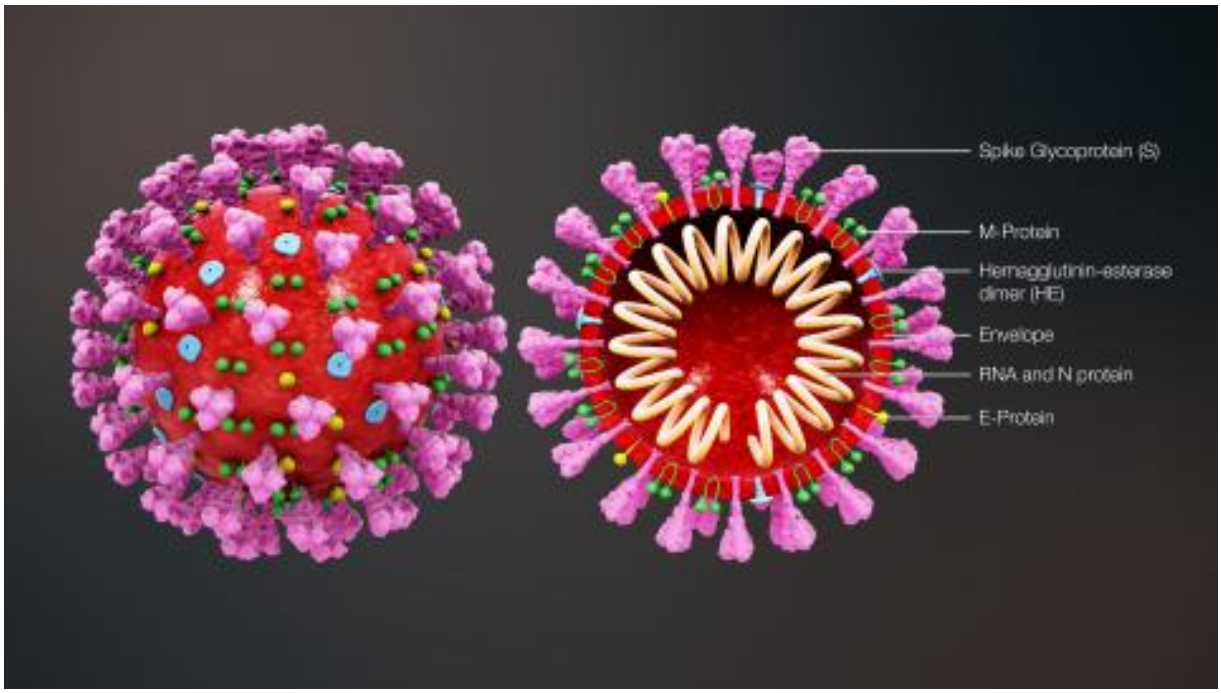

Figure 7: Anatomy of the COVID-19 virus. Source: American Society for Microbiology, https://asm.org/Articles/2020/January/2019-Novel-Coronavirus-2019-nCoV-Update-Uncoating

pathogens. It is typically used a concentration of one hundred to several hundreds of ppm. We propose to evaluate urea-hydrogen-peroxide complex (also known as “carbamide”) as a means of introducing H_2O_2 while maintaining highly anhydrous conditions. Other anhydrous biocidal agents we suspect will be soluble in super-critical CO_2 include quaternary amines such as benzalkonium chloride, and sodium dichloro-s-triazenetrione, also known as dichloroisocyanuric acid. Sodium dichloro-s-triazenetrione is powerful chlorinator and oxidizer. But unlike sodium hypochlorite (bleach), chemical stability considerations do not require that it

be delivered in the form of an aqueous solution. Note that a key characteristic of the three chemical reagents described above is that they are widely available and can be handled by unskilled personnel.

Ultra-dehydration may not turn out to be important to lethality, however, in which case a wider variety of water-borne biocidal agents may be employed. One leading candidate is peracetic acid, which has already demonstrated high biocidal activity in supercritical CO_2. In 2006, White et al. demonstrated greater than 6 log reduction of *B. stearothermophilus* spores for 5% peracetic acid in SC-CO_2.[8] This represents an extremely stringent test of biocidal activity. Accordingly, the question of what biocidal agents if any will ultimately be used in this application is not of central importance. We know supercritical CO_2 can deliver highly effective biocidal agents such as peracetic acid, and we know that supercritical CO_2 provides a convenient means of fully removing such biocidal agents at the end of the sterilization cycle. Therefore, the key questions are:

1) Can supercritical CO_2 perform these functions without damaging any of the delicate materials used in mask construction?
2) Can we experimentally verify that CO_2 provides a vehicle for delivery of biocidal agents into the deepest recesses of such microporous structures?

A.2.8. Construction of laboratory apparatus

The proposed work required the construction of two different types of apparatus to achieve two distinct goals. First, we needed a supercritical CO_2 pressure vessel large enough to treat whole masks, and ideally, many masks at a time. Second, we need an apparatus for processing

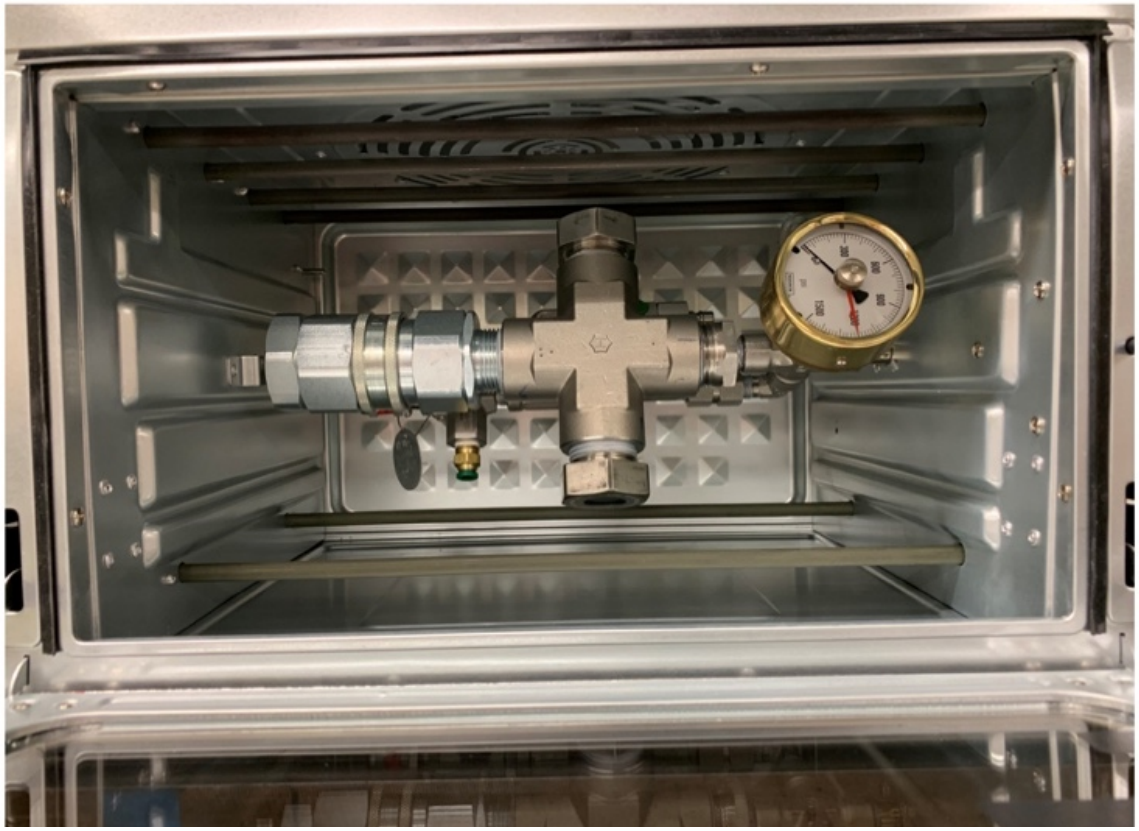

Figure 8: Fabric swatch test apparatus inside warming chamber with heating elements, convection fan, and rotisserie drive visible.

of virus-inoculated mask fabric swatches to demonstrate the microporous penetration capability of the proposed sterilization methodology. Moreover, we will ultimately need to demonstrate lethality against live COVID-19 virus, even if it is already implied by lethality against more robust bio-contaminant species. Such a compact SC-CO_2 processor must fit inside a standard bio-safety cabinet, and it also must meet all requirements for sterilizability. Evaluation of this compact SC-CO_2 processor in Sandia's existing BSL-2 laboratory was an immediate objective, but a 2nd SC-CO_2 processor was constructed in the event that access to live COVID-19 virus in an offsite BSL-3 facility could be arranged (working under the assumption that such an apparatus will be not returned once it enters a BSL-3 facility). Hereafter we will refer to these as the "fabric swatch test apparatus" and the "whole mask test apparatus".

Referring to Figure 8, the fabric swatch apparatus is a high-pressure cell that is filled with liquid carbon dioxide (CO_2) at room temperature, and then placed in a 37 C temperature-controlled chamber to affect the liquid-to-super-critical phase transition of CO_2. An operating temperature of 37 C was selected because it is above the supercritical temperature of carbon dioxide (31 C) and it ensures that mask materials will not experience temperature excursions in excess of what is normally encountered in the field. But, it's very likely that supercritical CO_2 processing at higher temperatures (e.g. 50 C) will prove to be permissible. This has important practical implications because as discussed later, accurate temperature control during vessel pressurization and depressurization presents some challenges.

The fabric swatch apparatus shown in Figure 8 also requires a CO_2 filling/venting apparatus. Early versions comprised a Size 1A CO_2 gas cylinder equipped with an internal syphon tube for dispensing liquid, and a custom-built gas handling system for dispensing of CO_2 liquid and venting of CO_2 gas. Later versions employed a much smaller 5 lb. CO_2 cylinder to allow the entire experimental apparatus to reside within the confines of a bio-safety cabinet.

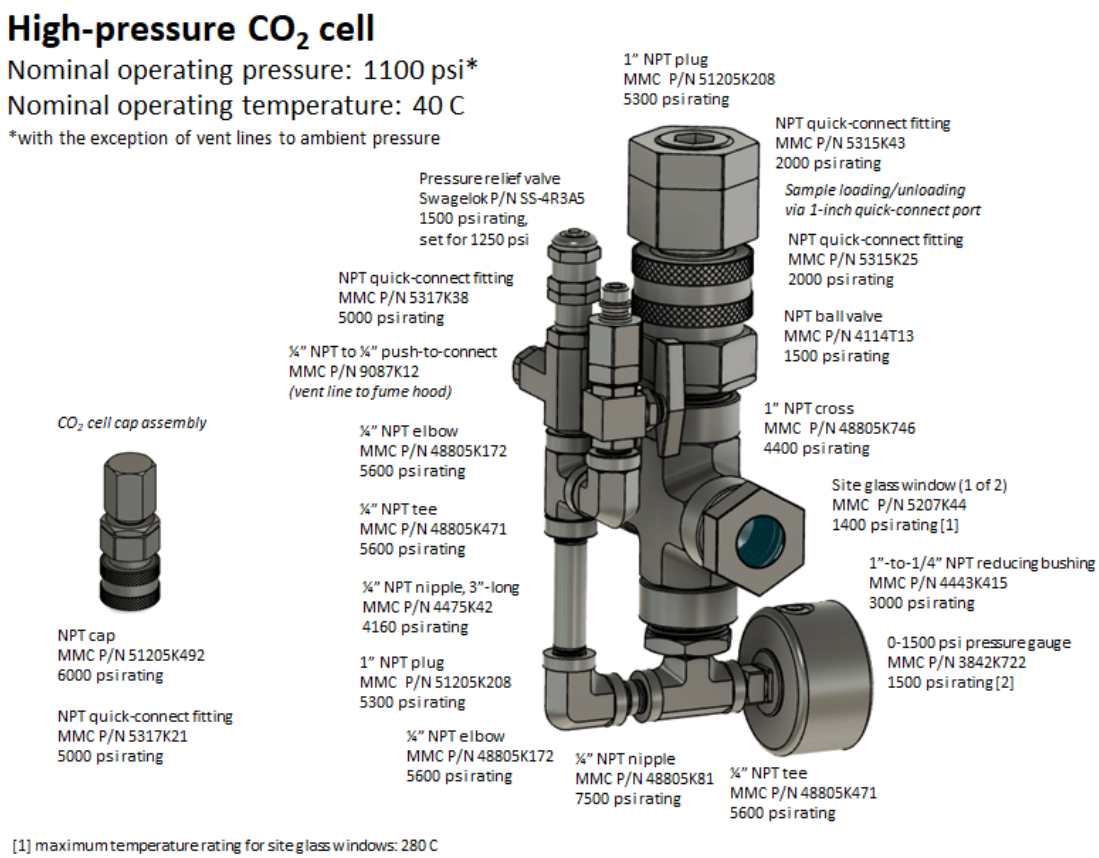

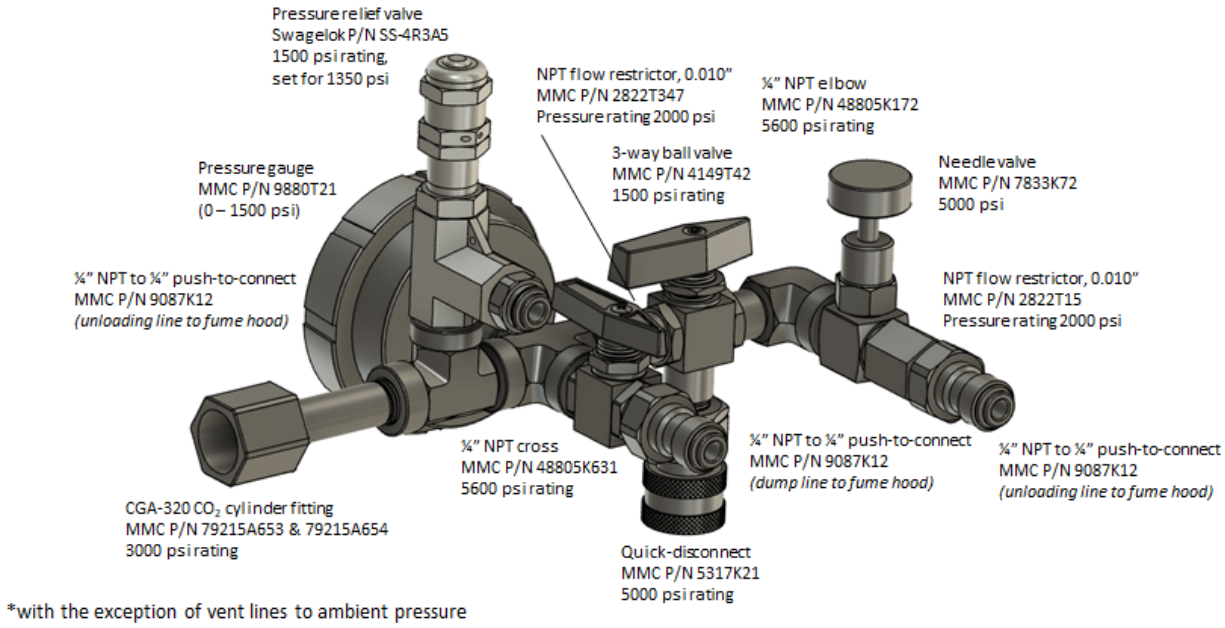

Figure 10: Design details of CO_2 loading/unloading apparatus

The high-pressure cell used for processing of fabric swatches is constructed entirely from commercial, off-the-shelf, pressure-rated, components procured from McMaster-Carr and Swagelok. There are no custom-made components used anywhere in high-pressure cell, or anywhere in the associated CO_2 filling/venting apparatus. The internal volume of the gas cell is 180 ml. A volume of approximately of 115 ml of liquified carbon dioxide added to the cell during the filling operation. The 4-port pressure cell is constructed from a 1-inch NPT cross. Port 1 is used for filling and venting of carbon dioxide. Ports 2 and 4 accommodate sight glass windows. This allows the level of CO_2 liquid to be determined by visual inspection, and visual confirmation of the liquid-to-super-critical phase transition once the high-pressure cell is placed in the warming chamber. Port 3 is used for sample loading and unloading. The system component with lowest pressure rating (1400 psig) is the site glass, McMaster-Carr P/N 5207K44. The pressure ratings of other components range from 1500 to 7500 psig, as documented in the figures below. Both the CO_2 filling/venting apparatus and the high-pressure cell have independent pressure gauges and pressure relief valves. Under normal operating conditions, after the sample (e.g. a 1 cm^2 swatch of N95 mask fabric) is loaded into the pressure cell, liquified CO_2 is added to the cell, and the pressure cell is placed in a warming chamber that is maintained at 37 C.

Operating procedure:

Loading of the CO_2 into the high pressure cell

1) Start with all valves in their closed/blocked positions.
2) Connect CGA 320 fitting to CO_2 cylinder equipped with syphon tube
3) Connect CO_2 gas cell to fill plumbing via quick-connect coupling.
4) Rotate 3-way valve gas delivery position.
5) Open ball valve on gas cell to permit filling.
6) Crack gas cylinder to begin filling cell.
7) Close ball valve on gas valve when desired liquid level is reached.
8) Close gas cylinder valve.
9) Rotate 3-way valve to venting position.
10) Crack needle valve to bleed off excess CO_2.
11) Disconnect CO_2 gas cell to fill plumbing via quick-connect coupling.
12) Rotate 3-way valve back to blocked position.
13) Install quick-connect cap to blank off gas cell fill port.

Unloading of CO_2 from the high pressure cell

14) Reconnect CO_2 gas cell to fill plumbing via quick-connect coupling.
15) Rotate 3-way valve to venting position.
16) Open ball valve on gas cell to permit venting.
17) Crack needle valve to slowly bleed off excess CO_2.
18) Rotate 3-way valve back to blocked position.

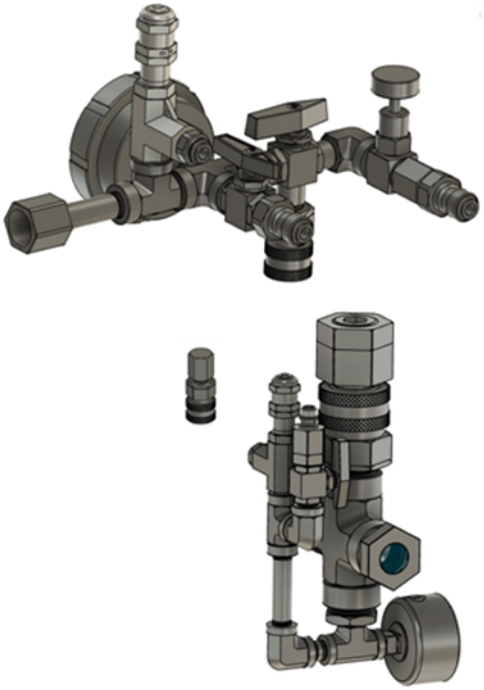

Figure 11: Operating procedure for loading/unloading CO_2 into fabric swatch test apparatus

The supercritical point for CO_2 is 31 C and 1080 psia. As noted earlier, we operate the cell at a temperature of 37 C and a pressure of 1200 psig to ensure that supercritical conditions are maintained throughout the duration of the disinfection cycle, which is nominally 1 hour. The warming chamber features a light to aid in visual detection of the liquid-to-super-critical phase transition, and both a circulating fan and a 3-rpm pressure cell rotisserie to promote isothermal conditions. Cell rotation is also desirable from the standpoint of mixing candidate biocidal agents. To ensure compatibility with candidate biocidal agents, all pressure cell components are stainless steel, with the exception of the sight glass windows which are borosilicate glass.

Figure 12: Anatomy of a siphon-tube CO_2 gas cylinder

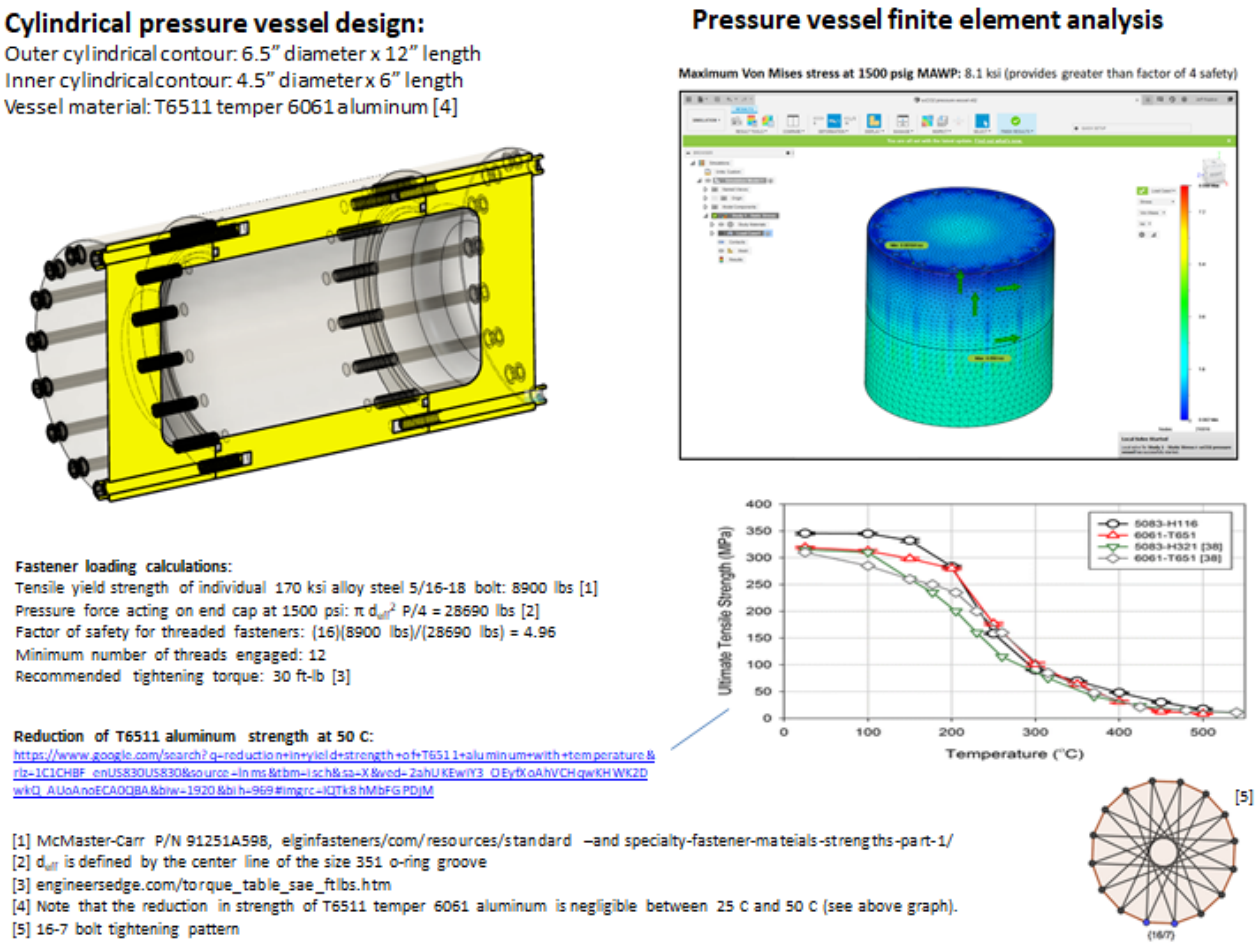

Figure 7: Summary of pressure vessel design for whole mask apparatus

The system component with the lowest maximum temperature rating (60 C) is the pressure gauge of the pressure cell (McMaster-Carr P/N 3842K722). The warming chamber employs a 35 W resistive heater that is powered by a fixed voltage (36 VDC) power supply. This low-power, voltage-limited, resistive heater is incapable of raising the oven temperature more than 15 C above ambient temperature. The use of an intrinsically power-limited heating element prevents the possibility of overheating due to user error or controller malfunction. Protection from overheating in the unlikely event of an ac/dc converter overvoltage malfunction is provided by 400 mA cartridge fuse at the line voltage input of the dc power supply. If somehow overheating were to occur, the pressure relief valve of the pressure cell would gradually vent CO_2 into the warming chamber, which is a vented enclosure that resides inside the bio safety cabinet. Implementation of redundant engineering controls to prevent over-pressurization by over overheating was deemed prudent in the unlikely event that the pressure relief valve malfunctions. The lack of temperature adjustment on the warming chamber also prevents a potential source of operator error.

Figure 4: Thick-walled aluminum pressure vessel constructed for whole mask testing.

Maximum Von Mises stress at 1500 psig MAWP: 8.1 ksi (provides greater than factor of 4 safety)

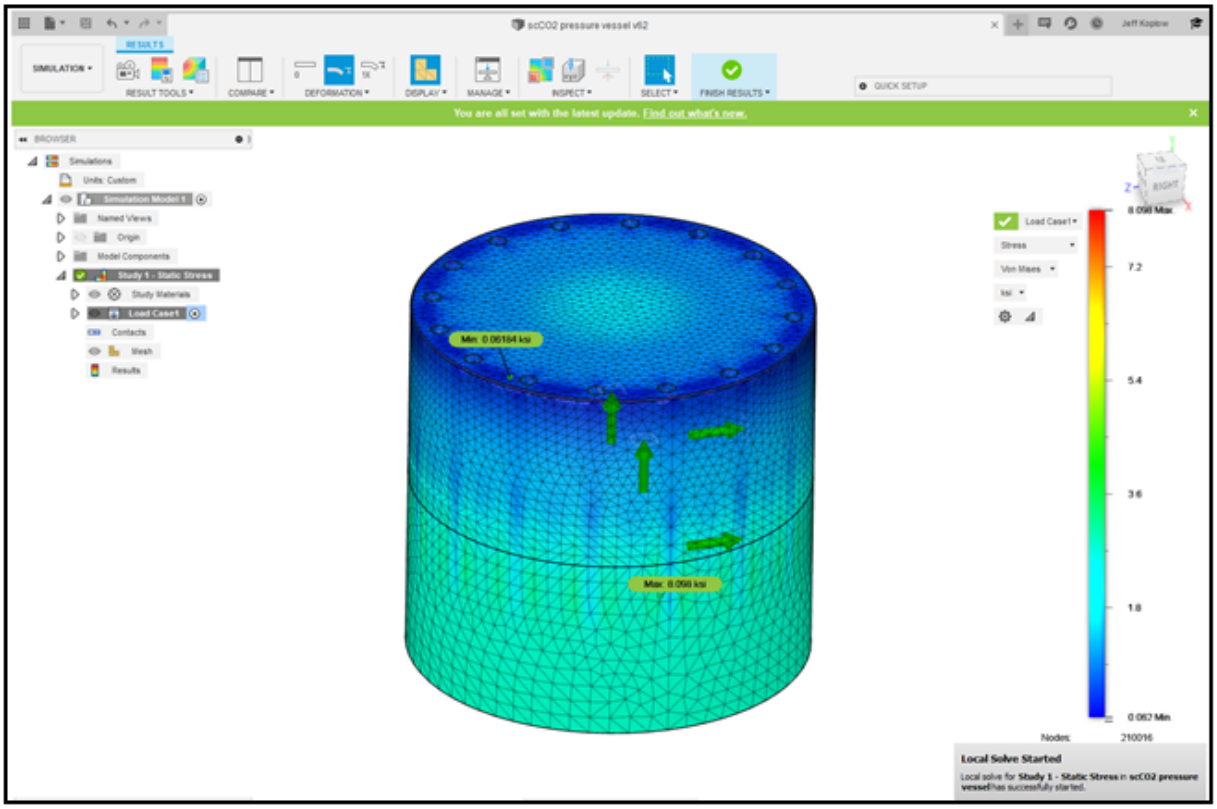

Figure 15: Finite element mechanical stress analysis of whole mask apparatus pressure vessel

Development of the whole mask test apparatus required construction of a much larger pressure vessel. Referring now to the cylindrical pressure vessel illustrated in Figures 13, 14, and 15, an internal diameter of 4.5” was required to allow 1860 masks to be loaded into the chamber with minimal folding or bending. The internal length of the cylindrical pressure vessel is 9.0”. This is large enough to allow eight 1860 masks to be treated at one time. The whole mask pressure vessel is constructed from T5611 temper alloy 6061 aluminum having a minimum wall thickness of 1.0”. The chamber comprises a central cylindrical tube and two end caps, each of which is sealed by EPDM o-rings and mechanically secured be a circular array of sixteen, size 5/16”-18 high-strength steel alloy bolts. Both the pressure vessel and bolts arrays used to construct this apparatus are engineered to have a factor of safety of approximately 5. Finite element analysis was used to calculate the stress field in the chamber walls and minimum factor of safety. This custom-built vessel was then hydrostatically tested at 2300 psi for 5 minutes prior to commissioning.

A.2.9. development of experimental protocols

We initially provided team member Oscar Negrete with samples of 8210 N95 masks that could be diced into samples and inoculated with the surrogate virus. Although the same anti-viral test protocol was eventually be applied to 3M 1860 masks, for initial testing we opted to conserve our very limited supply of 1860 masks for the time being. The 8210 N95 masks are however very similar in construction.

Figure 16: 8210 mask material used in early tests

Small swatches of N95 mask material were cut into 1 cm^2 squares and surface contaminated on the exterior with vesicular stomatitis virus (VSV), Indiana serotype strain. 10 μl of the virus suspension was used which equates to a starting concentration of 10^6 plaque forming units (pfu). Following one hour of air drying in a biosafety cabinet, one of test swatches was placed inside the super critical CO_2 chamber and the other in a petri dish as a control for the involvement of temperature and time in VSV decay.

Following application of supercritical CO_2 processing, virus was eluted from the mask material by soaking the mask square in 1 ml of virus culture medium. After 10 minutes of soaking, the liquid was centrifuged at 300 g for 2 minutes to concentrate the media at the bottom of the tube. 1 ml of media was also used to rinse the tubing used for the CO_2 gas vent line through which CO2 is released at the conclusion of the one-hour treatment cycle. A series of 10-fold dilutions were used to measure virus viability using a standard plaque assay on Vero cells. 48 hours after infection, plaques were counted and viral titers were calculated.

Prior to running the experiment with live surrogate virus, the team conducted two dry run experiments under the observation of bio-safety officer Natalie Jouravel and pressure-safety officer George Buffleben. The sequence of movements and operations performed by the team was carefully scrutinized to detect any potential opportunity for inadvertent release of surrogate virus. It was determined that the series of sample insertion, gas filling, gas venting, etc. operations required to perform the experiment precludes the possibility of virus release, is fully consistent with all pressure safety requirements, and that slowly vented CO_2 gas does not disturb the laminar flow field inside the bio safety cabinet.

The experimental first dry run did however reveal that the pressure relief valves used on the supercritical CO_2 fabric swatch cell were unreliable for this application. Upon actuation, the cooling effect of super-critical CO_2 flash evaporating to CO_2 gas caused enough localized cooling to prevent proper resealing of the o-ring inside the pressure relief valve. For this reason, we replaced our original pressure release valves (Swagelok P/N SS-4A3R5) with Circle Seal P/N 5180B-2MP-1400 pressure relief valves rated for operation down to a temperature of -100F. This solved the pressure relief valve malfunction.

A.2.10. Experimental Results

To evaluate the question of whether the construction materials of the N95 are altered or harmed in any way during supercritical CO_2 processing, early in this project we consulted with polymer chemist LeRoy Whinnery to compile a list required test criteria.

1) Pressure/flow-rate curve for air flow through N95 mask.
2) Glass transition temperature measurement of the fibrous polymeric material (melt-blown, non-woven, polypropylene fiber) used to construct the mask via differential scanning calorimetry.
3) Measurement of compression set and durometer hardness for elastomeric components.
4) Microscopy of cross-sectioned material samples to discern changes in polymeric fiber morphology.
5) Determination of the effect of supercritical CO_2 exposure to the electrostatic filtering properties of the mask.

Shortly thereafter, NIOSH, the government agency responsible for certification of respirator masks and other occupational safety equipment stood up a mask testing program. Under this new NIOSH program, research institutions working on candidate N95 sterilization techniques can send treated masks to NIOSH to verify that they still function properly. The battery of tests established by NIOSH and the specialized equipment on which such tests are run are exactly those used to certify N95 masks made by various manufactures before they can be placed on the market. To obtain adequate statistics, NIOSH requires participating institutions to submit 20 masks, 15 of which are given the proposed sterilization treatment, and 5 of which are used as control samples. These tests cover all aspects of mask performance such as pressure/flow characteristics, particle filtration efficiency, and questions surrounding proper fitting of masks to standardized mannequin test fixtures.

It will be recalled that the custom-built pressure chamber for whole mask testing was constructed with an internal diameter of 4.5” and an internal length of 9.0”. This is large enough to allow eight 1860 masks nested on inside another to be treated at one time. The set of fifteen 3M 1860 masks was processed in two batches, each subjected to the same cleaning protocol. In each cycle, the CO_2 pressure was gradually ramped to 1200 psi over a period of 15

minutes, maintained at 1200 psi (at a temperature of 37 C) for 60 minutes, and then ramped down to atmospheric pressure over a period of 15 minutes. This cleaning cycle was repeated 10 times to simulate the effect of multiple reuse. The ability to process multiple masks at one time helped reduce time and labor, but for follow on work we strongly recommend automation of the above cycle including closed loop pressure and temperature control. Conducting these operations manually was tedious and very time consuming.

Before the above batch processing of masks was executed, we conducted a variety of one-mask/one-cycle experiments to check for the following potential problems.

1) Warpage or deformation
2) Loss of mechanical strength
3) Loss of mechanical flexibility (e.g. due to fabric dehydration)
4) Chemical incompatibility with SC-CO_2 (e.g. the adhesive used to secure the foam nose cushion strip)
5) Damage to the elastomeric band used to hold the firmly mask in place

The results of such a test are shown in “before and after” figure below. The 1860 mask did not suffer from any of the above five problems. Although the CO_2 cleaning process did cause fading of its stenciled label on the 1860 mask, treated and untreated 1860 masks were otherwise indistinguishable.

Figure 17: Before and after photos of a 3M type 1860 N95 mask subjected to one 60-minute supercritical CO_2 treatment cycle.

Figure 18: Triplicate viral assays indicate that super-critical carbon dioxide alone does not exhibit biocidal activity against the VSV surrogate virus. This suggests that a biocidal additive such as peracetic acid will be required for N95 mask sterilization.

We also verified that a black sharpie marker could be used for colorfast labelling of the masks, and we tested a variety of RFID tags to demonstrate their compatibility with supercritical CO_2 cleaning. The ability to return masks to their original owners is important from the standpoint of successfully encouraging reuse.

Evaluation of Decontaminated N95 Respirators

NPPTL
National Personal Protective Technology Laboratory

Organization: Sandia National Laboratories

Date Tested: 7/15/2020 – 7/16/2020

Respirator Model(s): 3M 1860

Tests: Filtration with NaCl (modified version of STP-0059), Manikin Fit Factor with Static Advanced Headform, and Strap Integrity with Tensile Testing

Decontamination Method: New, never-used FFRs are treated with liquid-to-vapor supercritical CO_2 at a temperature of 37°C and a pressure of 1100 psig for 1 hour

Decontamination Cycles: 10 cycles

While decontamination and reuse of FFRs are not consistent with standard and approved usage, these options may need to be considered when FFR shortages exist. This assessment was developed to quantify the filtration efficiency and manikin fit factor[1] of an N95 respirator that has been decontaminated. This assessment is not to determine the effectiveness of the decontamination procedure at killing pathogenic microorganisms. The results provided in this report are specific to the subset of samples that were provided to NPPTL for evaluation. These results may be used to update the CDC guidance for Crisis Capacity Strategies (during known shortages).

20 respirators that were unworn and not subjected to any pathogenic microorganisms were submitted for evaluation. This included 15 respirators that were subjected to 10 cycles of the supercritical CO_2 decontamination process and an additional 5 respirators that served as controls. Figure 1 photos document the procedures used. Photos of the samples and information received are shown in Figures 2 and 3. The samples were tested using a modified version of the NIOSH Standard Test Procedure (STP) TEB-APR-STP-0059 to determine particulate filtration efficiency. The TSI, Inc. model 8130 using sodium chloride aerosol was used for the filtration evaluation. For the laboratory fit evaluation, a static manikin headform was used to quantify changes in manikin fit factor. The TSI, Inc. PortaCount® PRO+ 8038 in "N95 Enabled" mode was used for this evaluation. Additionally, tensile strength testing of the straps was performed to determine changes in strap integrity. The Instron® 5943 Tensile Tester was used for this evaluation. The full assessment plan can be found here.

Filtration Efficiency Results: None of the treated respirators measured more than 95%. See Table 1.

Manikin Fit Factor Results: The manikin fit factor showed passing fit factors (greater than 100) for 4 of the 5 respirators evaluated. See Table 2.

Strap Integrity Results: No visual degradation of the straps was observed. The top strap showed a less than 1.00% decrease in recorded force and the bottom strap showed a 2.18% increase in force. See Table 3.

Other notes: The respirator information on the front of the mask was discolored (turned from black to white). The inner surface of the respirators was tinted green in some places. See Figure 1.

Figure 19: Summary documentation for NIOSH tests conducted on fifteen SC-CO_2 treated 3M 1860 N95 masks and five control samples.

Figure 20: Left-hand panel: SC-CO_2 treated masks affixed to planar flange for flow resistance measurements. Center panel: SC-CO_2 treated masks tested for proper fit under standardized pressure/flow conditions. Right-hand panel: Discoloration resulting from transfer of dye from an adjacent mask during immersion in SC-CO_2. The use of a SC-CO_2 colorfast dye would be desirable to prevent such staining, because aesthetics has a bearing on the willingness of health care workers to reuse masks.

Referring now to Figure 18, test results from the virology laboratory indicate that SC-CO2 alone does not exhibit biocidal activity with respect to the with vesicular stomatitis virus (VSV) Indiana serotype strain surrogate virus. This is an indication that a biocidal agent such as peracetic acid will most likely be required. Lack of access to a BSL-3 facility precluded the same experiment with live corona virus, however.

The results of the standardized NIOSH mask tests are presented in Figures 19-23. The "Manikin Fit Factor" test data shown in Figure 21 collected suggest that:

(a) 10 cycles of SC-CO_2 treatment will likely not compromise mask fit in the intended application, but

(b) bending of the N95 masks to accommodate the small size of our SC-CO_2 test chamber measurably chamber degraded the fit factor of the masks.

Indeed it was apparent upon removal from the chamber that the mask fabric had taken a set to the bent geometry, and in particular that the bottom most mask in the stack of 8 masks (experiment #1) and 7 masks (experiment #2) was deformed more severely (splayed out) than the masks located above it. We suspect this accounts for sample 15 having an anomalously low fit factor, because samples 8 and 15 were the bottom-most masks in the experimental runs 1

and 2 respectively. Moreover, no such deformation was observed when a single N95 masks was processed in the chamber, presumably because the mask didn't need to be subjected to significant bending to make it fit within the chamber.

Table 2. Manikin Fit Evaluation

Manikin Fit Factor of Decontaminated N95s					
Respirator Model, Decon Method, # of cycles	**Treated Sample #**	**mFF Normal Breathing 1**	**mFF Deep Breathing**	**mFF Normal Breathing 2**	**Overall Manikin Fit Factor**
3M 1860, Supercritical CO2, 10 Cycles Static Advanced Medium Headform (Hanson Robotics)	**11**	173	56	165	101
	12	200+	77	180	127
	13	191	56	152	102
	14	200+	70	163	118
	15	70	43	55	**54**
	Control 4	200+	200+	200+	200+
	Control 5	200+	200+	200+	200+

Notes:

- Per OSHA 1910.134(f)(7), if the fit factor as determined through an OSHA-accepted quantitative fit testing protocol is equal to or greater than 100 for tight-fitting half facepieces, then the fit test has been passed for that respirator.
- This assessment does not include fit testing of people and only uses two exercises (normal and deep breathing) on a manikin headform.
- This assessment is a laboratory evaluation using a manikin headform and varies greatly from the OSHA individual fit test. This headform testing only includes normal breathing and deep breathing on a stationary (non-moving) headform; therefore, fit results from this assessment cannot be directly translated to using the standard OSHA-accepted test. Instead, this testing provides an indication of the change in fit performance (if any) associated with the decontamination of respirators.
- **BOLD** overall manikin fit factors < 100.

Figure 21: The "Manikin Fit Factor" test data collected strongly suggest that 10 cycles of SC-CO_2 treatment will not compromise mask fit. The small size of our SC-CO_2 test chamber forced us to bend the masks to some degree, and it was apparent that the mask fabric took a set to this bent geometry over time. This likely accounts for sample 15 having a low fit factor. In an actual SC-CO_2 washing machine, there would be no need to bend/compress the masks to fit them into the pressure chamber.

The remainder of the mask fit data is consistent with this interpretation as well. The mask fit scores for samples 11, 12, 13, and 14 were 101, 127, 102, and 118 respectively. When referenced to the control samples (4 and 5), this data is consistent with the adverse effect of mask bending, but less dramatic than sample 15 which had a fit score of only 54.

In aggregate these data suggest (but do not prove) that ten successive treatments in SC-CO_2 will not impair mask fit if a suitably sized chamber that does not subject the mask to mechanical

deformation is used. In addition, the data shown in Figure 22 strongly indicate that ten successive one-hour cycles of supercritical carbon dioxide do not adversely effect on elastomeric strap integrity.

At first glance, the data on mask filtration efficiency (Figure 23) looks problematic because the measured filtration efficiency had a mean value of 81% with a standard deviation of 7%. This is well below the 95% threshold for a properly functioning N95 mask. If this is due to de-poling of the electrostatically poled fibers in the mask material, and/or microscopic changes in fabric morphology, super-critical carbon dioxide cannot be used in this application.

Table 3. Strap Integrity Evaluation

Tensile Force in Respirator Straps of Decontaminated N95s (recorded force values are at 150% strain)			
Respirator Model, Decon Method, # of cycles	**Straps from Treated Sample #**	**Force in Top Strap (N)**	**Force in Bottom Strap (N)**
3M 1860, Supercritical CO2, 10 Cycles	**1**	2.676	3.020
	2	2.696	2.947
	3	2.751	2.903
	Decontaminated Strap Average	2.708	2.957
	Control 1	2.670	2.850
	Control 2	2.794	2.937
	Control Strap Average	2.732	2.894
	% Change ((Deconned - Controls) / Controls)	-0.88%	2.18%

Figure 8: 10X SC-CO_2 treatment of the 3M 1860 N95 masks caused no significant degradation of the elastomeric strap used to achieve proper fit.

But further inspection of the numerical data indicates that reductions in filtration efficiency are entirely attributable to leakage around the edges of the mask, and that this is true for all 10 ten mask samples; filtration efficiency percentage is equal to 100 percent minus maximum leakage percent in all table entries. This indicates that if SC-CO_2 treatment adversely effects fabric microstructure, the magnitude of the effect is insignificant.

It is regrettable that the very limited time and budget of this project precluded the construction of a larger chamber. But it is also fair to say that had we known how important the avoidance of mask bending effects would be to unambiguous test results, we would have diverted more resources towards chamber fabrication. Accordingly, we strongly recommend that the above testing of SC-CO_2 treatment in conjunction with NIOSH be repeated without the confounding variable of mask deformation. We further recommend that the loading/unloading of SC-CO_2 into the treatment chamber be automated to reduce labor and to ensure that conditions for

formation of the liquid CO_2 phase is avoided. According to thermocouple data, the difficulty of controlling upward and downward temperature excursions during pressurization and depressurization via manual valves likely resulted in frequent instances of liquid CO_2 formation. In this regard the tests performed were harsher than conditions encountered in a commercial SC-CO_2 washing machine.

Finally, in a separate set of experiments, the SC-CO_2 whole mask test chamber was used to evaluate the effect of SC-CO_2 exposure on various components used in hospital ventilator machines. In particular, there is interest in exploiting the gas-like volumetric-space-filling property of SC-CO_2 to sterilize long lengths of corrugated ventilator tubing. Much like N95 masks, such tubing was originally intended to be disposable. It was therefore not designed to survive thermal sterilization protocols such as autoclaving. The use of liquid sterilization agents is problematic because the extreme aspect ratio and highly corrugated shape of the tubing makes it difficult to ensure that all internal surfaces are fully wetted and fully rinsed. With the assistance of David Chandler, we obtained a complete set of what are normally considered one-time use ventilator components from Stanford University Hospital.

Table 1. Filter Efficiency Evaluation

Respirator Model, Decon Method, # of cycles	Treated Sample #	Flow Rate (Lpm)	Initial Filter Resistance (mmH_2O)	Initial Percent Leakage (%)	Maximum Percent Leakage (%)	Filter Efficiency (%)
3M 1860, Supercritical CO_2, 10 Cycles Min Fil Eff: 66.90% Max Fil Eff: 89.80%	**1**	85	7.2	11.9	15.5	**84.50**
	2	85	7.5	11.0	13.8	**86.20**
	3	85	8.4	9.59	12.0	**88.00**
	4	85	7.7	8.43	10.2	**89.80**
	5	85	7.5	16.0	23.6	**76.40**
	6	85	7.5	13.7	16.9	**83.10**
	7	85	7.4	11.7	14.5	**85.50**
	8	85	7.0	23.7	27.4	**72.60**
	9	85	7.5	28.6	33.1	**66.90**
	10	85	7.9	17.8	21.8	**78.20**
	Control 1	85	8.0	0.503	0.953	99.05
	Control 2	85	7.4	0.640	1.69	98.31
	Control 3	85	8.6	0.442	0.788	99.21

Notes:

- The test method utilized in this assessment is not the NIOSH standard test procedure that is used for certification of respirators. Respirators assessed to this modified test plan do not necessarily meet the requirements of STP-0059, and therefore cannot be considered equivalent to N95 respirators that were tested to STP-0059.
- **BOLD** filter efficiencies < 95%.

Figure 23: Inspection of the above numerical data for mask filtration efficiency indicates that reductions in filtration efficiency observed for SC-CO_2 treated masks are entirely attributable to leakage around the edges of the mask, and that this is true for all 10 ten mask samples. This strongly implies that if SC-CO_2 treatment adversely effects fabric microstructure, the magnitude of the effect is insignificant.

Referring now to Figure 24, this includes tubing, connectors, valves, and sensors.
The corrugated blue tubing along with its non-removable fittings did not exhibit any change or degradation during extended exposure to SC-CO_2. It was initially feared that leaching of SC-CO_2-soluable plasticizers might cause the corrugated flexible tubing to become brittle. But there was in fact no discernible change in the appearance, feel, or flexibility of the tubing after SC-CO_2 treatment. The PPE garment material did not exhibit any change or degradation either.

The only incompatibility observed was swelling/blistering of an elastomeric seal material used in component #1 of Figure 24. It is well known that the non-polar solvent properties of SC-CO_2

allow it infiltrate certain elastomers. An extreme example is Buna N rubber, which exhibits volumetric swelling greater than 50% after 1 hour of exposure to SC-CO_2 at 1200 psig when subsequently returned to atmospheric pressure. After a few days, the Buna N sample returns to its original size as CO_2 gradually escapes the elastomeric matrix. A subset of the elastomers vulnerable to SC-CO_2 infiltration will exhibit blistering if depressurization is not carried out very slowly. There are, however, other inexpensive engineering polymers that do not exhibit any of the above effects. For example, EPDM rubber o-rings swell by only 2 to 3% and are not vulnerable to blistering. Neoprene rubber is even better, swelling less than 1% and immune to blistering effects. This implies that substitution of neoprene rubber for elastomeric seals would render all ventilator components suitable for SC-CO_2 sterilization.

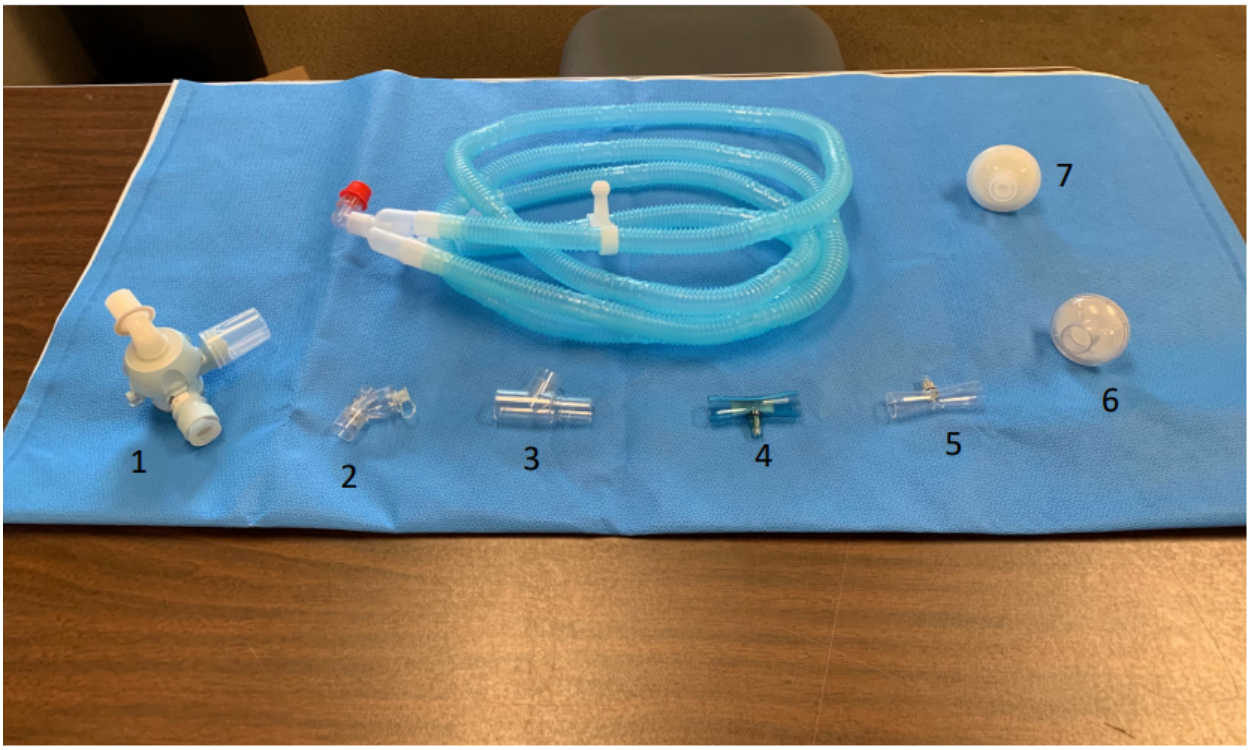

Figure 24: One-time use ventilator components laid out on top of a one-time use PPE garment, all of which were subjected to SC-CO_2 treatment.

A.2.11. Follow on work and real-world deployment

There are several objectives that were beyond the scope of our $54k project budget, even though numerous Sandians generously donated their time and subject matter expertise to help this project achieve its goals. If follow-on funding can be obtained, we recommend that the following work be prioritized.

1) Construction of larger SC-CO_2 pressure vessel will enable the NIOSH tests to be repeated without the confounding variable of mask bending. This will allow us to measure even a small reduction in mask filtration efficiency due to alteration of the fabric microstructure due to exposure to SC-CO_2 (if there is any). This larger pressure vessel should accommodate fifteen 3M 1860 N95 masks without any bending or compression of the mask material. It also be equipped with automated proportional valves that allow the addition and removal of CO_2 from the pressure vessel in a prescribed manner that does not result in uncontrolled temperature excursions.
2) Viral assay of mask fabric swatches contaminated with a non-pathogenic, BSL-2, surrogate virus, subject to the SC-CO_2 + peracetic acid protocol described by White[7] should be undertaken to demonstrate the micro-penetration capabilities of super-critical carbon dioxide when used as a vehicle to deliver peracetic acid.
3) An analogous experiment in a BSL-3 facility with live Corona virus would be desirable as well to directly demonstrate sterilization efficacy against COVID-19.

The remaining challenges pertain to real world deployment. As discussed earlier, there is existing infrastructure in the dry-cleaning industry that is presumably well suited to this application. But it also must be understood that:

a) The dry-cleaning industry is still in the process of transitioning from perchloroethylene to supercritical carbon dioxide. The ROI period for switching to eco-friendly supercritical carbon dioxide dry cleaning equipment is 2 to 4 years. As a result, in the dry-cleaning industry there are early adopters, those awaiting the results of early adaption, and hold outs that will continue using perchloroethylene for the foreseeable future.
b) Even if it could be proven that the dry-cleaning industry could safely handle some of the burden of N95 mask sterilization, public perception, concerns about potential liability, and politics would likely preclude this deployment scenario.

Accordingly, we envision working with the manufacturers of such SC-CO_2 dry cleaning equipment towards deployment dedicated machines for sterilization applications in the health care industry. The European Union has been far more aggressive than the U.S. in pushing towards environmentally friendly industrial processes. The EU may therefore be a good place to look for candidate vendors. See for example the campaign launched by international compressed gas distributor Linde:

https://americandrycleaner.com/articles/linde-launches-co2-brand-throughout-europe

We would also propose to conduct a technoeconomic analysis of the proposed N95 mask reuse technology. But at the outset, it should be understood that constructing a super-critical CO_2 cleaning apparatus is fairly simple. We just built a small unit in the span of a few days using off-the-shelf components and without a great deal of prior experience. To build a large capacity

machine, the most difficult item to get a hold of is the large steel pressure vessel (picture something the size of a large hot water heater). But there are companies who make such vessels for a wide variety of purposes, and the balance of other fabrication work relies on commonly available COTS parts and is fairly generic in nature.

The following two videos illustrate how quickly and cost effectively such a high-strength steel pressure vessel can be fabricated by industry. The following video is from Spuncast Inc. of Watertown, WI:

Spin casting thick-walled steel pipe: https://www.youtube.com/watch?v=OmApwBP2m4c

And here is a video from MJC engineering of Huntington Beach, CA that illustrate how end caps would be incorporated into such a spun cast steel pipe:

Forming of pressure vessel end caps: https://www.youtube.com/watch?v=DTJ_n6_4xwA

It will also be understood that spin-casting can be adopted to the fabrication of thick-walled steel pressure vessels with integral flanges, such as that required for the pressure vessel door.

Such a techno-economic study would also examine the cost savings associated with procurement of several hundred identical SC-CO_2 washing machines, whereas such machines are typically purchased individually by dry cleaning operations.

A.2.12. References

https://www.massdevice.com/u-s-defense-department-using-defense-production-act-to-boost-n95-masks-supply/;
https://www.beckershospitalreview.com/workforce/california-nurses-get-their-n95-masks-after-suspensions-spark-protest.html

[2] https://www.youtube.com/channel/UCG05UXgAI7mtRT_pN9TdSzg

[3] https://www.upi.com/Defense-News/2020/04/14/Battelle-awarded-415M-to-decontaminate-N95-masks-for-reuse/8881586885037/

[4] http://coolclean.com/2015/02/11/co2-cleaning-is-changing-the-garment-cleaning-industry/; https://www.greenapplecleaners.com/?co2

[5] "Solubility of Water in Super Critical Carbon Dioxide", A. N. Sabirzyanov, A,P. Il'in, A. R. Akhunov, and . M. Gumerov, *Thermophysical Properties of Materials*, Vol. 40, No. 2, pp. 231-234 (2002).

[6] See for example: https://www.tasteofscience.com/articles/1275/drying-with-supercritical-co2.html

[7] Effective terminal sterilization using supercritical carbon dioxide, A. White, D. Burns, T.Christensen, Journal of Biotechnology, Volume 123, Issue 4, 10 June 2006, Pages 504-515

A.3. Covid-19 LDRD: Extended Use of Face Masks, Thermal Disinfection and Spray-on Surface Active Layer

Mathew Celina

A.3.1. Objectives:

- Short thermal conditioning above 70°C has been reported to kill the Sars-CoV-2 virus (thermal disinfection). Does thermal exposure have noticeable consequences on mask materials and their filter performance? Could thermal treatment be a simple and viable alternative to gamma irradiation, UV illumination, or hydrogen peroxide exposure?
- For situations where no other options exist, could simple spray-on solutions containing easily available and low risk (non-toxic) disinfectants be prepared and applied to masks surfaces for 'refreshing' and extended wear, similar to a hand sanitizer?

A.3.2. Activities:

- Acquired multiple commercial mask types from PHS and UNMH in ABQ.
- Thermal conditioning at 65, 80 and 95C for 24 h with assessments for obvious shrinkage or unexpected material responses, and any aging of elastic straps.
- Preparation of simple non-toxic disinfectant solutions and application on mask surfaces via small hand held spray bottles. Visualization of disinfectant deposits via red dye.
- Use of surface infrared spectroscopy to assess micron layer residue of active ingredient and its surface retention at 25 and 37°C. Compounds evaluated included nonionic and anionic surfactants, benzalkonium chloride, chlorhexidine digluconate, anti-viral essential oil, citric acid or commercial cleaners (Pine-Sol), and comparison with commercial Lysol spray. Benzalkonium chloride is a common anti-microbial substance still on the FDA list for hand sanitizers and also used in commercial disinfectant sprays.
- Collaboration with the aerosol characterization team (6633/6775) to assess ongoing filtration performance after thermal conditioning and of masks with surface disinfectant deposits.
- Collaboration with bio-assay team (6633) for related efforts to assess the disinfectant properties on MS2 viral simulant of 3% Pine-Sol as surfactant and 0.3% benzalkonium chloride in water.

A.3.3. Results:

- Only minor mask specific material weaknesses were observed. Some warping or adhesion issue observed for one mask type. Most masks are able to handle thermal exposure for 24 h at 80-95°C, meaning they could be exposed multiple short times.
- Thermal conditioning of up to 24 h at 80 and 95°C, as well as gentle deposition of a spray-on solution containing isopropanol-water-surfactant-disinfectant on mask surfaces did NOT result in noticeable loss of filtration performance. Added disinfectant should offer longer lasting anti-viral properties than given by momentary disinfection offered by alcohol contact.

- In related efforts for general cleaning/disinfection, anti-viral efficacy of simple Pine-Sol/benzalkonium chloride in water was confirmed for MS2 viral simulant (work by 6633).

A.3.4. Spin-off:

Design of basic anti-viral disinfectant solution and their spray-on surface behavior allowed us to recommend a basic water-based custom disinfectant/cleaner solution for SNL purposes.

A.3.5. Publication:

Results published as journal paper in **"Polymer Degradation and Stability 179 (2020) 109251" Extended Use of Face Masks During the COVID-19 Pandemic - Thermal Conditioning and Spray-on Surface Disinfection** by Mathew Celina, Estevan Martinez, Andres Sanchez, Michael Omana, Dora Wiemann, Matthew Tezak, Tim R. Dargaville (Health and Biomedical Innovation, QUT, Australia)

A.4. Deactivation of SARS-CoV-2 by Boronic Acid-Functionalized Polymer

Brad H. Jones, George D. Bachand, Brooke N. Harmon, Philip R. Miller, James B. Ricken, Maxwell Stefan

A.4.1. Abstract

Boronic acid-modified polymers (BAMPs) can interact with glycoproteins and other glycosylated compounds through covalent binding of the boronic acid moieties to saccharide residues. As a first step toward evaluating the utility of BAMPs as SARS-CoV-2 antiviral agents, this COVID-19 rapid response LDRD was intended to examine the effect of BAMPs on SARS-CoV-2 spike glycoprotein and its subsequent binding with ACE2 receptor protein. Multiple different approaches were attempted in order to determine whether BAMPs based on poly(ethylene glycol) and poly(ethylenimine) bind the spike protein, but failed to produce a definitive answer. However, two different enzyme-linked immunosorbent assays clearly showed no discernable effect of boronic acid in inhibiting spike-ACE2 binding.

A.4.2. Summary of Approach and Results

Boronic acids (BAs) are mild Lewis acids with unique utility in biological applications due to their ability to reversibly bind to molecules possessing 1,2-diol functionalities, of which all saccharides and many related compounds constitute an important subset.[1-10] The covalent equilibrium between free BA and 1,2-diol versus the corresponding bound species – a cyclic boronate ester – is shown in Figure 1. The equilibrium constant K depends on the choice of BA and diol, as well as the pH.[11,12] In general, the boronate ester is favored at high pH, while the free, unbound species are favored at low pH. The pH over which this reversibility occurs is a complex function of several factors, but can be tuned over a broad range including physiological pH.

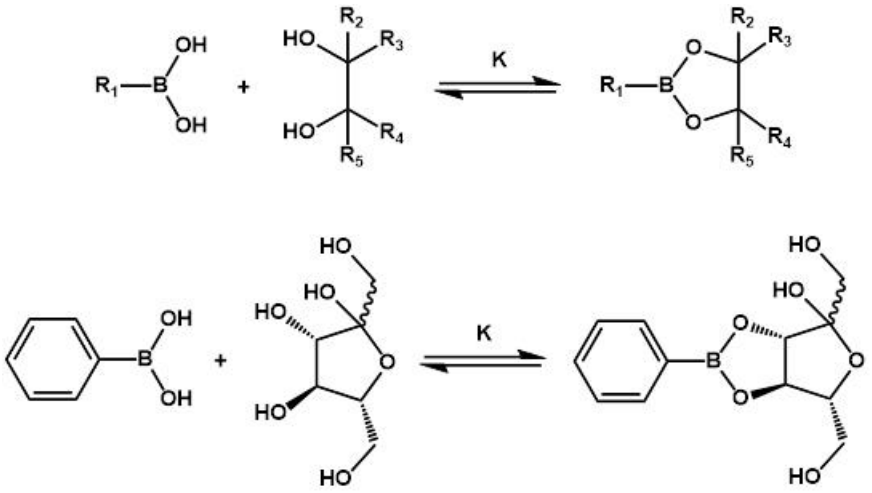

Figure 1. Reversible binding of 1,2-diols, including saccharides, to BAs. The top scheme shows a general equilibrium between the bound and unbound forms of arbitrary BAs and 1,2-diols. The bottom scheme shows this specific equilibrium for phenylboronic acid and fructose. Note that the BAs and boronate esters can exist in both trigonal and tetrahedral forms (uncharged and charged, respectively), but only the former are shown.

We, and others, have shown that BA-modified polymers (BAMPs) can be used to capture and aggregate cells via BA binding with saccharide residues of glycoproteins residing within the cell membrane.[13-16] More recently, we have shown that the BAMPs can be utilized as functional adhesives, for example, to bind articles to saccharide-rich materials such as cellulose paper or plant leaves.[17] At the advent of the infection process, enveloped viruses such as SARS-CoV-2 bind to host cells (*e.g.*, respiratory epithelial cells) via a transmembrane spike protein rich in glycans (polysaccharides).[18,19] Conformational changes in the S1 and S2 subunits of the spike protein are necessary for successful binding with the host receptor and viral uptake, making this protein an ideal target for rapid viral inactivation.[20] We hypothesized that BAMPs could effectively crosslink or otherwise bind the spike protein via its saccharide residues, inhibiting the intrinsic subunit dynamics and complexation with the host ACE2 receptor. Of particular note, recent published work has shown excellent antiviral activity against human coronavirus HCoV-229E in carbon quantum dots functionalized with BAs.[21]

This project was intended to probe the above hypothesis by studying the interactions between various BAMPs and SARS-CoV-2 spike protein. Specifically, we sought to determine (i) whether BAMPs can bind and/or aggregate the spike protein and, (ii) more importantly, whether BAMPs inhibit or otherwise affect the binding of the spike protein to ACE2. It was expected that positive confirmation of either of these phenomena would spur future research into the antiviral properties of BAMPs toward SARS-CoV-2 and other enveloped viruses.

Two different BAMPs were used in this work (Figure 2), a BA-functionalized poly(ethylene glycol) (PEG-BA) and a BA-functionalized poly(ethylenimine) (PEI-BA). These BAMPs were prepared as previously described.[15] Briefly, an 8-arm star, amine end-functionalized PEG of number-averaged molecular weight $M_n \sim 40$ kDa and a branched PEI of $M_n \sim 10$ kDa were used as starting materials. Phenylboronic acid was grafted to amine functional groups on both polymers via reductive amination

of 4-formylphenylboronic acid using sodium cyanoborohydride as a reducing agent. The resulting PEG-BA and PEI-BA possessed 7.3 and 5.6 BA units per polymer chain, respectively, as determined by ^{1}H nuclear magnetic resonance spectroscopy.[15] Furthermore, the successful introduction of BA units was confirmed through a simple gel test.[15] The BAMPs were dissolved in deionized water at 50 mg/mL and mixed with equal volumes of aqueous 50 mg/mL solution of a linear PEG end-functionalized with catechol (an aromatic diol that strongly binds BA[11]), designated hereafter as PEG-CAT. Immediately after mixing, a self-supporting hydrogel forms, confirming the successful generation of a cross-linked polymer network through BA-diol interaction.[22]

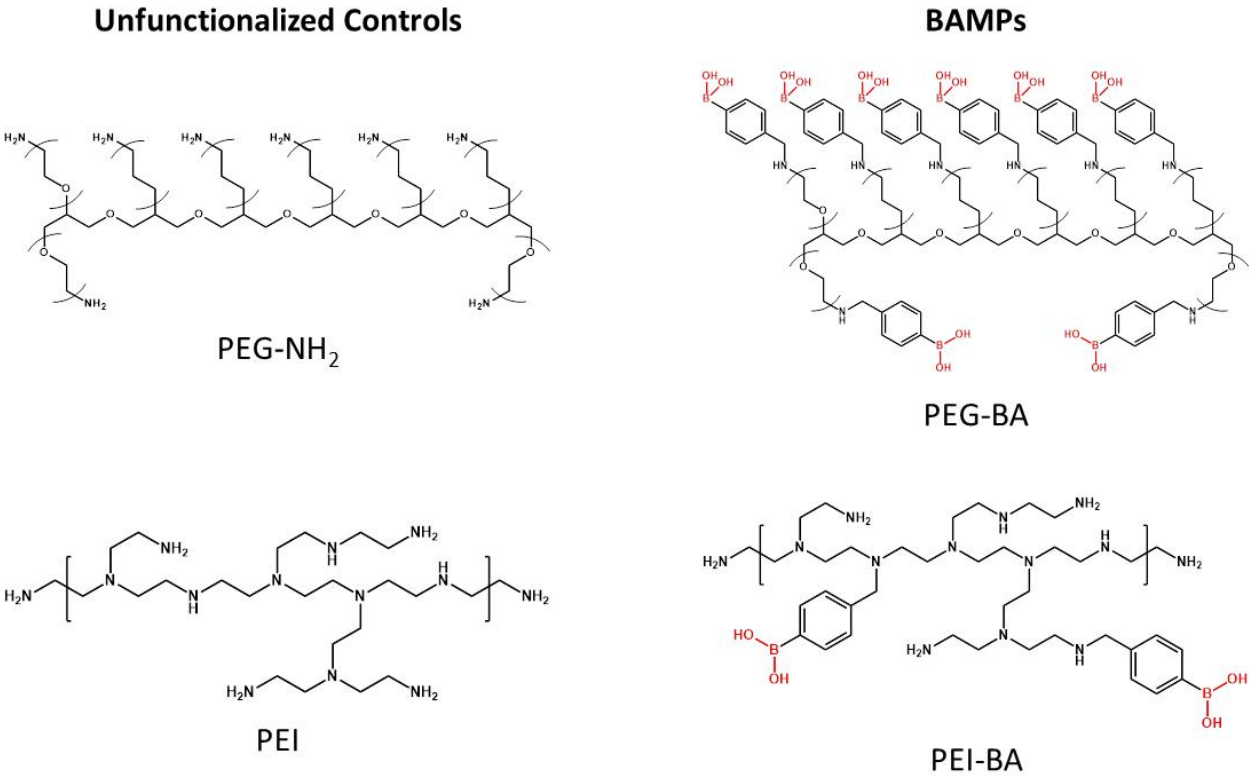

Figure 2. Starting polymers (unfunctionalized controls) and corresponding BAMPs used in this work. The BA functionalities are shown in red.

For a simple initial test of potential interactions between BAMPs and SARS-CoV-2 spike protein, buffered solutions of the two were mixed in a similar manner as the gel test described above. In a representative example, 47 μg recombinant SARS-CoV-2 S1 subunit protein (RayBioTech, Peachtree Corners, GA) was dissolved in 6 μL pH 7.4 phosphate buffered saline (PBS) for a concentration of 7.83 mg/mL. Separately, PEG-BA was dissolved in pH 7.4 PBS at 94 mg/mL. 0.5 μL volumes of the PEG-BA solution were added to the spike protein solution until a total of 2 μL PEG-BA solution was added (final concentrations 5.9 mg/mL spike protein, 23.5 mg/mL PEG-BA). The resulting solution did not exhibit any visual indication of gelation, nor the formation of a precipitate, and remained readily pipettable with each addition of PEG-BA. However, it is important to note that the model

system of PEG-BA and PEG-CAT combined at 10 mg/mL also failed to produce a gel. Indeed, in these types of tests, macroscopic gelation generally requires relatively high concentrations of the species responsible for crosslinking, whereas dilute solutions typically yield soluble microgels.23 Unfortunately, due to the high cost and limited availability of the spike protein (we obtained ~ 650 μg from RayBioTech and other sources), we were unable to perform a gel test at higher concentrations.

We further sought to employ gel electrophoresis to probe potential interactions between BAMPs and SARS-CoV-2 spike protein. Gel electrophoresis separates proteins and other macromolecules on the basis of their molecular size and charge. We conjectured that any binding of BAMP to saccharide residues of the spike would necessarily alter the molecular size of the BAMP-spike conjugate relative to the neat spike protein and, thus, be manifested in analysis by gel electrophoresis. We chose to use native polyacrylamide gel electrophoresis (native-PAGE), rather than the more common sodium dodecyl sulfate polyacrylamide gel electrophoresis (SDS-PAGE), as the latter involves denaturation of the protein analyte, whereas the former preserves the protein's inherent structure. Unfortunately, our attempts to obtain a reproducible band for even the neat spike protein were plagued by issues related to the use of old polyacrylamide gels. In addition, we avoided the use of the standard glycerol-based loading buffer typically used in native-PAGE, instead using low molecular weight PEG-based buffers, so as to avoid any interference of glycerol in BA-saccharide interaction. We suspect that the use of an unconventional buffer may have further contributed to our inability to reproducibly characterize the neat spike protein.

As a third approach to investigate potential BAMP-spike interaction, we attempted to functionalize surfaces with BAs, expose such functionalized surfaces to the spike protein, and indirectly evaluate BA-spike binding by determining the thickness of the surface via ellipsometry. Various methods for surface functionalization were attempted. Au surfaces were exposed to 4-mercaptophenylboronic acid, in order to graft the BA via the well-known Au-thiol interaction.[24] Alternatively, Si surfaces were exposed to an epoxide-functional silane, (3-glycidyloxypropyl) trimethoxysilane, after which the grafted epoxide was reacted with 3-aminophenylboronic acid. To illustrate the challenges associated with this general surface functionalization approach, Figure 3 shows the thickness (height) of the grafted BA for four replicates of Si surfaces identically functionalized by the latter method. The error bars indicate the standard deviation from several measurements in different locations across the same sample. The thickness of the grafted BA cannot be evaluated by ellipsometry within an accuracy of *ca.* 1 nm, which is on the order of the size of the spike protein.[25] Therefore, it was unsurprising to find that measurements next performed after subsequent exposure of these surfaces to the spike protein did not produce an increase in thickness within the error of the measurement. Thus, this method was insufficient to evaluate whether or not the spike protein binds to BAs.

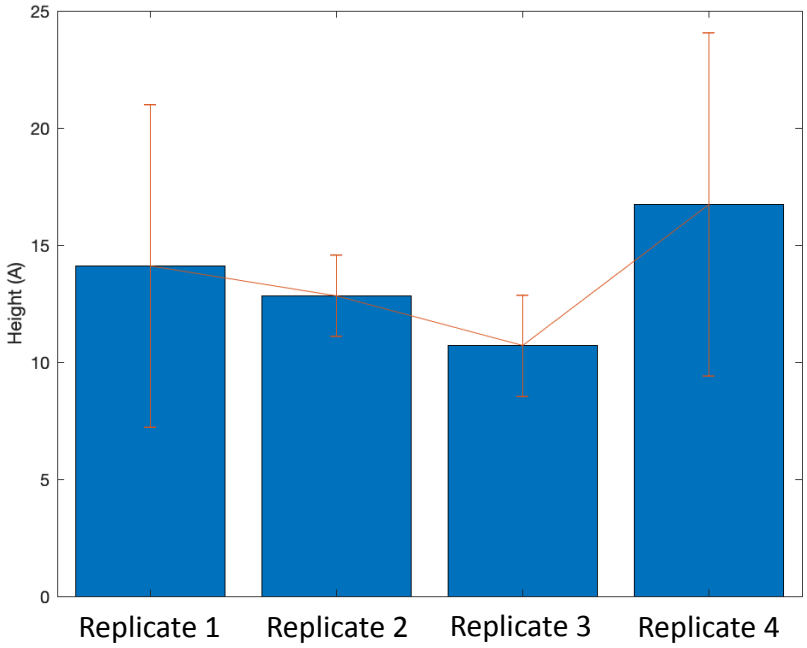

Figure 3. Representative example of thicknesses of BA-functionalized Si surfaces determined by ellipsometry.

While we were unable to obtain definitive information as to whether BAMPs can bind and/or aggregate SARS-CoV-2 spike protein, we were successfully able to evaluate, in part, the effect of BAMPs on the key spike-ACE2 interaction through the use of enzyme-linked immunosorbent assays (ELISAs). Figures 4 and 5 show the results of ELISAs performed on SARS-CoV-1 and SARS-CoV-2 spike proteins. The spike is adsorbed on polycarbonate surfaces in a 96 well plate, exposed and incubated to a solution of the polymer of interest, then exposed to ACE2, followed by a secondary antibody and an appropriate substrate to convert the amount of bound ACE2 to a quantitative optical readout.

The control curves in Figure 4(a) and Figure 5(a) clearly show that ACE2 binds to both spike proteins; increasing ACE2 concentration yields a larger absolute amount of bound ACE2, as evidenced by the increased absorbance of the sample. In the remaining panels, the polymer (or antibody, in the case of Figure 4(b) and Figure 5(b)) concentration is varied, while the subsequent ACE2 concentration is held constant. The positive control curves in Figure 4(b) and Figure 5(b) illustrate the outcome of the ELISA in a scenario where spike-ACE2 is effectively inhibited. The antibody m396 is known to inhibit spike-ACE2 binding for SARS-CoV-1, but not SARS-CoV-2. Confirming this notion, increasing concentration of m396 produced no significant change in the amount of ACE2 bound by SARS-CoV-2 spike, whereas increasing concentration of m396 clearly decreased the amount of ACE2 bound by SARS-CoV-1 spike.

Curiously, for both spike proteins, the addition of PEI and PEI-BA resulted in increasing amounts of ACE2 bound with increasing polymer concentration (Figure 4(c)-(d) and Figure 5(c)-(d)). Both PEI and PEI-BA are strong polyelectrolytes, possessing a high density of protonated amines in the

buffered conditions (PBS) used in this ELISA. We suspect that a significant amount of PEI became attached to the surface-bound spike through electrostatic interactions, in turn enhancing the amount of ACE2 deposited through the same mechanism. This outcome precludes (for the specific case of PEI) any determination of the effect of the BA on spike-ACE2 binding through this particular ELISA. On the other hand, Figure 4(e)-(f) and Figure 5(e)-(f) clearly show that both PEG-NH2 and PEG-BA had no effect on the amount of ACE2 bound by either SARS-CoV-1 or SARS-CoV-2 spike. More explicitly, these data indicate that the presence of BA in PEG-BA did not inhibit spike-ACE2 binding in either case.

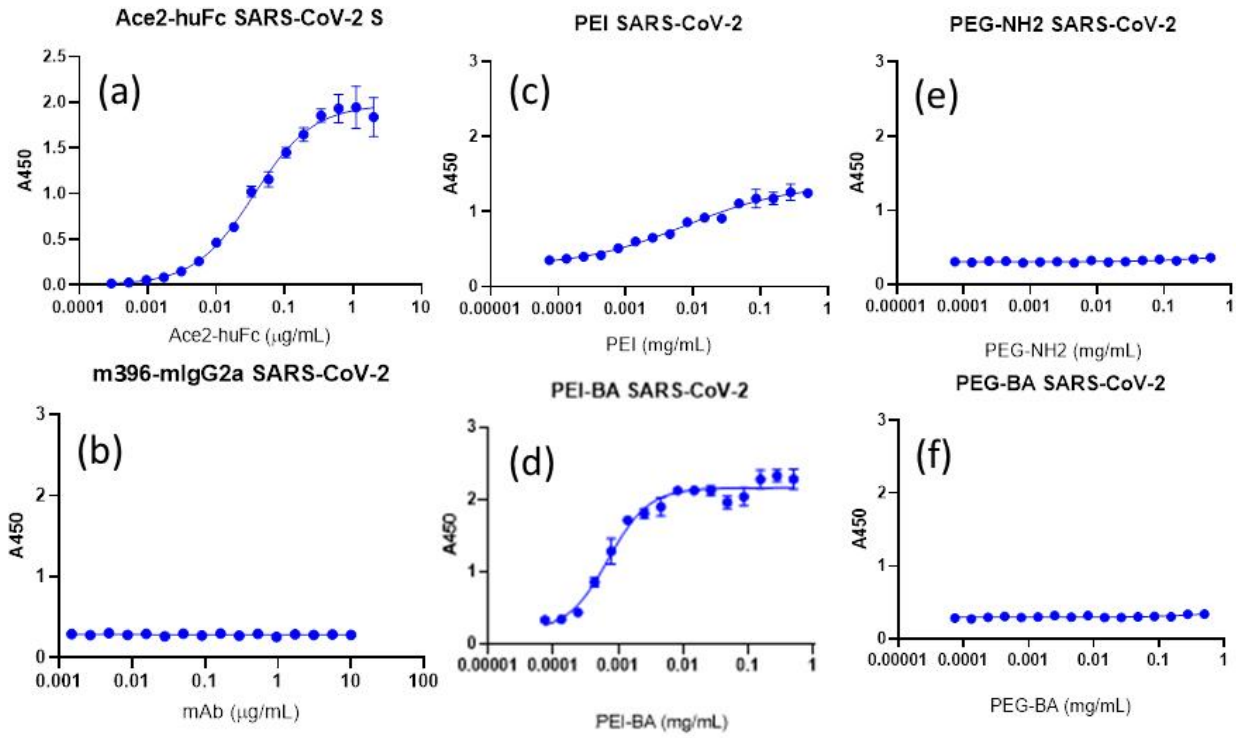

Figure 4. ELISA results for SARS-CoV-2 full trimeric spike protein attached to surface and exposed to **(a)** ACE2 (control curve), **(b)** m396 antibody, **(c)** PEI, **(d)** PEI-BA, **(e)** PEG-NH_2, and **(f)** PEG-BA. For **(b)-(f)**, the ACE2 concentration used was 0.01 ug/mL.

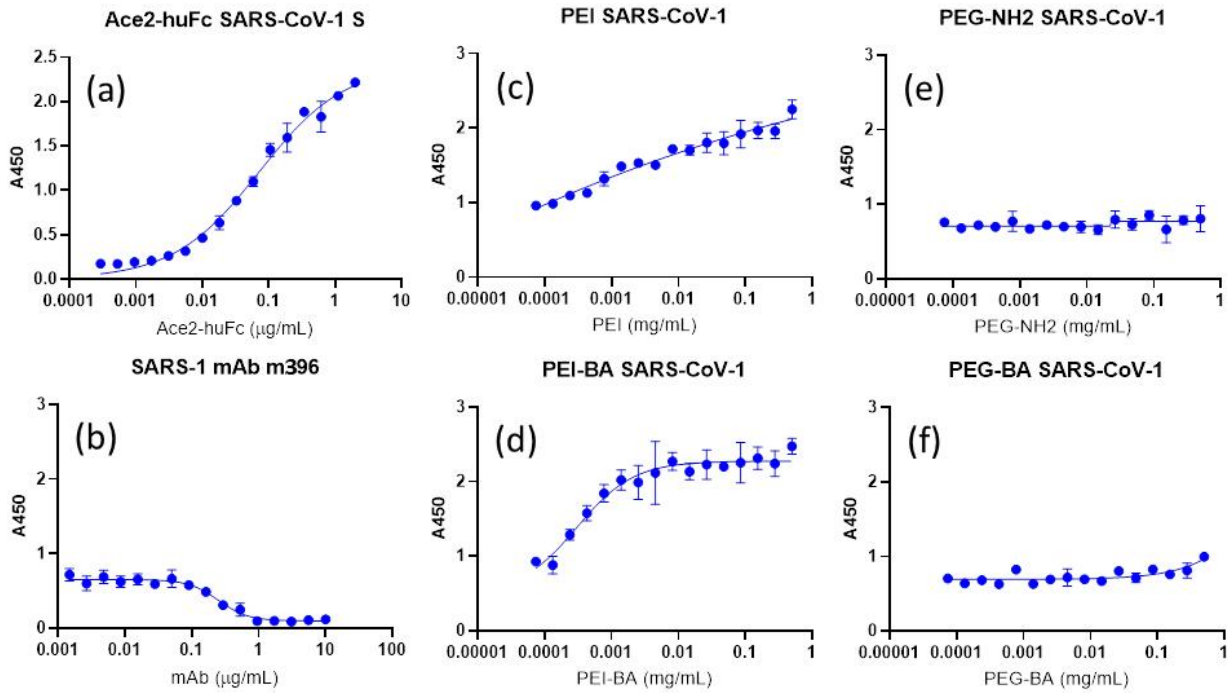

Figure 5. ELISA results for SARS-CoV-1 full trimeric spike protein attached to surface and exposed to **(a)** ACE2 (control curve), **(b)** m396 antibody, **(c)** PEI, **(d)** PEI-BA, **(e)** PEG-NH_2, and **(f)** PEG-BA. For **(b)-(f)**, the ACE2 concentration used was 0.033 μg/mL.

We also tested the same BAMPs in a commercial, ELISA-based SARS-CoV-2 inhibition kit. This test differed slightly from the ELISA depicted by Figures 4 and 5 in that the spike protein and polymer of interest were incubated together and simultaneously exposed to surface-bound ACE2. The results are shown in Figure 6. Note that, in this case, the data are expressed as a percent inhibition; in other words, 100% inhibition corresponds to no bound spike protein.

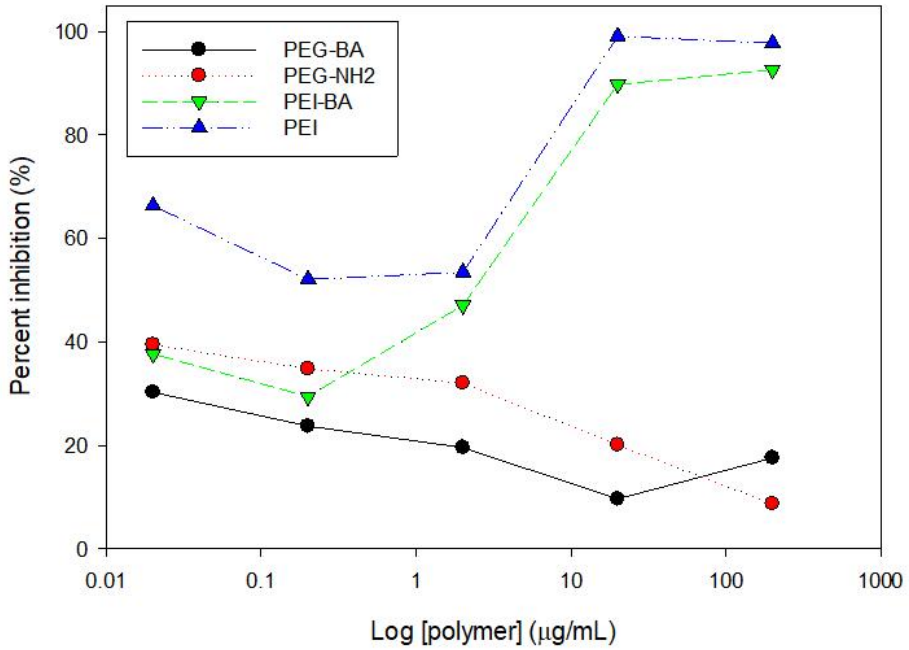

Figure 6. Inhibition of SARS-CoV-2 receptor binding domain recognition by surface-bound ACE2 after incubation of the former with BAMPs or unfunctionalized controls.

In this test, both PEI and PEI-BA strongly inhibited spike-ACE2 binding. We conjecture again that this outcome is derived from the polyelectrolyte nature of PEI. Electrostatic interactions may potentially disrupt the activity or structure of the spike, thereby reducing the efficacy of binding with ACE2. Nevertheless, the presence of BA does not impart any improvement in inhibition for PEI-BA relative to PEI. In contrast, PEG-NH_2 and PEG-BA both exhibited a marginal capacity to inhibit spike-ACE2 binding. More importantly, however, the presence of BA again does not impart any improvement in inhibition for PEG-BA relative to PEG-NH_2.

It is important to emphasize that the ELISAs are intended to interrogate only the spike-ACE2 binding event. The data presented here provide evidence that, contrary to our intended purposes, BAMPs do not interfere with this binding event. Lacking definitive information regarding the interaction of our BAMPs with the spike itself, two possible scenarios must be considered. On one hand, the BA moieties present in the BAMPs may simply have failed to form the desired boronate esters with spike saccharide residues under the conditions used for these ELISAs. In particular, the accessible residues in the spike protein, as well as the particular BA chemistry chosen, may perhaps require a higher working pH for appropriate binding. Alternatively, it may be possible that the BA moieties are, in fact, binding the spike protein via saccharide residues, yet the spike can still efficiently bind ACE2 in such a modified form.

Despite the fact that the presence of BA did not inhibit or otherwise affect spike-ACE2 binding in the ELISAs, we remained curious as to whether the presence of BA could disrupt other key,

downstream processes associated with viral infection, such as membrane fusion and viral entry. Therefore, two viral inhibition tests were further pursued, using Dengue virus (DENV) and bacteriophage Φ6 as surrogates in lieu of SARS-CoV-2. DENV is, of course, a mosquito-borne, enveloped virus that, like SARS-CoV-2, is amply decorated with glycoproteins.[26] Our test protocol with DENV involved infecting Vero cells with DENV; unfortunately, however, we were unable to obtain a proper control condition for successful infection of the Vero cells over the short duration of the project.

In contrast, the bacteriophage Φ6 is a well-known virus that infects Pseudomonas bacteria.27 Φ6 is relatively unique among bacteriophages in that it possesses a lipid membrane, similar to DENV and SARS-CoV-2. However, the spike protein of Φ6 is not glycosylated, and the process by which Φ6 recognizes and infects Pseudomonas is much different from SARS-CoV-2 and its characteristic spike-ACE2 process. Nevertheless, and quite interestingly, we found a significant inhibitory effect of BAMPs to Φ6 infection. Pseudomonas syringae were cultured and exposed to samples of Φ6 containing ca. 107 viral particles per sample, previously incubated with BAMP at 0.05 mg/mL. After allowing infection to occur for 2 days, the amount of Φ6 was evaluated as shown in Table 1. Relative to the control experiment in the absence of any polymer, the presence of the unfunctionalized polymers PEI and PEG-NH2 caused roughly an order of magnitude decrease in the quantity of Φ6 detected after infection. For PEG-BA, there was a further order of magnitude decrease in Φ6 relative to PEG-NH2. For PEI-BA, the polymer completely inhibited the Φ6 infection process, as no Φ6 was ultimately detected. There was a clear effect of the BA functionality in inhibiting Φ6 infection, particularly in the case of PEI-BA. It is important to note that Table 1 shows the result of a single experiment, the only experiment with Φ6 successfully completed over the short duration of this project; hence, to increase confidence in the reproducibility and associated outcome, this result should ideally be confirmed through future repetition.

Table 1. Φ6 counts after incubation with BAMPs for the indicated duration followed by infection of *Pseudomonas syringae*.

	PEI	PEI-BA	PEG-NH2	PEG-BA	Control
5 min	9e6	0	1e6	1.9e5	1.2e7
15 min	1.3e6	0	1.9e6	2.2e5	1.2e7
30 min	2.0e6	0	1.7e6	1.8e5	7e6
45 min	1.0e6	0	1e6	1.2e5	1.2e7

To reiterate, the spike protein of Φ6 is not glycosylated. Therefore, the inhibitory effect of the BA was somewhat surprising. It may be that the BA interacts with an alternative component of

Φ6, such as its characteristic phospholipids. However, in truth, the mechanism by which the inhibitory effect of the BA is derived is wholly unclear at this point. If the BA targeted a component of Φ6 that is universally found in a wide variety of viruses, then these BAMPs would reasonably be expected to exhibit broad anti-viral behavior. Until additional information regarding the specific mechanism is uncovered, or inhibition tests are successfully completed with other viruses, such a notion is purely speculative.

A.4.3. Summary

It remains unclear from the experiments attempted as to whether BAMPs can effectively crosslink or otherwise bind SARS-CoV-2 spike protein. Regardless, initial results from two different ELISAs clearly show no appreciable effect of the BA functionality in inhibiting spike-ACE2 binding relative to unfunctionalized controls. In contrast, an initial test of the effect of BAMPs on Φ6 bacteriophage infection showed a marked inhibitory effect due to the BA functionality, although this outcome is of dubious relevance to SARS-CoV-2. We recommend that any future efforts to evaluate the fundamental nature of interaction between BAMPs and the spike proteins of enveloped viruses focus on the development and implementation of experimental protocols that enable determination of the appropriate conditions (*e.g.*, pH, BA selection) necessary to enforce BA-spike binding.

A.4.4. References

(1) James, T. D.; Sandanayake, K. R. A. S.; Shinkai, S. Saccharide Sensing with Molecular Receptors Based on Boronic Acid. Angew. Chem. Int. Ed. 1996, 35, 1910-1922.
(2) Yang, W.; Gao, X.; Wang, B. Boronic Acid Compounds as Potential Pharmaceutical Agents. Med. Res. Rev. 2003, 23, 346-368.
(3) Bull, S. D.; Davidson, M. G.; van den Elsen, J. M. H.; Fossey, J. S.; Jenkins, A. T. A.; Jiang, Y.-B.; Kubo, Y.; Marken, F.; Sakurai, K.; Zhao, J.; James, T. D. Exploiting the Reversible Covalent Bonding of Boronic Acids: Recognition, Sensing, and Assembly. Acc. Chem. Res. 2013, 46, 312-326.
(4) Wu, X.; Li, Z.; Chen, X.-X.; Fossey, J. S.; James, T. D.; Jiang, Y.-B. Selective Sensing of Saccharides Using Simple Boronic Acids and Their Aggregates. Chem. Soc. Rev. 2013, 42, 8032-8048.
(5) Guan, Y.; Zhang, Y. Boronic acid-containing hydrogels: synthesis and their applications. Chem. Soc. Rev. 2013, 42, 8106-8121.
(6) Brooks, W. L. A.; Sumerlin, B. S. Synthesis and Applications of Boronic Acid-Containing Polymers: From Materials to Medicine. Chem. Rev. 2016, 116, 1375-1397.
(7) Akgun, B.; Hall, D. G. Boronic Acids as Bioorthogonal Probes for Site-Selective Labeling of Proteins. Angew. Chem. Int. Ed. 2018, 57, 13028-13044.
(8) Ryu, J. H.; Lee, G. J.; Shih, Y.-R. V.; Kim, T.-I.; Varghese, S. Phenylboronic Acid-polymers for Biomedical Applications. Curr. Med. Chem. 2019, 26, 6797-6816.

(9) Antonio, J. P. M.; Russo, R.; Carvalho, C. P.; Cal, P. M. S. D.; Gois, P. M. P. Boronic acids as building blocks for the construction of therapeutically useful bioconjugates. Chem. Soc. Rev. 2019, 48, 3513-3536.
(10) Stubelius, A.; Lee, S.; Almutairi, A. The Chemistry of Boronic Acids in Nanomaterials for Drug Delivery. Acc. Chem. Res. 2019, 52, 3108-3119.
(11) Springsteen, G.; Wang, B. A detailed examination of boronic acid–diol complexation. Tetrahedron 2002, 58, 5291-5300.
(12) Yan, J.; Springsteen, G.; Deeter, S.; Wang, B. The relationship among pKa, pH, and binding constants in the interactions between boronic acids and diols—it is not as simple as it appears. Tetrahedron 2004, 60, 11205-11209.
(13) Amaral, A. J. R.; Pasparakis, G. Macromolecular cell surface engineering for accelerated and reversible cellular aggregation. Chem. Commun. 2015, 51, 17556-17559.
(14) Amaral, A. J. R.; Pasparakis, G. Rapid Formation of Cell Aggregates and Spheroids Induced by a "Smart" Boronic Acid Copolymer. ACS Appl. Mater. Interf. 2016, 8, 22930-22941.
(15) Bachand, G. D.; Greene, A.; Jones, B. H.; Ko, R. Cell Gels – Building Reversible Networks from Boronic Acid and Cell Membrane Chemistry. SAND2017-10056R, Sandia National Laboratories, 2017.
(16) Amaral, A. J. R.; Pasparakis, G. Cell Membrane Engineering with Synthetic Materials: Applications in Cell Spheroids, Cellular Glues and Microtissue Formation. Acta Biomater. 2019, 90, 21-36.
(17) Miller, P. R.; Jones, B. H. Reversible Binding Tissue Adhesive. SD # 15288, Sandia National Laboratories, 2020.
(18) Watanabe, Y.; Allen, J. D.; Wrapp, D.; McLellan, J. S.; Crispin, M. Site-specific glycan analysis of the SARS-CoV-2 spike. Science 2020, DOI: 10.1126/science.abb9983.
(19) Shajahan, A.; Supekar, N. T.; Gleinich, A. S.; Azadi, P. Deducing the N- and O-glycosylation profile of the spike protein of novel coronavirus SARS-CoV-2. Glycobiology 2020, DOI: 10.1093/glycob/cwaa042.
(20) Shang, J.; Wan, Y.; Luo, C.; Ye, G.; Geng, Q.; Auerbach, A.; Li, F. Cell entry mechanisms of SARS-CoV-2. Proc. Nat. Acad. Sci. 2020, DOI:10.1073/pnas.2003138117.
(21) Łoczechin, A.; Séron, K.; Barras, A.; Giovanelli, E.; Belouzard, S.; Chen, Y.-T.; Metzler-Nolte, N.; Boukherroub, R.; Dubuisson, J.; Szunerits, S. Functional Carbon Quantum Dots as Medical Countermeasures to Human Coronavirus. ACS Appl. Mater. Interf. 2019, 11, 42964-42974.
(22) He, L.; Fullenkamp, D. E.; Rivera, J. G.; Messersmith, P. B. pH responsive self-healing hydrogels formed by boronate–catechol complexation. Chem. Commun. 2011, 47, 7497-7499.
(23) Thorne, J. B.; Vine, G. J.; Snowden, M. J. Microgel applications and commercial considerations. Colloid Polym. Sci. 2011, 289, 625-646.
(24) Pensa, E.; Cortes, E.; Corthey, G.; Carro, P.; Vericat, C.; Fonticelli, M. H.; Benitez, G.; Rubert, A. A.; Salvarezza, R. C. The Chemistry of the Sulfur-Gold Interface: In Search of a Unified Model. Acc. Chem. Res. 2012, 45, 1183-1192.
(25) Wrapp, D.; Wang, N.; Corbett, K. S.; Goldsmith, J. A.; Hsieh, C.-L.; Abiona, O.; Graham, B. S.; McLellan, J. S. Cryo-EM structure of the 2019-nCoV spike in the prefusion conformation. Science 2020, 367, 1260-1263.
(26) Rey, F. A. Dengue virus envelope glycoprotein structure: New insight into its interactions during viral entry. Proc. Nat. Acad. Sci. 2003, 100, 6899-6901.
(27) Phillpotts, R. J.; Thomas, R. J.; Beedham, R. J.; Platt, S. D.; Vale, C. A. The Cystovirus phi6 as a simulant for Venezuelan equine encephalitis virus. Aerobiologia 2010, 26, 301-309.

A.5. Variable Chain Length Carboxylic Acids as Modifiers to Enhance the Antiviral Efficacy of Sodium Dodecyl Sulfate

Patrick D. Burton and Matt Tezak

Exists as a standalone SAND Report: SAND2020-5940.

A.6. Self-Disinfecting Polymeric Coatings

Cody Corbin, Bryce Ricken, Lauren Atencio, Jesse Cahill, Andres Sanchez, Anne Grillet, Sara Dickens, Martin Nemer

Exists as a standalone SAND Report: SAND2020-5621R

A.7. Disinfectant corrosivity with shipboard HY80 steel

Michael A. Melia, Jason M. Taylor, Mark Tucker

A.7.1. Abstract

Many disinfectants are used to eliminate the SARS-CoV-2 virus from surfaces, ranging in efficacy and materials compatibility, with corrosion of infrastructure materials being a concern for many applications. The aim of this study is to determine the corrosivity of a hydrogen peroxide-based disinfectant, DF-200 (Decontamination Formulation-200) and Bleach (sodium hypochlorite) when in contact with a shipboard relevant alloy in HY80 steel. The corrosion rate was similar for wrought and cast HY80 specimens after 1 hour immersion in the Bleach and DF-200 solutions however at longer immersion times the corrosion rate for samples immersed in the DF-200 solution reduced by over an order of magnitude, due to the natural dissipation of hydrogen peroxide.

Atmospheric exposures of HY80 specimens with crevice forming washers showed the impact these disinfectants have on crevice corrosion in a humid environment with and without a disinfectant residue and contamination (NaCl). The Bleach solution caused the most corrosion when residue remained on the surface, having more crevice sites with local attack. DF-200, when diluted to 10% strength, showed minimal localized corrosion/crevice corrosion, similar to the control samples with no disinfectant. The residue left behind from DF-200 exhibited corrosion inhibitor behavior for the exposures performed on specimen with NaCl loading.

A.7.2. Introduction

The decontamination formulation, DF-200, is being widely used for decontamination of critical infrastructure worldwide via licensed commercial suppliers versus the SARS-CoV-2 virus that causes COVID-19 [1]. There is little quantitative corrosion data for DF-200 and similar

decontamination formulations. Laboratory based reports suggest hydrogen peroxide based disinfectants can cause corrosion [2], however there is a major lack of corrosion data that replicates or utilizes real world scenarios, unfortunately a commonality with other disinfectants [3-8]. The unknown corrosion behavior is limiting the use of high virus kill efficacy formulations like DF-200 for naval shipboard and aircraft applications given the current pandemic to maintain military readiness. The hydrogen peroxide-based DF-200 has been shown to have a seven-9's (99.99999%) effective virus kill efficacy.

The DF-200 formulation consists of mild solvents, inorganic salts, a low concentration of hydrogen peroxide (~3.5%), a hydrogen peroxide activator, and water. Outperforming similar, more aggressive formulations and other varieties of disinfectants, DF-200 has been shown to be effective against coronaviruses and similar viruses, measured by log kill as shown in Table 1 below [9]. In tests at Kansas State University, DF-200 was shown to rapidly and completely inactivate a >5Log10 concentration of Bovine Coronavirus with a one minute contact time even in the presence of a 50% organic loading [9]. Based on these results, DF-200 can effectively be used to disinfect facilities against SARS-CoV-2 – even with high organic or soil loads. Most other disinfectants are repelled or inactivated by the high organic loadings that could surround SARS-CoV-2 and never actually encounter the virus, hence it survives [10]. For example, 10% chlorine Bleach achieves high efficacy against pathogens in laboratory tests but often fails in the field because it does not penetrate organic matter [11, 12].

Table 1: Virus kill efficacy of common types of disinfectants. Note that the efficacy estimates are not intended to include all disinfectants but only examples of low efficacy and high efficacy products without organic loading

Log_{10} Kill	**Percent Kill (%)**	**Remaining Virus from original 10,000,000 present**	**Representative Disinfectants**
1	90	1,000,000	
2	99	100,000	
3	99.9	10,000	Ethyl Alcohol, Quaternary Amines (Quats)
4	99.99	1000	
5	99.999	100	
6	99.9999	10	10% Chlorine Bleach
7	99.99999	1	DF-200

The purpose of this work is to determine meaningful, quantitative corrosion data using the DF-200 formulation on a shipboard relevant metal (HY80 steel). Electrochemical corrosion data was collected under full immersion conditions to show an extreme corrosion case and reveal trends in corrosion response over long exposure times. Atmospheric corrosion experiments were then used to show how residue from multiple DF-200 cleaning cycles can impact corrosion rates when a crevice exists on a part. The hypothesis tested is if the residue from the DF-200 chemistry is rinsed from a coupons surface, then the likelihood for corrosion after proper application is negligible compared to what typically occurs over the tests' time period. This study will also

provide needed information as little to nothing is known about their long term damage to the equipment they are used on, especially with respect to corrosion.

A.7.3. Methods:

Material: The disinfectants tested are a solution of dilute household Bleach (0.825 vol% sodium hypochlorite, pH~9.5) and DF-200, a 3-part solution:

- **Part 1:** 1.6% n-Alkyl(C12-16)-N, N-dimethyl-N-benzylammonium chloride (CAS 85409-22-9)
- **Part 2:** 3.99% Hydrogen peroxide (CAS 7722-84-1)
- **Part 3:** 1% Diacetin (Glycerol diacetate – CAS 25395-31-7)

The DF-200 solution will be used at its full strength (49:49:2) and after dilution to 10%, both had a pH of ~10.

Table 1: HY80 steel nominal composition (wt%)

Iron, Fe	93.1
Nickel, Ni	3.23
Chromium, Cr	1.80
Copper, Cu	≤ 0.25
Molybdenum, Mo	0.60
Silicon, Si	0.35
Carbon, C	0.18
Manganese, Mn	0.40
Phosphorous, P	≤ 0.025
Sulfur, S	≤ 0.025
Titanium, Ti	≤ 0.020
Vanadium, V	≤ 0.030

High strength low alloy (HSLA-12) steel, nominal composition shown in **Table 1**, also referred to as HY80 steel, was provided by the Naval Research Lab (NRL) in the cast and forged condition. All samples were cut from a 1” x 1” x 6” casting/wrought product and cut into 1” x 1” squares, roughly 1/8” thick. All samples for the humidity-controlled experiments (48 wrought

and 36 cast samples) were drilled through their center face with a 0.265" diameter hole. One face of all samples prior to electrochemical measurements and humidity-controlled experiments were ground to a 400 grit finish with SiC paper.

Initial electrochemical experiments: Electrochemical tests were carried out using a standard three electrode cell with a Pt mesh counter electrode and a Ag/AgCl (saturated KCl) reference electrode (+0.197 V vs. standard hydrogen electrode (SHE)). Electrochemical measurements were performed on a Biologic VSP-300 multichannel potentio/galvanostat. The measurements included a 1- or 24-hour open circuit potential (OCP) measurement, followed by a potentio-electrochemical impedance spectroscopy (EIS) measurement, and then after a 5 minute OCP, a Tafel polarization scan.

The EIS measurements were performed at OCP from a frequency range from 100,000 to 0.01 Hz at 10 pts./decade and sinusoidal voltage amplitude of V_{RMS} = 10 mV. Impedance data was fit to an equivalent circuit containing a solution resistance (R_s) in parallel with one or two Randle's circuits, depending on the number of time constants observed in the data. See **Figure 1** for an example of a circuit. From this equivalent circuit a polarization resistance (R_p) could be determined which is known to be inversely proportional to corrosion rate. The Tafel polarization scan was performed from -250 mV below the OCP to 250 mV above the OCP at a scan rate of 10 mV/min. Tafel extrapolation was used to determine the Tafel constants, β_a and β_c, along with the corrosion potential (E_{corr}) and corrosion current density (i_{corr}), which is directly proportional to corrosion rate [13].

Experiments were performed using deionized (DI) water, 1.44 M NaCl (expected concentration caused by salt loading used for humidity exposure samples), 10 vol% Bleach (0.825% sodium hypochlorite), 10 vol% DF-200, 10 vol% part 1 of DF-200, and 10 vol% part 2 of DF-200. Each test was replicated a minimum of two times.

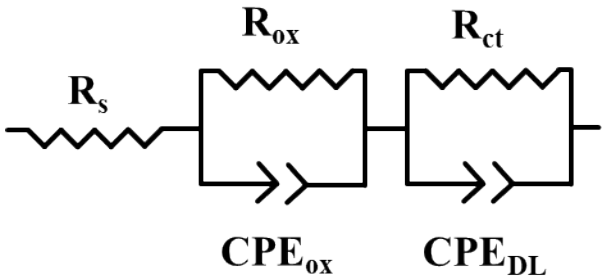

$$R_p = R_{ct} + R_{ox} \propto \frac{1}{i_{corr}} = \frac{1}{corr.rate}$$

Figure 1: Equivalent circuit used to fit EIS data and relationship between resistances and corrosion rate.

Disinfectant and salt loading exposures with crevice former: One side of the samples was polished to a 400 grit finish; the other side was left as the cut surface from sectioning which was

covered with Kapton tape. Prior to applying the Kapton tape, the samples were marked with a scribe and weighed to allow for mass loss measurements after exposures.
Disinfectants were applied via misting from a spray bottle with the conditions described in **Table 2**. Specimens were sprayed roughly 15 times to reach a disinfectant loading of ~0.25 L/m^2 from each solution, depicted in **Figure 2** for the 10% Bleach specimens. The specimen marked as "no rinse" means after the disinfectant was applied to the surface, the solution sat on the surface for ~30 minutes after which it was force dried with dry N_2 to evaporate all water from the surface, leaving disinfectant residue on the surface. Samples marked as "rinsed" means after the solution sat on the samples surface for 15 minutes, then the disinfectant solution was thoroughly rinsed off with DI water and dried with dry N_2. These steps for applying disinfectant were repeated 3 times to simulate multiple cleaning cycles. After the disinfectant was deposited, half of the coupons were loaded with 50 µg/cm^2 of NaCl salt using an inkjet printing method [14].

Figure 2: Picture of sprayed on disinfectant loading to a set of samples, ~0.25 L/m^2 coverage.

Table 2: Disinfectant and salt loading	
Disinfectant?	Salt (NaCl)
No disinfectant	None
10% Bleach – no rinse	None
10% Bleach – rinsed	None
10% DF200 – no rinse	None
10% DF200 – rinsed	None
Full DF200 – no rinse	None

No disinfectant	50 µg/cm^2
10% Bleach – no rinse	50 µg/cm^2
10% Bleach – rinsed	50 µg/cm^2
10% DF200 – no rinse	50 µg/cm^2
10% DF200 – rinsed	50 µg/cm^2

Full DF200 – no rinse	50 μg/cm^2

Following the disinfectant and salt loading, a ceramic crevice forming washer was fastened to the surface of all samples with 316L stainless fasteners (bolt, nut, and washers) at a torque of 20 lbs./in. The sample after the ceramic washer was applied is shown in **Figure 3**. Each condition for wrought samples had 4 replicate coupons while cast samples had 3 replicate coupons. These samples were then loaded into a humidity-controlled chamber (Associated Environmental Systems LH-10 Temp/Humidity Test Chamber, MA, USA) at a relative humidity of 95% and a temperature of 35°C for 2 weeks.

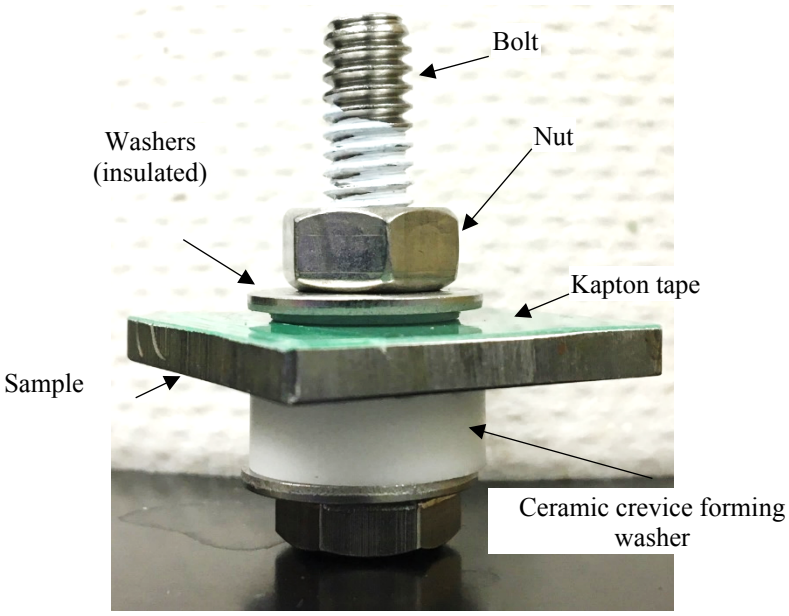

Figure 3: HY80 steel sample preparation with a ceramic washer, torqueing (20 ft.-lbs.) and electrical isolation from the stainless steel bolt/washers.

Characterization of samples: All samples were imaged with a Keyence VHX 5000 after grinding with 400 grit paper, after the disinfectant was applied to the surfaces, and after the exposures. The images after the exposures and all subsequent analyses were performed on the samples after the crevice forming washers were removed.

Corrosion product was removed per ASTM G1-03 with a 1.0 M diammonium citrate solution at 80°C and a 40 minute soak time [15]. Gravimetric mass loss was performed for all samples after corrosion product was removed. Imaging of the corrosion damage after corrosion product removal was performed using a Zeiss Supra 55-VP field emission scanning electron microscopy (SEM), in secondary and backscattered electron imaging modes. A working distance of 8 mm and accelerating voltage of 10 kV were used for all SEM imaging. White light interferometry was also performed on a set of specimens with a Zygo NexView. All data was processed using DigitalSurf MountainMaps.

A.7.4. Results and Discussion:

Electrochemical measurements: Representative electrochemical measurements of the wrought HY80 material are shown in **Figures 4** and **5**,with a schematic of Tafel extrapolation shown in **Figure 4(b)**. Experiments performed after a 1-hour open circuit potential (OCP) hold are shown in **Figure 4** for specimens immersed in DI water, 1.44 M NaCl, 10% Bleach, and 10% DF-200. Optical images after the experiments are show in **Figure 4(a)** with general corrosion caused by all solutions starting from the o-ring, however there are no major signs of crevice corrosion. The representative Tafel polarization measurements are shown in **Figure 4(b)**, unsurprisingly showing DI water to elicit the lowest current density response compared to the other three solutions. **Figure 4(c)** shows the polarization resistance (R_p) determined by equivalent circuit (from Figure 1) fitting of the EIS measurements which correlate well with the corrosion current density (i_{corr}) tabulations in **Figure 4(d)**, determined by Tafel extrapolation. After an hour of full immersion, the expected corrosion rate from each solution rank from lowest to highest as; DI water < 1.44 M NaCl < 10% Bleach < 10% DF-200.

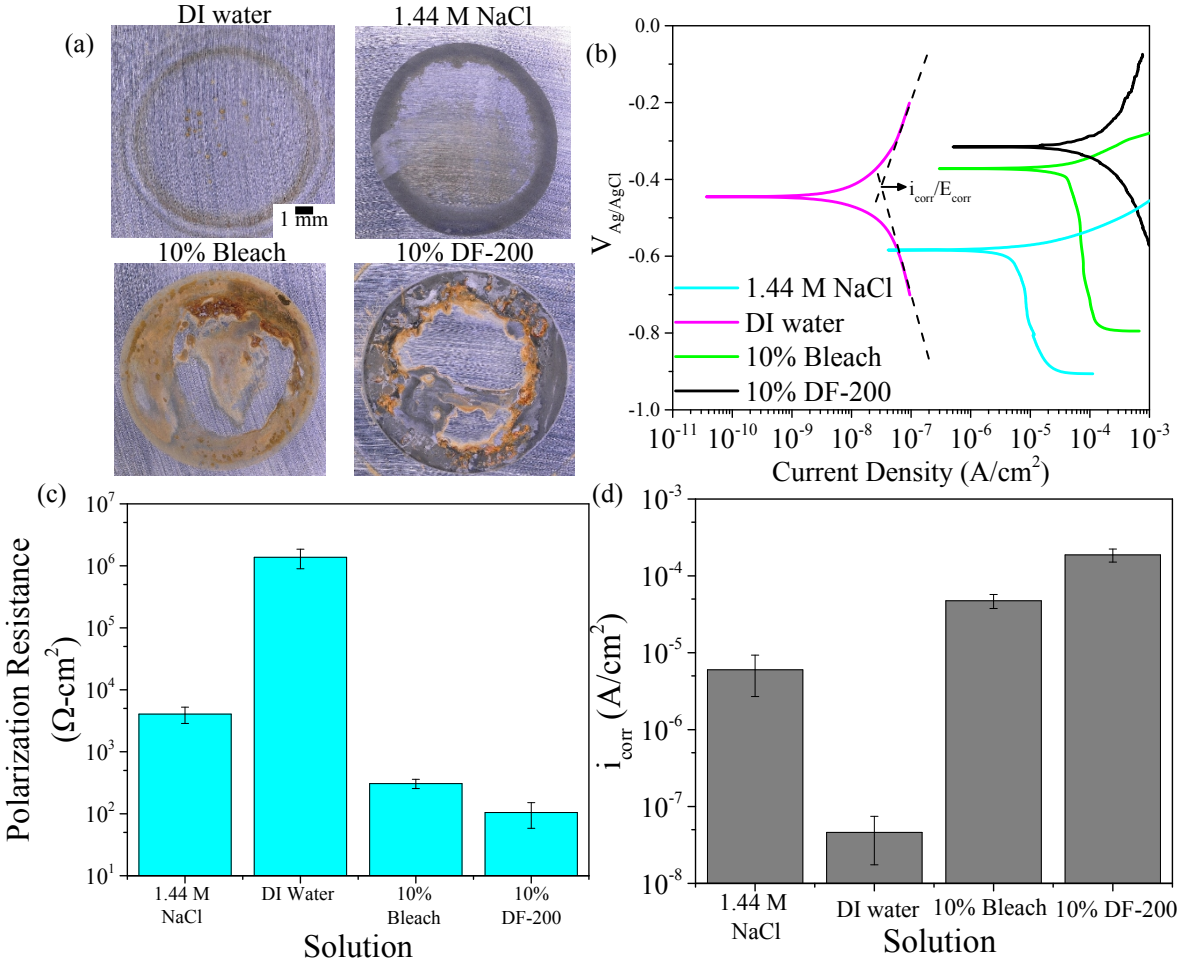

Figure 4: Electrochemical measurements performed after 1 hour OCP on HY80 steel (both wrought and cast) showing the (a) optical images after immersion, (b) representative Tafel polarization measurements, (c) the polarization resistance from EIS, and (d) the corrosion current density from the Tafel polarization measurements. Error bars represent standard error of the data.

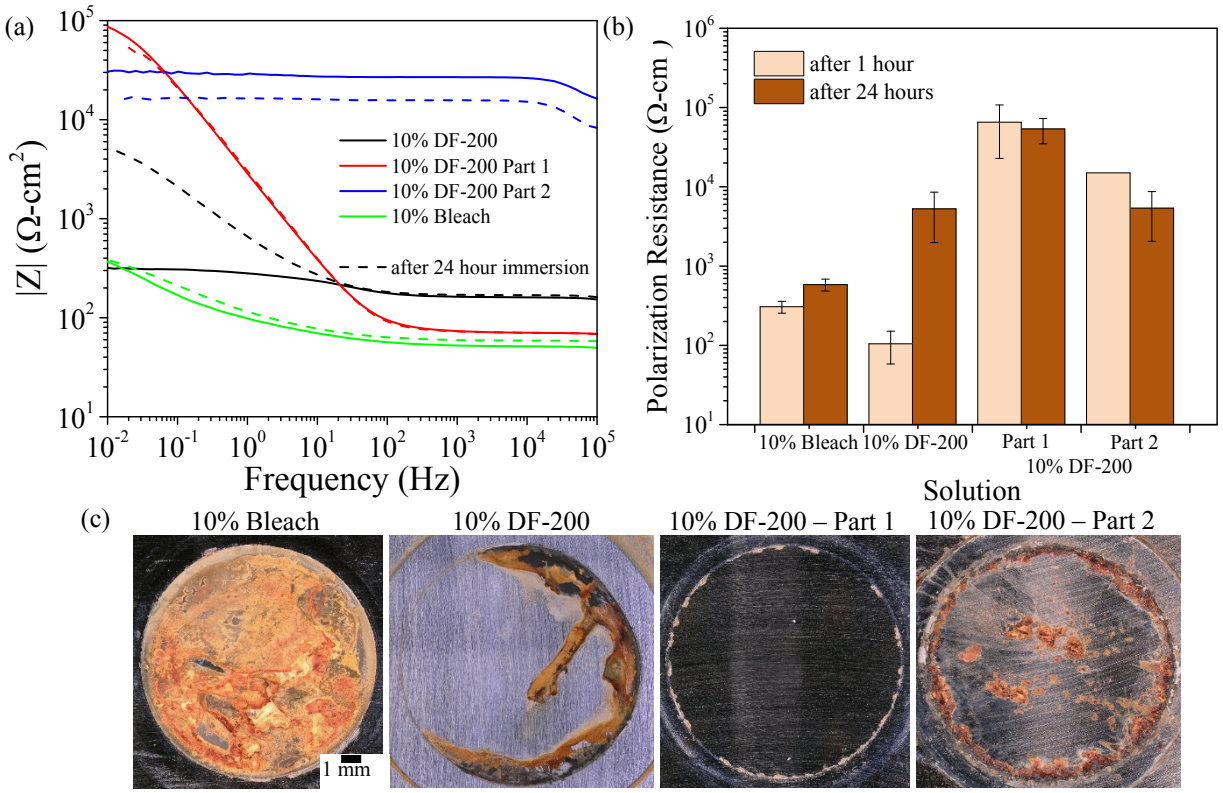

Figure 5: Electrochemical measurements performed after 1 (solid lines) and 24 (dashed lines) hour OCP holds on HY80 steel with (a) representative Bode Magnitude plots, (b) the polarization resistances from EIS for these Bode Magnitude data, and (c) optical images after the 24 hour immersion tests. Error bars represent standard error of the data.

After a 24-hour immersion, the samples exposed to 10% DF-200 show roughly an order of magnitude increase in impedance magnitude/R_p, as shown in **Figure 5(a)** and **(b)**. The consumption/dissipation of H_2O_2 (an oxidizer) was the main reason for the R_p /impedance magnitude of samples immersed in 10% DF-200 to increase by over an order of magnitude. This suggests that if there was DF-200 residue on a surface, it would become less corrosive the longer it remains on the surface. Also, specimens immersed in Part 1 of the DF-200 formulation showed minimal corrosion activity after a 24-hour immersion per the images in **Figure 5(c)**. This is in direct contrast to the 10% Bleach solution which showed a consistent corrosion rate/R_p over the 24-hour period and substantially more coverage of corrosion product than all other samples in **Figure 5**.

These electrochemical measurements showed that hydrogen peroxide, the primary virus killing surfactant, was the main cause for initially rapid corrosion rates caused by the 10% DF-200 formulation because it acts as an oxidizer. However, this corrosion rate diminishes rapidly due to dissociation of the H_2O_2 caused by consumption during corrosion reactions or by dissociation with exposure to light [16]. Not captured in the present study, and many studies on disinfectants, was the interplay between the surfactants and detritus/organic matter, other pathogens, and the virus itself. For peroxide-based disinfectants this is critical when considering the corrosivity of

the disinfectant, along with its efficacy, because more peroxide will be consumed by the other factors, leaving less to cause corrosion.

Crevice/atmospheric corrosion experiments: Electrochemical measurements are a sound way to quantify and capture trends in how a solution, in this case disinfectants, will cause corrosion over an extended period in a full immersion environment. However, in many relevant scenarios to disinfectants, materials are not in full immersion for extended times. Hence, atmospheric corrosion experiments at a constant relative humidity were performed, with the bonus of showing how susceptible these materials may be to crevice corrosion when exposed with a crevice former on their surface. Incorporation of rinsing procedures and the deposition of NaCl were also used to better simulate potential scenarios where those aspects of an environment come into play, both critical to a shipboard application.

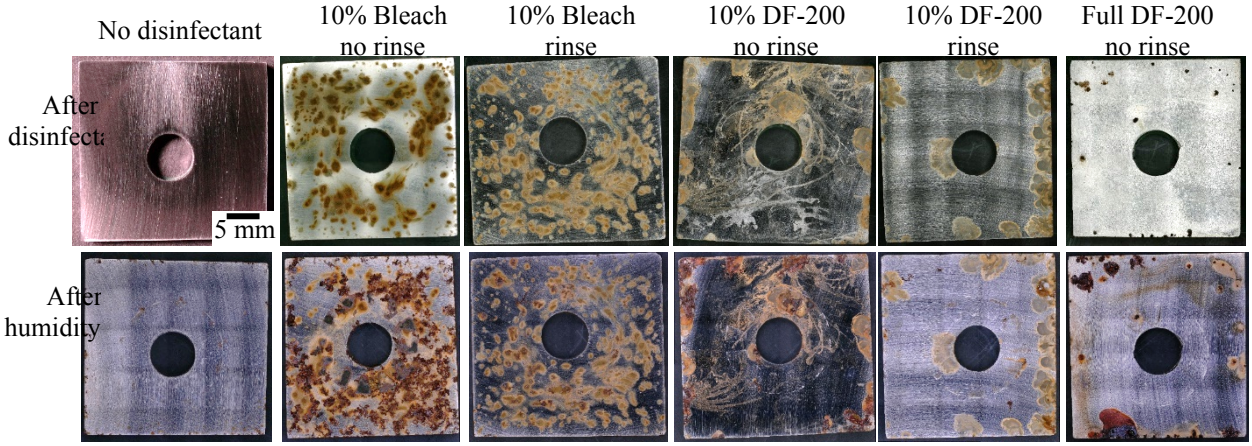

Figure 6: Optical images taken of the atmospheric exposure, crevice corrosion samples after the labelled disinfectant was applied to their surface and after the 2 week long exposure to 95% relative humidity. These samples were **not loaded with NaCl** prior to the humidity exposure experiment.

Optical images of the crevice samples are shown in **Figures 6** and **7** for samples that were free of NaCl loading (**Figure 6**), and those samples that had 50 μg/cm^2 deposited on their surface (**Figure 7**). Corrosion occurred in some capacity after the different disinfectants were applied to the coupon surfaces, regardless of the disinfectant used. The corrosion caused by the Bleach solution after the 3 disinfecting cycles showed > 1 mm diameter corrosion spots covering the entire surface. Many of these spots were noticed after the first disinfecting cycle. Corrosion caused by spraying on the 10% DF-200 formulation primarily emanated from the edges of the samples. The initiation of corrosion at edges could be caused by an increase in defects sites at edges, which were not finished with grinding paper, or caused by the meniscus that forms at the edge leading to an enhanced effect from hydrogen peroxide. Lastly, the fully concentrated DF-200 formulation showed similar corrosion at edges although the attack was not as spread out and the residue left behind on the surface appeared to be significantly more than the dilute disinfectants. These results were consistent for the cast HY80 samples as well.

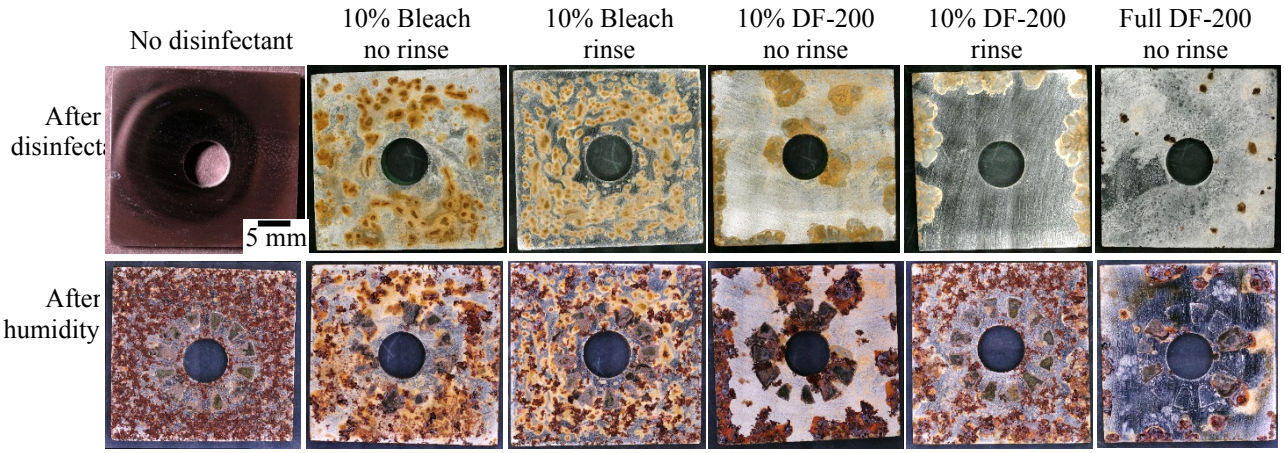

Figure 7: Optical images taken of the atmospheric exposure, crevice corrosion samples after the labelled disinfectant was applied to their surface and after the 2 week long exposure to 95% relative humidity. These samples were loaded **with 50 µg/cm^2 of NaCl** prior to the humidity exposure experiment.

The bottom row of images in **Figures 6** and **7** show the samples after the 2 week exposure to a 95% relative humidity environment. In **Figure 6** the specimens with no disinfectant or NaCl loading showed some corrosion product forming near the edges and at the crevice washers, this was also shown for the Bleach and DF-200 samples that had their disinfectant rinsed off. The specimen with Bleach residue present on the surface showed additional local corrosion at the previously corroded spots as well as dark colored corrosion spots where the crevice former sat on the surface. Additional corrosion caused by residue from sodium hypochlorite was been observed by others (Gunderson et al. [17]). The crevice corrosion was less obvious on the disinfected samples with the DF-200 residue (10% and full-strength formulations), but additional corrosion was observed at the edges of samples at the previously corroded regions. Regardless of the disinfectant type, if residue was left behind on a sample, additional corrosion was observed. That said, the only disinfectant that resulted in a noticeable increase in corrosion rate (roughly double) compared to the specimens without disinfectant on the surface were those with residue from the 10% Bleach solution, per **Figure 8**.

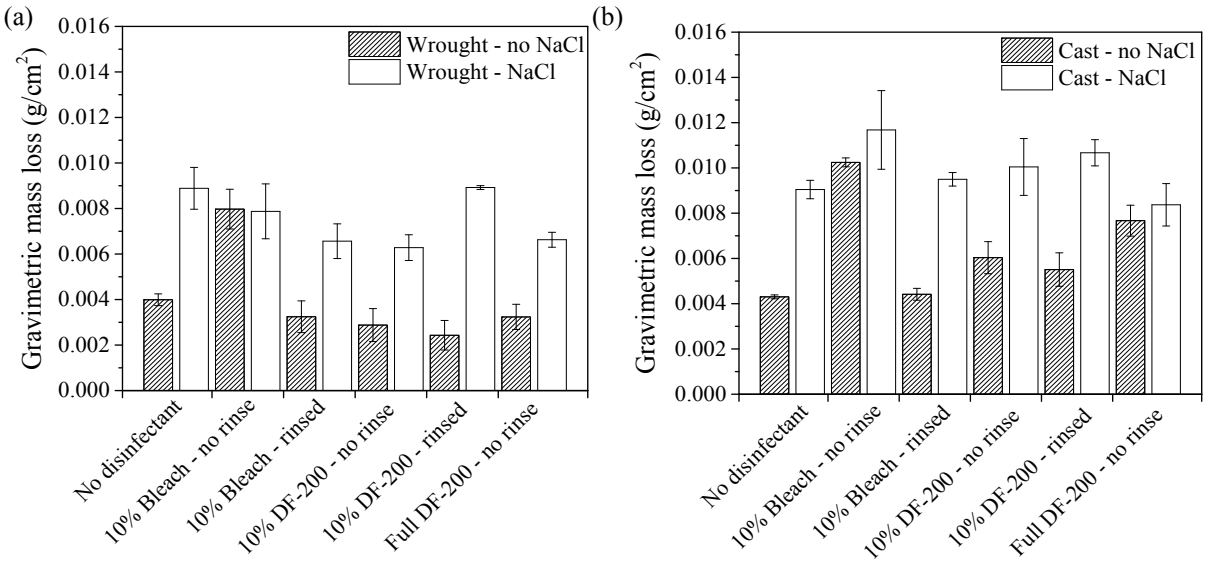

Figure 8: Plots for (a) wrought and (b) cast HY80 material showing gravimetric mass loss measurements for all crevice specimens exposed to the 95% relative humidity for two weeks, after corrosion product was removed.

S

pecimens with NaCl loadings are shown in the bottom row of **Figure 7** after 2 week exposures to provide evidence for crevice corrosion on all samples, by the dark spots surrounding the hole through each sample. The corrosion morphology was similar for the "no disinfectant", 10% Bleach (rinsed and no rinse conditions), and the rinsed 10% DF-200 samples. Crevice corrosion occurred on the specimen with DF-200 residue present, however it tended to not occur at every crevice washer tooth, and the local corrosion occurring across the rest of the sample was not as extensive as the other conditions. This type of behavior may suggest the surfactants present in the DF-200 formulation can behave as an inhibitor to corrosion caused by NaCl.

Across the board, corrosion rates determined by gravimetric mass loss (**Figure 8**) roughly doubled when NaCl was present compared to samples without NaCl. This result was consistent for HY80 steel in the cast condition. The general corrosion caused by the NaCl containing environments, used a relatively low salt load of 50 μg/cm^2 NaCl, conservative compared to many shipboard environments, but still proved to be more aggressive when compared to the surfactants used in the DF-200 formulation [18, 19]. However, the specimen with sodium hypochlorite residue consistently showed corrosion rates comparable to the specimen with NaCl on their surface.

To quantify the crevice corrosion attack, the severity of crevice corrosion under each crevice tooth was counted for each sample and designated as having; "no corrosion", "less than half the area of the crevice site was corroded", and "more than half the area of the crevice site was corroded". Results for this analysis are shown in **Figure 9**. Similar trends were observed when comparing the wrought and cast HY80 materials. The only non-NaCl loaded **Figure 9 (a, b)** specimens that consistently showed more than half the area of the crevice sites to be affected by corrosion was the 10% Bleach – no rinse and Full DF-200 – no rinse samples. Regardless, a

majority of specimens showed some sign of crevice corrosion, usually along the crevice tooth edge, shown in **Figure 10**, but it was often covering less than half the crevice tooth area.

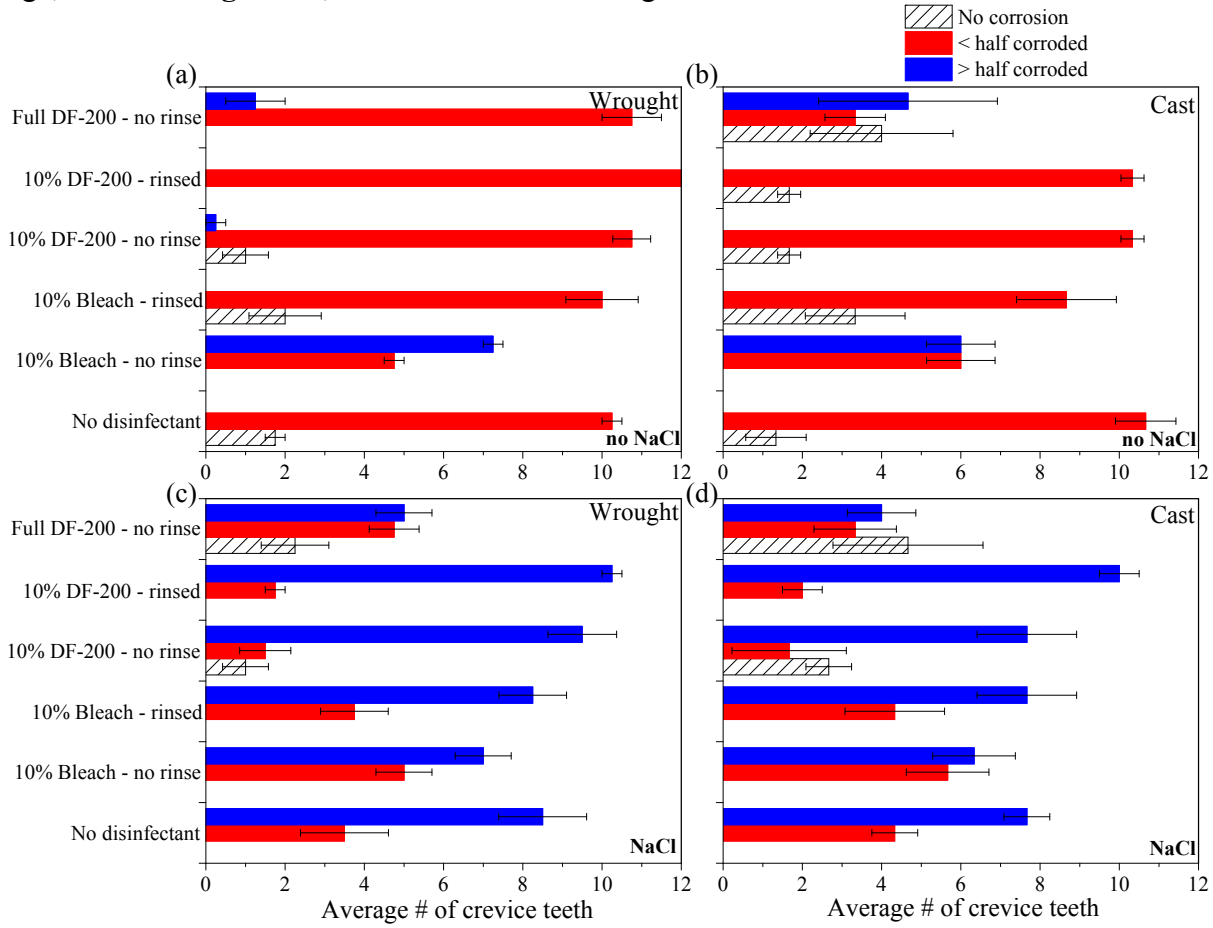

Figure 9: Plots quantifying the average crevice teeth that showed corrosion attack for the (a, c) wrought and (b, d) cast material (a, b) without NaCl loading and (c, d) with NaCl loading. The error bars represent standard error.

Compared to samples without NaCl loading, samples with NaCl showed the majority to have crevice teeth with more than half the area affected by corrosion. The 10% Bleach – no rinse samples exhibited the same behavior as if NaCl wasn't there, shown in **Figure 9 (c, d)**, suggesting Bleach behaves similar, if not more aggressivly, to NaCl. This greater than half area coverage of crevice corrosion for nearly all samples can be seen in **Figure 11**, showing samples in (a) – (e) to consistently have shallow (and occasionally deep) attack at the crevice teeth. Specimens with the Full DF-200 formulation on their surfaces were the only condition where most crevice teeth had no corrosion or less than half areal coverage of the crevice site. Large areas of minimal corrosion on the NaCl loaded specimen were observed for samples that had the DF-200 formulation residue present, most dramatically shown in **Figure 11 (f)**. This apparent prevention of corrosion points again to the possibility that the surfactants used in the DF-200 formulation can behave as an inhibitor to corrosion attack [20].

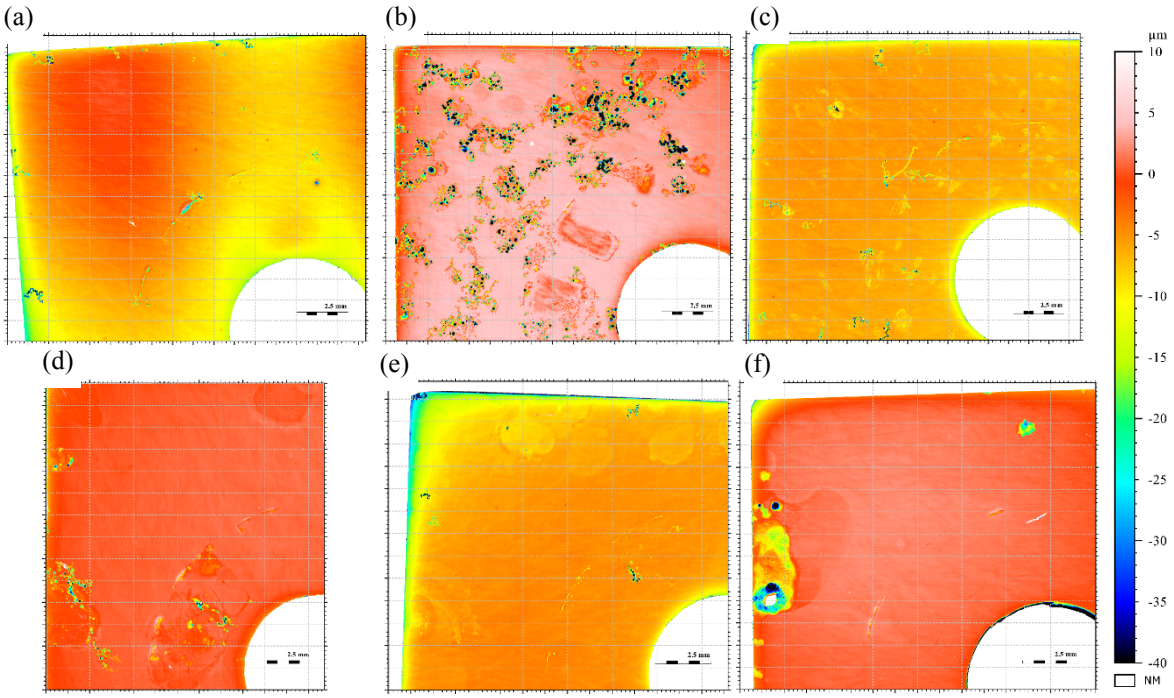

Figure 10: Representative white light interferometry heat maps showing corrosion attack depth for wrought HY80 crevice corrosion samples after the 2 week atmospheric exposure for samples with no NaCl loading and (a) no disinfectant, (b) 10% Bleach – no rinse, (c) 10% Bleach – rinsed, (d) 10% DF-200 – no rinse, (e) 10% DF-200 – rinsed, (f) Full DF-200 – no rinse.

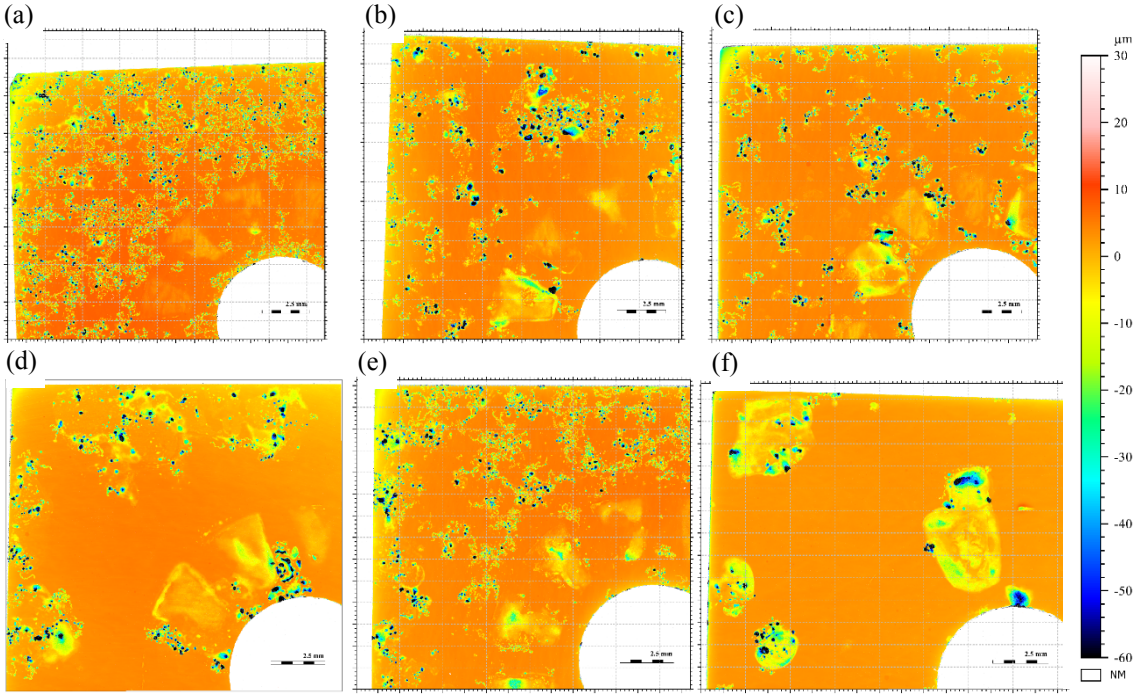

Figure 11: Representative white light interferometry heat maps showing corrosion attack depth for wrought HY80 crevice corrosion samples after the 2 week atmospheric exposure for samples with 50 µg/cm^2 NaCl loading and (a) no disinfectant, (b) 10% Bleach – no rinse, (c) 10% Bleach – rinsed, (d) 10% DF-200 – no rinse, (e) 10% DF-200 – rinsed, (f) Full DF-200 – no rinse.

A closer look at the localized corrosion caused by the disinfectant residue and NaCl loading is shown by secondary electron images in **Figures 12** and **13**. Most of the typical corrosion morphology for these specimens, regardless of disinfectant, was localized pitting or filament-like corrosion, also shown in **Figures 10** and **11**. Signs of crevice corrosion are shown in every image, for every sample, typically accompanied by an area of more intense local corrosion next to the crevice area that typifies the local corrosion shown elsewhere on the sample (pitting/filament-like corrosion).

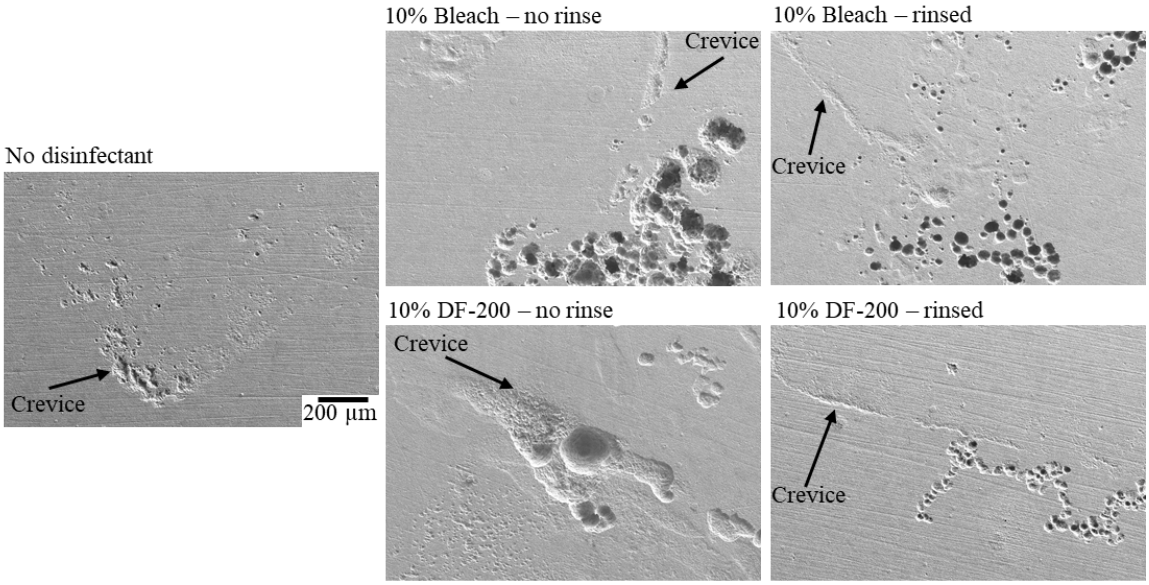

Figure 12: Secondary electron micrographs of crevice samples with their corrosion product removed. All images were taken at a location where the crevice forming washer was intact with the sample. These samples did not have NaCl loading on them. The "Crevice" label indicates an edge of the crevice former.

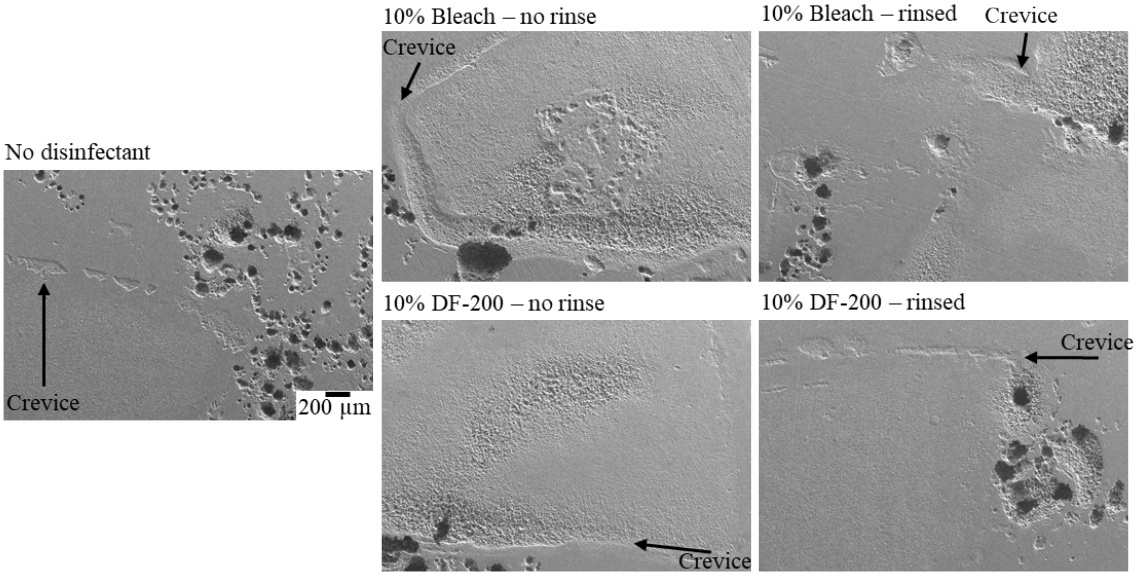

Figure 13: Secondary electron micrographs of crevice samples with their corrosion product removed. All images were taken at a location where the crevice forming washer was intact with the sample. These samples had 50 µg/cm^2 of NaCl loading on them. The "Crevice" label indicates an edge of the crevice former.

The hydrogen peroxide-based disinfectant, DF-200, did cause corrosion when in contact with HY80 steel, yet there are a range of factors to consider when quantifying its corrosivity that are often not employed by the corrosion community (contact time, number of cycles, organic load, etc.). Future work for these and other disinfectants should consider organic carbon loading/detritus that will be found on most surfaces and show its impact on the corrosion

response. Hydrogen peroxide is known to react with surface contaminates (organics, viruses, etc.), rapidly lowering its concentration and likely why anecdotal evidence suggests hydrogen peroxide-based disinfectants are considered relatively non-corrosive. Also, for the DF-200 disinfectant, incorporating a corrosion inhibitor may be a viable route to mitigating the possibility for corrosion. However, changing the formulation by incorporating an inhibitor would require further experimentation to ensure the inhibitor does not adversely affect the virus killing power/efficacy.

This study provides a quantitative analysis of corrosion behavior and rate for a shipboard relevant metal, HY80 steel, when exposed to two disinfectant formulations, Bleach and DF-200. HY80 steel was shown to be susceptible to general/localized corrosion attack when in contact with both disinfectants. Electrochemical experiments suggest the relatively large corrosion rates at early immersion times caused by the DF-200 disinfectant were controlled by hydrogen peroxide, as H_2O_2 dissipated the polarization resistance increased, from 100 Ω-cm^2 to 6,000 Ω-cm^2 after 24 hours of immersion, suggesting the corrosion rate decreases with time. Corrosion caused by Bleach (sodium hypochlorite solution) saw minimal change in its polarization resistance over time, ranging from 300 to 400 Ω-cm^2, meaning its corrosion rate remained large regardless of immersion time.

All disinfectant formulations showed signs of local corrosion after 3 cycles of disinfecting and rinsing/drying. Corrosion by the Bleach solution caused more corrosion spots to form on the surface than the DF-200 formulation. After the atmospheric corrosion exposures, samples with Bleach solution residue showed signs of crevice corrosion and coverage of localized corrosion on the remainder of the surface. The Bleach residue samples exhibited similar damage morphology, coverage, and mass loss to samples that were loaded with 50 μg/cm^2 NaCl. Crevice corrosion was prominent on all samples that were loaded with NaCl, regardless of disinfectant, and the mass loss measurements increased in magnitude (roughly doubling) compared to specimens without NaCl. Regardless of disinfectant, if the specimen was thoroughly rinsed prior to the atmospheric exposure, the material behaved as if the disinfectant was not applied (except for the corrosion spots formed during the disinfecting cycles).

The corrosion caused by Bleach was more widespread and intense than the DF-200 formulation (in both dilute and fully concentrated conditions). The residue left behind from the DF-200 formulation caused crevice corrosion attack to a similar severity as the samples without any disinfectant on the surface. Corrosion damaged caused by the full concentration DF-200 samples covered less area than the 10% dilute samples, however this corrosion tended to be more localized, penetrating deeper. Additionally, DF-200 residue showed signs of inhibiting crevice corrosion and the filament-like localized corrosion for specimens loaded with NaCl, a result requiring further investigation.

A.7.5. Acknowledgements

The authors would like to acknowledge the contributions from J. Bruce Kelley for numerous conversations and guidance regarding the DF-200 chemistry, Patrick D. Burton for providing the

disinfectant solutions, Jie Er Yang and Christina Profazi for their help with sample preparation, and Matthew Draper from the Naval Surface Warfare Center Carderock Division for providing the HY80 material. Sandia National Laboratories is a multimission laboratory managed and operated by National Technology & Engineering Solutions of Sandia, LLC, a wholly owned subsidiary of Honeywell International Inc., for the U.S. Department of Energy's National Nuclear Security Administration under contract DE-NA0003525.

A.7.6. References:

[1] Sandia Decon Formulation for Mitigation and Decontamination of CBW Agents, in, 2019.
[2] K. Nakamura, Y. Yamada, Y. Takada, T. Mokudai, H. Ikai, R. Inagaki, T. Kanno, K. Sasaki, M. Kohno, Y. Niwano, Corrosive effect of disinfection solution containing hydroxyl radicals generated by photolysis of H₂O₂ on dental metals, Dental Materials Journal, 31 (2012) 941-946.10.4012/dmj.2012-098
[3] L. Bonin, V. Vitry, M.G. Olivier, L. Bertolucci-Coelho, Covid-19: effect of disinfection on corrosion of surfaces, Corrosion Engineering, Science and Technology, (2020) 1-3.10.1080/1478422X.2020.1777022
[4] G. Tranchida, F. Di Franco, S. Virtanen, M. Santamaria, Effect of NaClO disinfection/cleaning on passive films on AISI 316L, Corros. Sci., 165 (2020) 108415.https://doi.org/10.1016/j.corsci.2019.108415
[5] S. Uchida, T. Satoh, J. Sugama, N. Yamashiro, Y. Morishima, T. Hirose, T. Miyazawa, Y. Satoh, K. Iinuma, Y. Wada, M. Tachibana, Effects of Hydrogen Peroxide on Corrosion of Stainless Steel, (III), J. Nucl. Sci. Technol., 42 (2005) 66-74.10.1080/18811248.2005.9726365
[6] T. Vasudevan, S. Muralidharan, S. Alwarappan, S.V.K. Iyer, The influence of N-hexadecyl benzyl dimethyl ammonium chloride on the corrosion of mild steel in acids, Corros. Sci., 37 (1995) 1235-1244.https://doi.org/10.1016/0010-938X(95)00028-I
[7] B. Pierozynski, I.M. Kowalski, The Influence of Hypochlorite-Based Disinfectants on the Pitting Corrosion of WeldedJoints of 316L Stainless Steel Dairy Reactor, International Journal of Electrochemical Science, 6 (2011) 3913-3921
[8] S. Abban, M. Jakobsen, L. Jespersen, A practical evaluation of detergent and disinfectant solutions on cargo container surfaces for bacteria inactivation efficacy and effect on material corrosion, African Journal of Biotechnology, 12 (2013) 3689-3698
[9] J.M. Bieker, C.A. Souza, C.V. Williams, M.D. Tucker, R.D. Oberst, S. Kapil, Rapid Inactivation of SARS-like Coronaviruses, in, Sandia National Laboratories, Sandia National Laboratories, 2004.
[10] P.W. Krug, T. Davis, C. O'Brien, M. LaRocco, L.L. Rodriguez, Disinfection of transboundary animal disease viruses on surfaces used in pork packing plants, Veterinary Microbiology, 219 (2018) 219-225.https://doi.org/10.1016/j.vetmic.2018.04.029
[11] S. Chiu, B. Skura, M. Petric, L. McIntyre, B. Gamage, J. Isaac-Renton, Efficacy of common disinfectant/cleaning agents in inactivating murine norovirus and feline calicivirus as surrogate viruses for human norovirus, American journal of infection control, 43 (2015) 1208-1212.https://doi.org/10.1016/j.ajic.2015.06.021
[12] Y. Hong, P.J. Teska, H.F. Oliver, Effects of contact time and concentration on bactericidal efficacy of 3 disinfectants on hard nonporous surfaces, American journal of infection control, 45 (2017) 1284-1285.https://doi.org/10.1016/j.ajic.2017.04.015
[13] D.A. Jones, Principles and Prevention of Corrosion, Prentice Hall, 1996.
[14] E. Schindelholz, R.G. Kelly, Application of Inkjet Printing for Depositing Salt Prior to Atmospheric Corrosion Testing, Electrochem. Solid-State Lett., 13 (2010) C29-C31.10.1149/1.3473724
[15] ASTM G1.03,
[16] B.R. Petigara, N.V. Blough, A.C. Mignerey, Mechanisms of Hydrogen Peroxide Decomposition in Soils, Environmental Science & Technology, 36 (2002) 639-645.10.1021/es001726y
[17] R. Gundersen, B. Johansen, P.O. Gartland, L. Fiksdal, I. Vintermyr, R. Tunold, G. Hagen, The Effect of Sodium Hypochlorite on the Electrochemical Properties of Stainless Steels in Seawater With and Without Bacterial Films, CORROSION, 47 (1991) 800-807.10.5006/1.3585855
[18] D.D.N. Singh, S. Yadav, J.K. Saha, Role of climatic conditions on corrosion characteristics of structural steels, Corros. Sci., 50 (2008) 93-110.https://doi.org/10.1016/j.corsci.2007.06.026

[19] I.M. Allam, J.S. Arlow, H. Saricimen, Initial stages of atmospheric corrosion of steel in the Arabian Gulf, Corros. Sci., 32 (1991) 417-432.https://doi.org/10.1016/0010-938X(91)90123-7
[20] A.A.-T. Ali, A.A. Shaikh, A.A. Abdullah, Performance Variation of Quaternary Amine Corrosion Inhibitors as a Function of Hydrocarbon Chain Length with Respect to Temperature, in: SPE International Oilfield Corrosion Conference and Exhibition, Society of Petroleum Engineers, Aberdeen, Scotland, UK, 2018, pp. 13.

DISTRIBUTION

Email—Internal

Name	Org.	Sandia Email Address
Gil Herrera	01000	herregv@sandia.gov
Ben Cook	01970	bkcook@sandia.gov
Cody Corbin	01833	wcorbin@sandia.gov
Mathew Celina	01853	mccelin@sandia.gov
Brad H. Jones	01853	bhjones@sandia.gov
Wahid Hermina	01850	wlhermi@sandia.gov
Michael A. Melia	01852	mamelia@sandia.gov
Edward Cole	05000	coleei@sandia.gov
Grant A. Rossman	05422	grossma@sandia.gov
Patrick D. Burton	06633	pdburto@sandia.gov
Jeffrey Koplow	08341	jkoplow@sandia.gov
Technical Library	01977	sanddocs@sandia.gov

This page left blank

Sandia National Laboratories is a multimission laboratory managed and operated by National Technology & Engineering Solutions of Sandia LLC, a wholly owned subsidiary of Honeywell International Inc. for the U.S. Department of Energy's National Nuclear Security Administration under contract DE-NA0003525.